ADVANCING THROUGH APPLIED SCIENCE AND TECHNOLOGY

EDITOR
Assist. Prof. Dr. Serkan GÜLDAL

İKSAD
Publishing House

ADVANCING THROUGH APPLIED SCIENCE AND TECHNOLOGY

EDITOR

Assist. Prof. Dr. Serkan GÜLDAL

AUTHORS

Prof. Bunyamin AKSAKAL

Prof. Dr. Mustafa TOMBUL

Prof. Dr. Yağmur UYSAL

Prof. Dr. Yusuf URAS

Assist. Prof. Dr. Feridun KARAKOÇ

Assist. Prof. Dr. Hasan Üstün BAŞARAN

Dr. Burak TANYERI

Dr. Çağrı ÜN

Dr. Jamal Eldin Fadoul Mohammed IBRAHIM

Res. Assist. Dr. Melih CANLIDINÇ

Lecturer Sinan GUNEŞ

Res. Assist. Ahmet DAYANÇ

Cevher Kursat MACIT

Ersoy YILMAZ

Fatih Enes ALP

Gamze ISPIRLIOGLU KARA

Merve HORLU

MSc. Şule TÜRKÖNER

İKSAD
Publishing House

(The Licence Number of Publicator: 2014/31220)
TÜRKİYE TR: +90 342 606 06 75
USA: +1 631 685 0 853
E mail: iksadyayinevi@gmail.com
www.iksadyayinevi.com

It is responsibility of the author to abide by the publishing ethics rules.
Iksad Publications – 2023©

ISBN: 978-625-367-333-8
Cover Design: İbrahim KAYA
October / 2023
Ankara / Türkiye
Size = 16x24 cm

CONTENTS

PREFACE

In this comprehensive volume, we embark on a journey through various facets of contemporary research and innovation, spanning diverse fields of science and technology. Each chapter offers unique insights and contributions, advancing knowledge and understanding in their respective domains. Here, we provide a brief overview of the chapters and their key contributions:

Chapter 1: Energy Efficient Through Near-Zero Energy Building Approach Across the Lifecycle of Existing Public Buildings

Continuing our journey, we shift our attention to energy efficiency in existing public buildings. This chapter explores the near-zero energy building approach as a sustainable solution, emphasizing strategies to reduce energy consumption, improve building performance, and minimize environmental impact.

Chapter 2: Advance in Lithium-Ion Batteries: An Overview

Transitioning to the realm of energy technology, we delve into the advancements in lithium-ion batteries. This chapter addresses critical challenges, explores emerging technologies, and underscores the pivotal role of lithium-ion batteries in shaping our evolving energy landscape.

Chapter 3: Fuel Injection Strategies to Improve After-Treatment Thermal Management in Diesel Engine Systems: A Review

Our journey takes us into the world of automotive technology. Chapter 4 provides a comprehensive review of fuel injection strategies in diesel engine systems. It highlights how these strategies can enhance after-treatment thermal management, leading to reduced emissions and improved engine performance.

Chapter 4: Tribological Effects of Cobalt and Boron on Copper-Based Composites

Shifting our focus to materials science and tribology, Chapter 5 explores the tribological effects of cobalt and boron on copper-based composites. This study investigates the addition of these elements to enhance the properties of copper, offering valuable insights into their impact on hardness, wear resistance, and microstructure.

Chapter 5: Exploring the Interplay of Structural and Magnetic Properties in Technologically Enhanced Eu-Doped GdMnO3 Materials

Continuing our exploration of materials science, Chapter 6 delves into the intricate interplay between structural and magnetic properties in technologically enhanced materials. It focuses on Eu-doped GdMnO3 materials and their potential applications in advanced technologies, shedding light on their magnetic and structural behavior.

Chapter 6: Rocket Motor Thrust Analysis with CFD

Venturing into the realm of aerospace and computational fluid dynamics (CFD), Chapter 7 analyzes rocket motor thrust. This chapter explores the complexities of rocket propulsion, offering insights into optimizing thrust performance for space exploration and beyond.

Chapter 7: Hydrogeochemical Characterization and Health Implications of Freshwater Springs in the Fatmalı-Önsen Region, Turkey

Our journey concludes with a unique chapter on hydrogeochemistry. This chapter provides a deep understanding of the hydrogeochemical characteristics and health implications of freshwater springs in the Fatmalı-Önsen region of Turkey, adding a thought-provoking dimension to our exploration.

The content and accuracy of each chapter are the sole responsibility of their respective authors, whose expertise and dedication have been pivotal in shaping this compilation.

We extend our heartfelt gratitude to IKSAD International Publishing House for their support in bringing this volume to fruition. Their commitment to disseminating cutting-edge research has made this endeavor possible.

We also express our appreciation to the esteemed chapter authors for their dedicated contributions, which have enriched this compilation with valuable insights and expertise.

These chapters collectively contribute to the expanding realm of knowledge, offering valuable perspectives and solutions in their respective fields. We hope this volume inspires further exploration and innovation, fostering a deeper understanding of the multifaceted world of science and technology.

With the highest regards,

Assist. Prof. Serkan Güldal

Adiyaman University

CHAPTER 1

ENERGY EFFICIENT THROUGH NEAR-ZERO ENERGY BUILDING APPROACH ACROSS THE LIFECYCLE OF EXISTING PUBLIC BUILDINGS

Lecturer Sinan GÜNEŞ[1]

Prof. Dr. Mustafa TOMBUL[2]

DOI: https://dx.doi.org/10.5281/zenodo.10500455

1 Ankara University, Faculty of Applied Sciences, Department of Real Estate Development and Management, Ankara, Türkiye, sinan.gunes@ankara.edu.tr, ORCID 0000-0001-7753-8333

2 Ankara University, Faculty of Applied Sciences, Department of Real Estate Development and Management, Ankara, Türkiye, mustafa.tombul@ankara.edu.tr, ORCID 0000-0002-1875-8042

INTRODUCTION

One of the primary causes of climate change is the carbon emissions released from energy sources derived from fossil fuels. According to data from 2022, building construction and related activities constitute the largest share in both global final energy use (36%) and carbon emissions resulting from energy consumption (46%) (Figure 1). Therefore, the building and construction sector takes a central role in efforts to reduce greenhouse gas emissions. Hence, there is a growing need for further action to reduce emissions and promote a low-carbon, sustainable built environment.

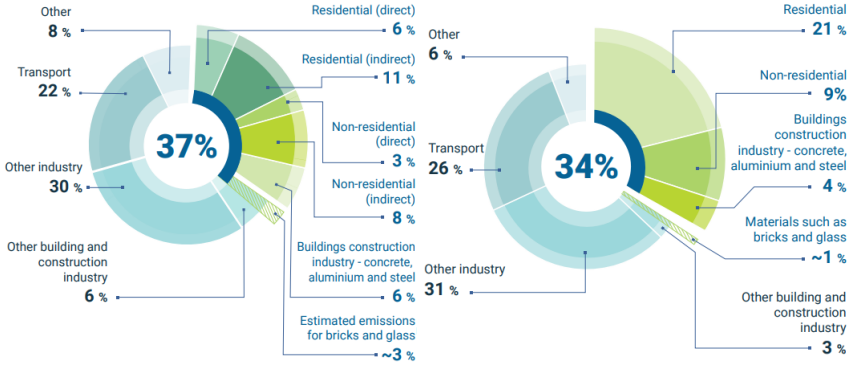

Figure 1: (a) "Global Share of Final Energy Use in Buildings and Construction Sector (b) Global Share of Emissions from Buildings and Construction Sector (United Nation Environment Programme, 2022)

The operational energy demand for functions within buildings, including heating, cooling, water heating, lighting, cooking, and other purposes, accounts for approximately 30% of the total final energy demand. This demand has increased by approximately 4% compared to 2020, reaching 135 EJ, surpassing the previous value in 2019 by 3% (United Nation Environment Programme, 2022). Global growth in fuel use in the building sectors from 2010 onwards has been concentrated on electricity, natural gas, and traditional biomass usage, with a recent surge in electricity consumption contributing to an increase in CO2 emissions (Figure 2).

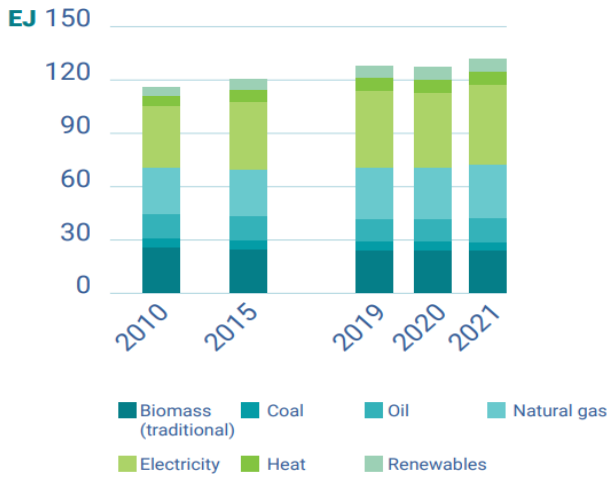

Figure 2: Global Final Energy Use in the Building Sector by Fuel Type (United Nation Environment Programme, 2022)

The increase in carbon emissions released into the environment due to energy consumption in buildings, along with the growing challenge of accessing cost-effective energy, are considered significant barriers to the development of a sustainable built environment. The primary drivers of this situation can be attributed to the global population growth and the expansion of building use (International Energy Agency, 2022).

The energy intensity in buildings (final energy use per square meter) has been consistently decreasing by approximately 0.5% to 1% since 2010. However, it has been emphasized within the Sustainable Development Scenario (SDS) that in order for energy efficiency in buildings to sustainably continue, there should be a minimum annual decrease of 2.5% in energy intensity per square meter (Figure 3).

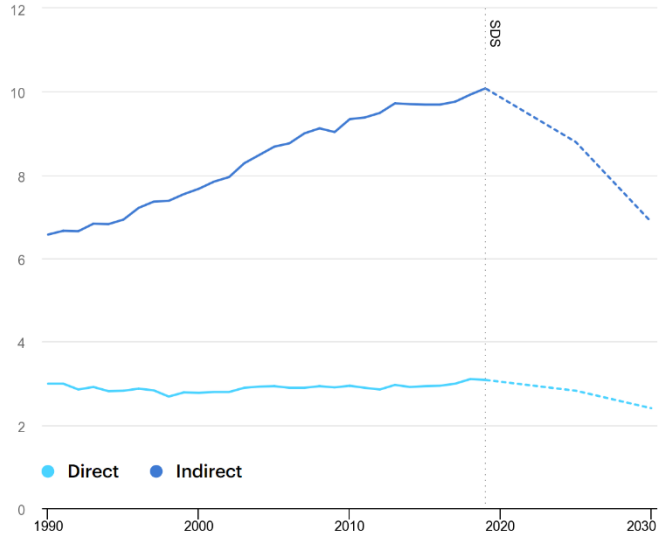

Figure 3: Within the scope of the SDS, CO2 emissions related to energy consumption in buildings, 2000-2030 (International Energy Agency, 2020)

Although total energy efficiency expenditures in buildings saw a relative decrease as of 2018, they remained above the $250 billion threshold as of 2022. However, a decline in these investments is anticipated in the short-term future (Figure 4). The slowdown is attributed to investments in energy-efficient building systems continuing in countries such as the United States and China, while investments within the EU countries are slowing down. Nevertheless, the real estate market continues to invest due to the increase in Environmental, Social, and Governance (ESG) scores, which serve as promising metrics for the sector, leading to the adoption of green buildings and green building rating systems (Global Environmental Social and Governance Benchmark, 2022).

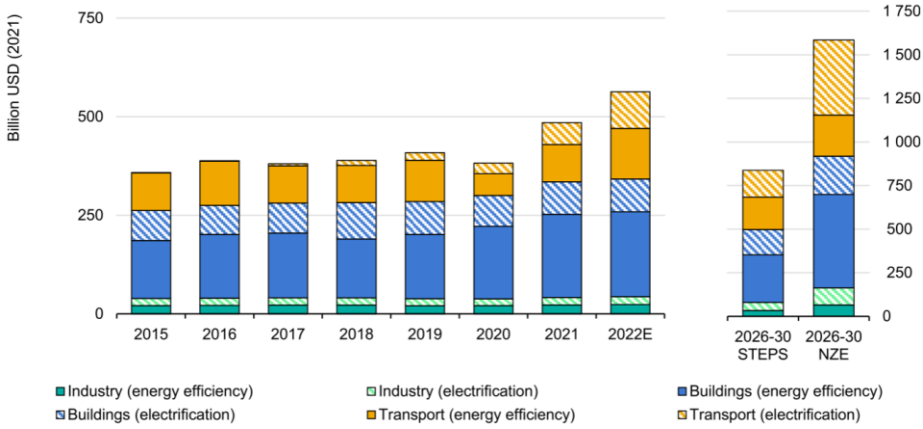

Figure 4: Global energy efficiency investments by sector (International Energy Agency, 2022)

The evaluation of efforts aimed at designing nearly Zero Energy Buildings (nZEB) for existing public buildings should encompass environmental, technological, economic, and social variables. Furthermore, it is crucial to approach the process dynamically, identify risks, and incorporate monitoring and review procedures. Anticipated gains or challenges during the operational phase should be outlined, and life-cycle costs must be comprehensively considered. The validity of proposed models should be confirmed, aligning them with legal regulations and objectives. Given its inherently interdisciplinary and multi-stakeholder nature, this process should be thoroughly examined from various perspectives and addressed by all stakeholders.

In current energy efficiency initiatives for existing buildings, decision-making mechanisms are typically treated as static processes. Additionally, the risks and potential challenges of the process are not subject to monitoring and evaluation. Consequently, the criteria considered during the decision phase fail to provide insights into the post-renovation situation, hindering problem-solving efforts.

Within the building energy efficiency sector, it is essential for stakeholders, including users, contractors, financiers, and administrators, to ensure that the outcomes of the process generate added value from a sustainable environmental perspective. This research proposes a process design that aims to provide user comfort, maximize profitability for contractors in the shortest time, ensure robust cash flow for financiers, and

offer sustainable, feasible, and scalable solutions for administrators while minimizing the environmental impact through dynamic process design. The study presents a perspective on this dynamic process design and offers recommendations.

1. IMPLEMENTING THE NEARLY ZERO ENERGY BUILDING APPROACH IN EXISTING PUBLIC BUILDINGS

Public buildings represent a significant share of energy consumption and a strategic area for achieving environmental and economic sustainability. The application of the near-zero energy building approach to existing buildings starts with the near-zero energy building approach, setting out the basic principles and potential benefits of this approach. We then describe the tools that complement the approach, such as life cycle assessment (LCA) and life cycle cost analysis (LCC). These tools will help us to understand and optimise the environmental and economic impacts of energy efficiency projects. Under the concept of deep renovation, we examine how existing buildings can be transformed and energy efficiency improved. We then focus on performance indicators to assess the impact of energy efficiency projects. Finally, we conclude the approach by addressing the energy efficiency implications of understanding and managing building occupant behaviour, which plays an active role in achieving energy saving targets.

The paper is an introduction to the journey of understanding the complexity of implementing energy efficiency and addressing the challenges and proposing solutions to improve the energy efficiency of existing public buildings.

1.1 Nearly Zero Energy Building Approach

The process of converting existing buildings into nZEBs, which is applied in the world and conceptually known and targeted in our country, is a sensitive process that should be implemented by considering many variables together ((Attia et al., 2017; Brambilla et al., 2018; Di Giuseppe et al., 2017; Fotopoulou et al., 2018; Irulegi et al., 2017; Semprini et al., 2017; Wells et al., 2018). The best results of this process depend on the dynamic design of the process and the consideration of the demands of all stakeholders. In the European Union (EU), efforts have been made in the context of reducing primary energy consumption in buildings; following the 2007 Climate and Energy Package, which aimed to reduce primary energy consumption by 20% by 2020, increase the share of renewable energy production by 20%, and

reduce greenhouse gas emissions by 20% compared to the 1990 level, the 2030 Climate and Energy Framework and the European Roadmap for 2050 have been published. According to these frameworks, greenhouse gas emissions are expected to be reduced by 40% compared to the 1990 level, the share of renewable energy is expected to increase to 32%, and energy efficiency is expected to improve by at least 32.5% (European Commission, 2023).

Reducing energy consumption and the use of energy from renewable sources in the construction sector constitute fundamental steps to reduce the EU's energy dependency and greenhouse gas emissions. The construction sector has been defined as a key sector in achieving the Sustainable Development Goals set by the EU and the United Nations (UN), particularly in efforts to achieve the 20/20/20 targets. Additionally, many of the sustainable development goals set by the UN's Agenda 2030 affect the construction sector. In its forecasts for 2050, the EU aims to achieve net-zero greenhouse gas emissions within the framework of the European Green Deal. To achieve this goal, the UN also emphasizes the urgent implementation of Sustainable Development Goals.

The concept of nZEB, defined as buildings with very high energy performance (Official Journal of the European Union, 2018), is expressed as energy that can be significantly met with renewable resources produced in the building. The nZEB definitions, which reflect the national, regional or local conditions of the member states by EPBD and indicate a numerical indicator of primary energy use expressed in annual kWh/m2, are detailed. The primary energy factors used in determining the use of primary energy are based on national or regional annual average values, taking into account the relevant European standards.

It is stated that the Member States need to provide quantitative definitions of "very high energy performance" and "energy significantly obtained from renewable resources", and also the meaning of "primary energy (total, non-renewable or renewable)" to be used in the numerical performance indicator and "near" are phenomena that need to be redefined in each country.

One of the provisions restructured with the updated EPBD is related to the introduction of cost-effectiveness (cost-optimality). A comparative methodology framework is provided in the Delegated Regulation No. 244/2012, which completes the renewal of the EPBD, for the minimum

energy performance requirements for buildings and their elements to be achieved at a cost-optimal level (Arambula Lara et al., 2015; Zangheri et al., 2022). The optimum cost level is defined as "the level of energy performance that leads to the lowest cost over the estimated economic life cycle". The methodology includes defining reference buildings and implementing energy efficiency measures to reduce primary energy consumption and select economically the most advantageous solutions (D'Agostino et al., 2021, 2022; Yang et al., 2016).

The concept of optimum cost, which plays a critical role in determining the minimum energy target level for both building renovation and new buildings, is intertwined with nZEB (Figure 5). According to the European Commission Recommendation on the Guidelines for nearly zero-energy buildings, a single performance level cannot be determined for nZEBs across Europe. It has been stated that flexibility is needed to take into account the impact of climate conditions on heating and cooling needs and the cost-effectiveness of energy efficiency and renewable energy resource packages.

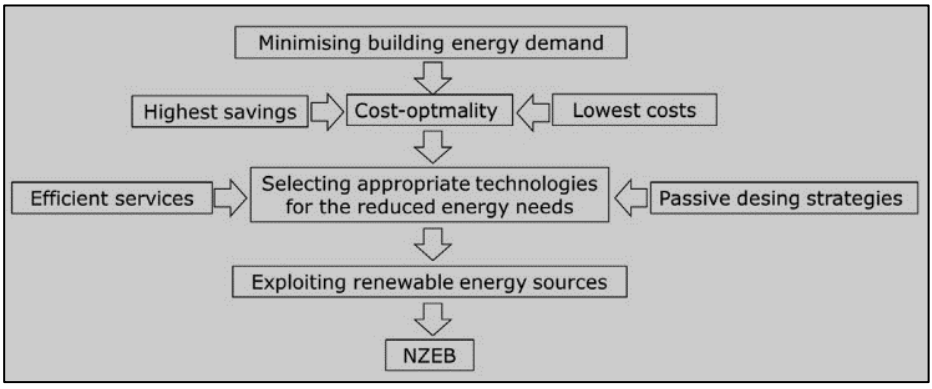

Figure 5: The nZEB consept

The main goal of energy efficiency studies in buildings is to reduce building energy consumption and create a more environmentally friendly structure without compromising comfort levels. The path to follow to increase energy efficiency in the process of renovating existing buildings is primarily to minimize the energy demand of the building within the framework of budget and technological possibilities. Then, meeting part of the remaining energy need from renewable energy sources forms an important part of this process. If a minimum of 60% energy efficiency can be achieved with a deep renovation study in a building and the annual total energy demand can be met

from renewable sources, the criteria for zero energy buildings (nZEB) are met (Economidou & Bertoldi, 2014).

The building energy need can be reduced with energy efficient design, planning, and applications depending on a number of variables such as the type, size, age, and location of the building (Figure 6). In this context, measures such as high-performance thermal insulation in the building envelope, high-efficiency heating, cooling and ventilation systems, lighting and heat recovery systems, variable speed and high-efficiency pump and fan selection, free cooling applications, implementation of automatic control and automation systems/energy management systems, selection of efficient office devices can be considered.

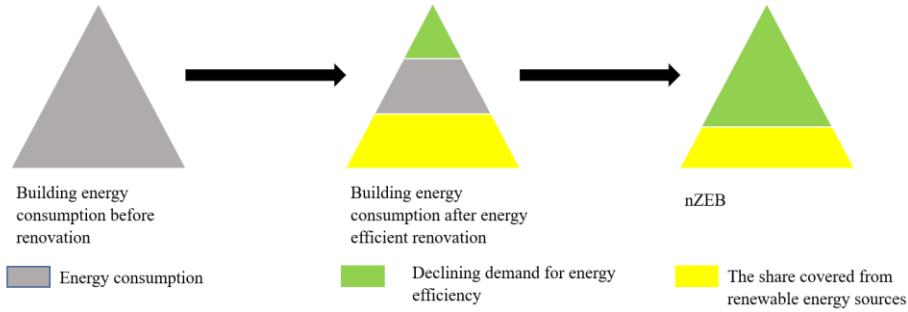

Figure 6: Processes aimed at increasing energy efficiency in building (Republic of Türkiye Ministry of Environment Urbanization and Climate Change, 2020)

The literature review conducted for the renovation of existing buildings with the nearly zero-energy building approach has included results related to nZEB design and potential energy savings that can be achieved with these design principles. It has been found that the established framework related to the subject has been examined in all its aspects, and in some studies, this framework is questioned, and new methods are proposed with the studies conducted. The relationship of design principles with user behavior, deep renovation applications, and economic feasibility has been revealed and policy criticisms have been made at national and international scales. However, no studies have been encountered where all economic, social, environmental, technical, and legal processes are carried out together. In addition, the fact that the process is mostly handled statically, not including risk analysis with monitoring and review processes, not revealing the gains or difficulties expected to be achieved during the operation period, one-sided handling of life cycle costs, not confirming the validity of the designed

models, not associating legal regulations and compliance with targets, examining this process which needs to be carried out interdisciplinary and multi-stakeholder by nature in one way or not being handled comprehensively and not being handled in terms of all stakeholders are considered as gaps in the studies conducted in this field.

When the reasons why the process could not be handled holistically are analysed,difficulties encountered in obtaining physical data related to existing buildings, limited possibilities of strategy determination due to low performance of future energy consumption prediction models, limited interdisciplinary education opportunities in the field of energy efficiency and therefore possible difficulties and insufficient cooperation problems that may be experienced in teamwork that will form comprehensive thought can be listed.

By considering the impact of energy-efficient transformation on climate change, there is a need for strategic visions that adopt international targets where relevant disciplines can communicate, financial opportunities and communication opportunities are expanded for high cooperation, especially related institutions and organizations act together on data sharing and for public buildings, which are among the most problematic areas in terms of energy consumption, to become energy efficient.

1.2. Life Cycle Assessment (LCA)

Life Cycle Assessment (LCA) refers to the process that aims to increase resource use efficiency and reduce liabilities by evaluating the potential impacts on the environment throughout the entire life cycle of a product or service, including production, distribution, use, and end of life (European Environment Agency, 2023). LCA is often referred to as "cradle to grave" analysis (Jiménez-González et al., 2000). The key elements of LCA are: (1) identification and measurement of relevant environmental burdens such as consumed energy and raw materials, produced emissions and wastes; (2) evaluation of the potential environmental impacts of these burdens; and (3) evaluation of existing options to reduce these environmental impacts.

Life Cycle Impact Assessment (LCIA) covers all environment-related inputs such as mining, crude oil, water and land use, as well as air, water and soil emissions such as carbon dioxide and nitrogen oxide. Guidelines and requirements for LCA are available in ISO 14040 and 14044 (International Organization for Standardization, 2006).

In the goal and scope stage of the life cycle assessment, the product or service subject to the evaluation is first defined. A functional base reference is chosen for comparison and the required level of detail is defined. Then a goal is set that defines the scope, including purpose, application, and target audience. Finally, it is decided whether there needs to be a critical review of this goal.

In the inventory analysis stage for the evaluation, a data compilation and an inventory analysis of what is taken from and released into the environment should be performed. The final inventory provides a list of all inputs and outputs associated with the life cycle of the product or service.

In impact assessment, resource use and produced emissions are classified according to their potential impacts and quantified for a limited number of impact categories. They are then evaluated in terms of their relative importance for the purpose of the LCA study. The results of inventory analysis and impact assessment within the scope of life cycle assessment goal are discussed in terms of contributions presented, suitability, robustness, data quality, and limitations, and any opportunities to reduce the adverse effects of products or services on the environment are systematically evaluated.

The LCA framework (International Organization for Standardization, 2006): includes processes such as extracting an inventory related to natural resources and environmental emissions occurring along with water, energy and other raw materials used in the service provision process, evaluating possible environmental impacts associated with these inputs and outputs, and systematically and comparatively evaluating the results and presenting them to decision-makers (Figure 7).

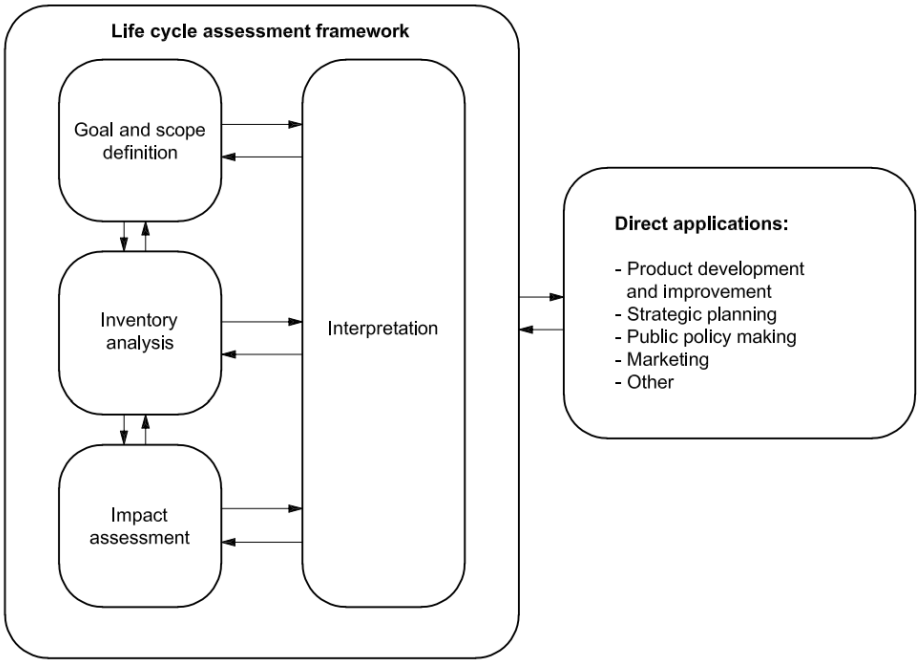

Figure 7: LCA framework (International Organization for Standardization, 2006)

1.3. Life Cycle Cost (LCC)

In studies aimed at renewing existing buildings in an energy-efficient manner, ensuring economic feasibility, determining sustainable and affordable financing models for the implementation of the study, are dependent on the healthy continuation and completion of renovation works (Ascione et al., 2017; Di Giuseppe et al., 2017; Guardigli et al., 2018; Hamdy et al., 2017; Semprini et al., 2017; Tagliabue et al., 2018).

Life Cycle Costs (LCC) are expressed as the sum of cost estimates for both equipment and projects determined by an analytical study, and the total costs experienced throughout the entire life of the product or service (Barringer et al., 1996). The purpose of the LCC analysis is to select the lowest cost approach among a range of alternatives and thus reach the shortest term acquisition cost.

LCC analysis helps decision-makers justify their choice of equipment and processes based on total costs rather than the initial purchase price. Operating, maintenance, and disposal costs often far exceed all other costs. The best balance between cost elements is achieved when LCC is minimized

(Landers, 1997). However, it should be kept in mind that LCC will give the best results when combined with good reasoning by considering many variables together, especially aesthetics and science.

Various variables such as initial investment costs, energy costs, efficiency rates, payback periods, net present value calculations, and lifetime costs should be considered for comprehensive cost analyses for efficiency-enhancing projects and scenarios. As a result of these analyses, scenarios and projects that both have appropriate payback periods and successfully meet indoor quality targets are determined. The energy efficiency increase rates that can be achieved in the context of energy efficiency-enhancing projects are presented in detail in Table 1.

Table 1: Energy efficiency increase rates related to energy efficient projects (Republic of Türkiye Ministry of Environment Urbanization and Climate Change, 2020)

Savings Level	Energy consumption reduction rate (%)	Description
Low	%5-10	Short payback period (<3 years)
Medium	%10-20	Short to medium payback period (<6 years)
High	%20-40	Long payback period – deep renovation (>6 years)
Very High	%40-70	Long payback period (energy efficiency measures, renovations, renewable energy systems, cogeneration/trigeneration systems, etc.)

There are problems of high-cost initial investments and long payback periods for building owners and the Administration in front of the energy improvement of existing buildings. Therefore, different renovation strategies need to be evaluated through the measurement of economic sustainability in relation to the provision of energy efficiency aimed at reducing energy consumption and carbon emissions. In this context, in order to measure the economic sustainability of various design alternatives, determining net present value (NPV), discounted payback period (DPP) and global cost factors are among the most commonly used methods. However, it is necessary to prepare economic studies from this perspective in order to reduce energy costs and associate economic feasibility with the targeted energy efficiency rate and other stakeholder expectations, based on the fact that the studies focus only on economic feasibility during the construction process, do not make predictions related to the operating period, environmental factors remain in the background, international targets and user behaviors are ignored.

Energy-efficient transformations have economic benefits in the medium and long term as well as environmental benefits. The existence of these benefits offers a solution to reduce high initial investment costs. In order to make the economic benefits of energy efficiency measurable and reflect them in economic feasibility studies, it is necessary to make the environmental social and technical efficiency of buildings measurable by scoring, finding the efficiency value by calculating the purchase-sale values of buildings before and after energy-efficient transformation, and selecting an energy-efficient transformation project with dynamic project valuation methods that take into account the time value of money.

1.4 Deep Renovation

The energy consumed and needed by existing buildings and the alternatives to be put forward to meet this energy need to be economically feasible, applicable in terms of current construction conditions and technologies, and need to be supported by legal permits. In making existing buildings energy efficient, technical possibilities are also important alongside financial instruments (Agliardi et al., 2018; Ahmad et al., 2018; Ascione et al., 2017; Brambilla et al., 2018; Ciancio et al., 2020; Di Giuseppe et al., 2017; Fotopoulou et al., 2018; Irulegi et al., 2017; Medved et al., 2021; Rosso et al., 2020; Salata et al., 2020; Santangelo & Tondelli, 2017; Semprini et al., 2017; Wells et al., 2018). In this context, it is envisaged that the cost-optimal solutions, which are the lowest cost, least harmful to the environment, most profitable for financiers and contractors, income-generating in the medium and long term, applicable with current techniques, and can be developed with evolving technology, will respond to the variables demanded by all stakeholders.

Studies to increase energy efficiency with deep renovation, which is widely used and encouraged by international authorities in renovation works to reduce energy costs of existing buildings, reduce energy consumption and achieve savings, are widely used worldwide. In this context, studies to increase the energy efficiency of existing buildings with deep renovation are frequently encountered especially in recent years (Agliardi et al., 2018; Ascione et al., 2017; Camporeale & Mercader-Moyano, 2021; Eliopoulou &

Mantziou, 2017; Ferreira et al., 2017; Fotopoulou et al., 2018; Guardigli et al., 2018; Hamdy et al., 2017; Salvalai et al., 2017; Semprini et al., 2017). At the macro level, deep renovation, unlike traditional strengthening applications, is envisaged to consider the system as a whole, and it is expected to present energy savings of at least 30% as output, although it varies by regions and conditions.

As a result of the studies conducted, it is seen that the application of deep renovation is at the forefront of the most effective and recommended technical studies in ensuring the energy-efficient transformation of existing buildings. Numerous studies have been encountered where energy-efficient renovation is evaluated together with factors such as architectural design techniques, economic feasibility, and new methods have been proposed in addition to established knowledge. However, it is necessary to prepare economic studies from this perspective in order not to evaluate all these factors together, not to achieve the expected effect from energy-efficient transformation and to associate energy costs reduction and economic feasibility with the targeted energy efficiency rate and other stakeholder expectations.

In addition to the environmental benefits of energy-efficient transformations, there are also economic benefits in the medium and long term. The existence of these benefits offers a solution to reduce high initial investment costs. In order to make the economic benefits of energy efficiency measurable and reflect them in economic feasibility studies, it is necessary to make the environmental, social, and technical efficiency of buildings measurable by scoring, finding the efficiency value by calculating the purchase-sale values of buildings before and after energy-efficient transformation, and selecting an energy-efficient transformation project with dynamic project valuation methods that take into account the time value of money.

There is no common deep renovation definition established at regional or international level, and it varies between regions. According to the survey results applied for the preparation of the technical report prepared by the Global Building Performance Network (GBPN), there is a clear distinction

between "deep renovation" and "deep retrofit". Experts from Europe have found that renovation is the most commonly used term, while experts from the US generally use retrofit. In general, all terms are primarily related to building shell regarding a deep renovation aiming at reducing all terms in depth. The definition of retrofit mainly focuses on mechanical systems of the building.

In Europe, most definitions focus on heating, cooling, ventilation, and hot water, and generally emphasize that these should lead to at least 75% improvement after building renovation. Most commonly, deep renovation in the US requires improvements in the range of 30% - 50%, but this is based on total energy consumption including plug load. The relevant targets or final energy consumption after a deep renovation / retrofit project should be specified at local level within the values stated in definitions depending on climate zones, loads and building type.

The EPBD published by the EU is recognized as an authority worldwide on the issue of energy-efficient renovation of buildings (Official Journal of the European Union, 2012). Although this directive does not directly mention the concept of "deep renovation", it regulates practices aimed at ensuring maximum energy performance with minimum requirements for existing building units and building elements subject to major renovation. According to the EPBD, a "major renovation" means renovating a building in the following cases:

(a) The total cost of renovation work related to the building shell or technical building systems is higher than 25% of the building value, excluding the value of the land where the building is located,

(b) More than 25% of the building's exterior shell surface undergoes renovation.

This definition also defines a "window of opportunity" for "in-depth renovation". The minimum energy requirement will be determined by individual member states. However, it should be based on EPBD Article 4, which stipulates minimum energy performance requirements for building elements that form part of the building's exterior shell and have a significant

impact on the energy performance of the building's exterior shell when they are replaced.

In recent years, stakeholders and politicians in the EU have started to show increasing interest in deep renovations. Other deep renovation definitions encountered in the research conducted by GBPN are as follows:

RENOVATE EUROPE; Deep renovation can provide a decrease in energy consumption between 60% and 90% for most buildings in Europe. When this building renovation takes place, all existing energy-saving technologies should be included (Shnapp et al., 2013).

EURIMA & Laustsen; A renovation classification of 2, 4, 6 or 10 is made, expressing the systematic decreases in energy performance as a factor, and it provides a decrease in energy consumption by 50%, 75%, 84% or 90% respectively compared to the performance before renovation (Economidou & Bertoldi, 2014).

IEA; Deep renovation is a renovation that does not lock the savings potential. Deep renovation can only be carried out when the overall energy performance of the building is taken into account when designing the renovation program (Shnapp et al., 2013).

ROCKWOOL; Normally, deep renovation is carried out using a cost-optimal approach, associated with a major renovation of a building or buildings and/or as part of the standard 30-40 years renovation cycle. In low-performing buildings, energy performance can generally be improved fourfold or between 65% - 95% by reducing final energy consumption compared to pre-renovation levels (Shnapp et al., 2013).

BPIE (Building Performance Institution Europe); in-depth renovation is the process of capturing all of the potential to reduce energy demand in one or several steps if not possible, depending on the typology of a building and the climate zone.

Energy in buildings is generally used in the form of electrical energy and thermal energy. During the building design process, various studies are carried out, usually using energy modeling software, to optimize energy consumption and increase efficiency. These modeling programs offer

powerful tools where factors such as heating/cooling loads, ventilation loads, lighting and electrical system designs in existing buildings can be calculated holistically and design optimization (optimization) can be done. In building renovation projects, a detailed analysis of current energy consumption is required to determine the targeted energy efficiency improvements. In Figure 8, the relationships between different systems contributing to energy consumption are graphically shown. This provides a guide to better understand energy consumption and identify improvement opportunities.

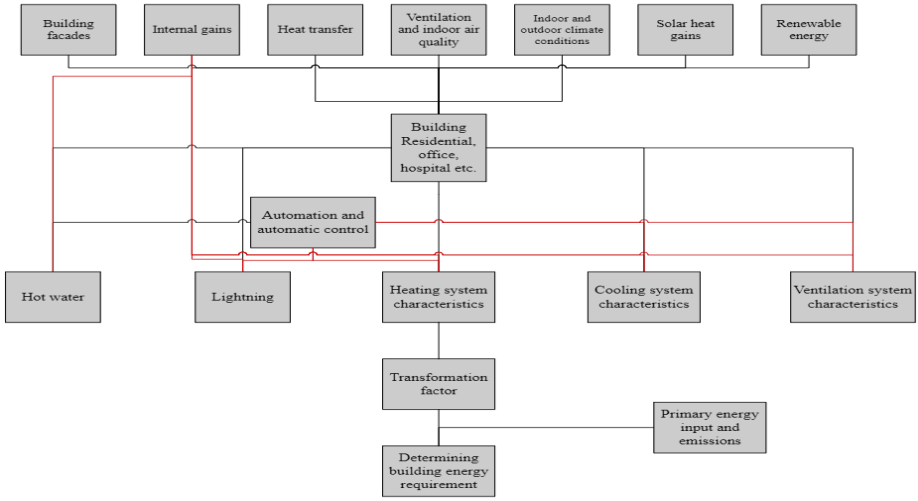

Figure 8: Relationships of energy consumption areas and systems in buildings (Republic of Türkiye Ministry of Environment Urbanization and Climate Change, 2020)

The energy need of a building arises from the total of heating, cooling, ventilation, hot water supply, lighting, elevator, electrical appliances and other energy consumption sources related to the use of different systems inside it. These energy consumptions have a structure that varies at different hours of the year. In Figure 9, an example of the Sankey Diagram (building energy flow diagram), which is frequently used in building energy consumption analyses, is presented (Momber et al., 2010).

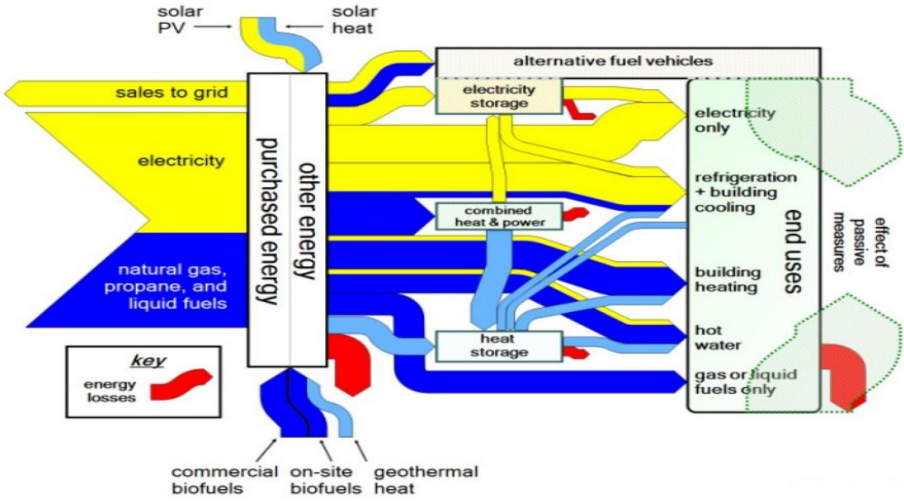

Figure 9: Sankey (Energy Flow) Diagram in Building Energy Analysis

The Sankey Diagram is a tool used to make a detailed analysis of the energy consumed between the systems used in buildings. This analysis is a fundamental starting point to determine whether energy efficiency can be improved and how these improvements can be made. Tools such as energy measurement and monitoring systems and energy modeling programs are used in these processes. After reducing the energy need, the remaining energy need can be met with appropriate renewable energy sources depending on the initial investment costs and the purpose of use of the building. However, the energy consumption of a building over its lifetime will be significant compared to the initial investment costs made. Therefore, when evaluating energy costs, factors such as total costs that will arise over the life of the building and annual CO2 emissions should also be taken into account.

Deep renovation, which aims to ensure energy efficiency through the combined use of variables such as especially the exterior shell of the building, mechanical systems, heating, cooling, ventilation and hot water systems, generally aims for an energy improvement of 30-50%. Deep renovation, which means comprehensive energy renovation, should be carried out in accordance with the targets specified in national and international legal regulations in terms of final energy consumption; depending on the climate region where the buildings are located, the moving and dead loads they are exposed to throughout the year and the type of building. The renovation work should also be designed with a nearly zero-energy building approach to allow the building to meet its own energy at maximum level. In this context,

architectural, static and mechanical projects of existing public buildings should be examined, advantages and disadvantages of existing materials and materials and systems envisaged to be used within the scope of renovation should be revealed, design process related to renovation project and construction activity should be prepared using modern techniques such as Building information modeling (BIM) technologies with the data obtained.

1.5 Performance Indicators Related to Energy Efficiency in Buildings

Improving energy performance is one of the most important processes that need to be carried out in the energy-efficient improvement of existing public buildings. The Energy Management System (EnMS), prepared within the scope of ISO 50001, aims to continuously improve energy performance (Republic of Türkiye Ministry of Environment Urbanization and Climate Change, 2020). EnMS is defined as a set of activities systematically carried out to reduce the energy used and increase the energy efficiency of the institution for existing public buildings without reducing service quality. With an effective EnMS, energy efficiency of around 10-15% can be achieved just with the awareness created, and with a systematic roadmap, determining all energy consumption points and implementing techno-economically feasible projects, energy efficiency up to 40-50% can be possible.

The EnMS defined according to the ISO 50001 standard is based on the principle of continuous improvement of energy performance. Studies for continuous improvement of energy performance can be achieved by adopting a systematic approach based on energy management known as the Deming Cycle, which is Plan - Implement - Check - Take Precautions. In daily applications, attention is paid to energy use and continuous improvement of energy performance is taken as a basis (Figure 10).

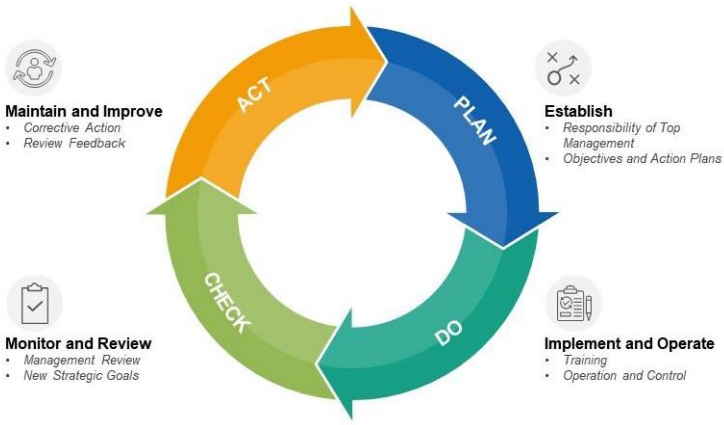

Figure 10: Deming Cycle for Energy Performance Improvement (Deming, 1982)

The Energy Management System (EnMS), which can be applied to buildings of all scales and in many sectors including the building sector, can be carried out alone or in harmony with other management systems. In buildings where EnMS is implemented, besides improving energy performance, financial benefits, compliance with legal obligations, and many non-energy external and internal benefits can also be provided:

Financial Returns:

- Reduction in Energy Imports: Reducing energy consumption nationwide reduces dependence on energy imports, thereby increasing the country's energy security.
- Decrease in Costs: Reducing energy consumption provides a significant decrease in the institution's energy costs, which increases profitability.
- Continuous Operation: The energy consumption and operating conditions of the equipment are constantly monitored. This allows faults and service interruptions to be predicted and prevented in advance.

Legal Compliance:

- Continuous Compliance: It is mandatory to continuously comply with legal regulations related to energy use, and this ensures the institution fulfills its legal obligations.
- Reduction of CO2 Emissions and Future Compliance: Reducing CO2 emissions facilitates compliance with current and future environmental regulations.

External Gains:

- Social Responsibility Image: The institution emphasizes its social responsibility more by providing energy efficiency, and this creates a positive impression on the public.
- Fighting Climate Change: By increasing energy efficiency, the institution supports the fight against climate change and reduces its environmental impacts.

Internal Gains:

- Participation of Senior Management: Senior management plays a guiding role in improving holistic energy performance.
- Coordination: Coordination is provided between units, which contributes to more efficient operation of business processes.
- Improvement of Working Conditions: When energy efficiency is achieved in businesses, working conditions improve, productivity increases, and employee health problems decrease.
- Sense of Belonging: Employees establish more connection with a sense of belonging by being part of contributing to the institution's energy efficiency goals.
- Reduction of Energy-Related Risks: Energy efficiency measures provide safer working conditions for personnel.
- Awareness Training: Awareness training makes employees more conscious about energy saving and increases job performance. This also contributes to strengthening corporate identity.
- Tracking Innovations: Tracking innovations that emerge in the process of improving energy performance increases the competitive advantage of the institution.

In the installation of the Energy Management System, getting an effective result is associated with the healthy operation of managerial and strategic structuring as well as technical structuring. In this context, the necessary steps for establishing EnMS (Figure 11):"

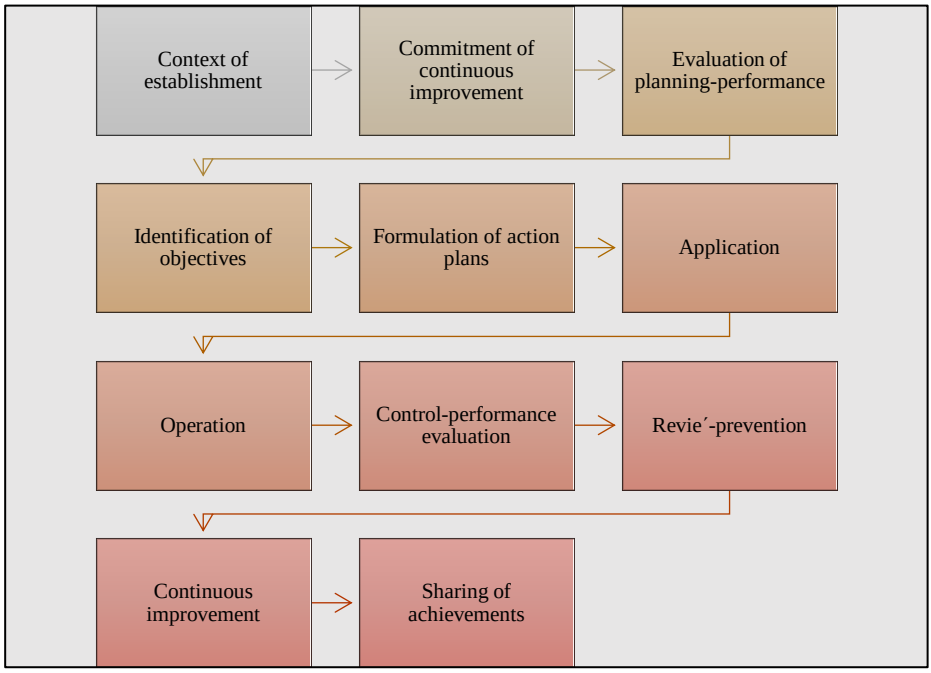

Figure 11: Stages of EnMS Installation (Republic of Türkiye Ministry of Environment Urbanization and Climate Change, 2020)

The planning of the process consists of performance evaluation, setting goals, and creating action plans. In performance evaluation, the energy use analysis of the facility is made and efficiency opportunities are determined with the values taken as a basis for improvements in energy performance. In this context, data/consumption collection and monitoring, creation of Energy Reference Line, determination of Energy Performance Indicators, and analysis of energy use should be carried out.

A criterion pool should be created for determining performance indicators by comparing the reports of the World Bank, International Energy Agency, Ministry of Energy and Natural Resources, Ministry of Environment and Urbanization, and sector reports. The performance criteria included in the relevant reports as a result of detailed studies conducted by these institutions/organizations, which are considered authorities in studies on energy efficiency worldwide, should be matched considering qualities such as building type and characteristics, climatic characteristics of the working area, availability of monitoring and evaluation, and final performance indicators

should be created. It should be possible to monitor and update throughout the entire life cycle of the process.

1.6 Determining Building User Behaviors

It is considered important that studies aimed at reducing energy consumption in buildings and the transition to nZEB do not compromise comfort in buildings. Therefore, within the scope of the research, it is necessary to know the building user behaviors first and to consider them in the process in order to transition to nZEB in existing public buildings (Attia et al., 2017; Rinaldi et al., 2018; Yousefi et al., 2017).

In the renovation of existing public buildings, the durability, safety, indoor quality, and regulatory requirements of the building should be met first. While ensuring good indoor quality in buildings, it is aimed that buildings consume as little energy as possible and have low CO2 emissions. To reach these goals, the current energy consumptions of the buildings should be analyzed, and comfort elements that are currently lacking for the parts to be included in the renovation should be determined along with energy performance and/or energy efficiency targets.

Regarding the determination of user behaviours, it is necessary to determine the characteristics of the building users such as gender, age, duration of building use, heating, cooling, lighting information, as well as the frequency of use of rooms, halls and classrooms, which vary according to building types. An inventory list used in heating, cooling and lighting in buildings should be created, knowing the shape and usage frequencies of these inventory and systems by users allows predicting user behaviors. In addition to this, revealing the problems experienced by users and user requests also contributes to measuring user behaviors in the energy-efficient transformation of existing buildings. There are many studies worldwide where data on user behaviors in buildings are produced with the help of surveys and building inventory lists. After meaningful data is obtained, determining behaviors affecting energy efficiency is defined as a multi-criteria decision-making process.

Studies show that there is a correlation between energy use and building characteristics with user behaviors, and there is a strong relationship between user behaviors and built environment characteristics with building age. In addition to this, ambient temperature on building performance also directly affects performance by increasing fuel consumption due to heating

systems' usage times causing an increase. Studies show that it is possible to renovate existing public buildings as nearly zero-energy buildings and make them energy efficient without reducing comfort facilities for building users and considering them in the process contributes positively. However, it is seen as a gap in the literature that studies on determining user behaviors are not considered as part of the process in buildings to be renovated within nZEB and user details remain superficial.

2. CONCLUSIONS AND RECOMMENDATIONS

It is emphasized that the environmental, technical, economic, social, and legal dimensions of the studies carried out on energy efficiency in buildings should be considered separately. Not evaluating these studies with a holistic approach can lead to a lack of full understanding of energy efficiency and the development of limited solution options. Stakeholders in the energy efficiency sector need to collaborate to ensure that the outputs of the process provide sustainable environmental benefits. This requires a process design that does not harm nature with comfort for users, profitability for contractors, cash flow for financiers, and sustainable and applicable solutions for the administration.

The goals of energy saving and reduction of CO2 emissions require creating a roadmap compatible with national and international objectives. Increasing the energy efficiency of public buildings requires important steps such as interdisciplinary communication, financial support, and adopting international targets.

The environmental and economic benefits of energy efficiency offer the potential to reduce high initial costs. It is important to make these benefits measurable and score environmental, social, and technical factors for the selection of energy-efficient transformation projects to determine the value of energy efficiency projects. In addition, energy-efficient transformation projects should be designed with modern techniques such as the zero-energy building approach.

Also, planning the process, performance evaluation, setting goals, and creating action plans are important. At this stage, an energy use analysis should be performed, energy performance indicators should be determined, and data should be monitored. A criterion pool based on performance criteria of organizations such as the World Bank, International Energy Agency, Ministry of Energy and Natural Resources, Ministry of Environment,

Urbanization and Climate Change should be created, and these criteria should be used for monitoring and updating the process. In this way, energy efficiency in buildings can make a significant contribution to building a sustainable future.

In line with the research title “Clean, Accessible and Secure Energy Supply” within the framework of Green Deal Compliance called the new growth strategy that includes basic goals such as ending net greenhouse gas emissions by 2050 determined by the EU and zeroing dependence on resource use in economic growth; The research conducted should serve sustainable growth with the green transformation of Turkey's economy and industry, one of the objectives of the Green Deal.

REFERENCES

Agliardi, E., Cattani, E., & Ferrante, A. (2018). Deep energy renovation strategies: A real option approach for add-ons in a social housing case study. *Energy and Buildings*, *161*, 1–9. https://doi.org/10.1016/j.enbuild.2017.11.044

Ahmad, T., Chen, H. X., Guo, Y. B., & Wang, J. Y. (2018). A comprehensive overview on the data driven and large scale based approaches for forecasting of building energy demand: A review. *ENERGY AND BUILDINGS*, *165*, 301–320. https://doi.org/10.1016/j.enbuild.2018.01.017

Arambula Lara, R., Pernigotto, G., Cappelletti, F., Romagnoni, P., & Gasparella, A. (2015). Energy audit of schools by means of cluster analysis. *Energy and Buildings*, *95*, 160–171. https://doi.org/10.1016/j.enbuild.2015.03.036

Ascione, F., Bianco, N., De Masi, R. F., Mauro, G. M., & Vanoli, G. P. (2017). Energy retrofit of educational buildings: Transient energy simulations, model calibration and multi-objective optimization towards nearly zero-energy performance. *Energy and Buildings*, *144*, 303–319. https://doi.org/10.1016/j.enbuild.2017.03.056

Attia, S., Eleftheriou, P., Xeni, F., Morlot, R., Ménézo, C., Kostopoulos, V., Betsi, M., Kalaitzoglou, I., Pagliano, L., Cellura, M., Almeida, M., Ferreira, M., Baracu, T., Badescu, V., Crutescu, R., & Hidalgo-Betanzos, J. M. (2017). Overview and future challenges of nearly zero energy buildings (nZEB) design in Southern Europe. *Energy and Buildings*, *155*(2017), 439–458. https://doi.org/10.1016/j.enbuild.2017.09.043

Barringer, H. P., Weber, D. P., & Weber, D. A. (1996). Life Cycle Cost Tutorial. *Fifth International Conference on Process Plant Reliability*.

Brambilla, A., Salvalai, G., Imperadori, M., & Sesana, M. M. (2018). Nearly zero energy building renovation: From energy efficiency to environmental efficiency, a pilot case study. *Energy and Buildings*, *166*, 271–283. https://doi.org/10.1016/j.enbuild.2018.02.002

Camporeale, P. E., & Mercader-Moyano, P. (2021). A GIS-based methodology to increase energy flexibility in building cluster through deep renovation: A neighborhood in Seville. *Energy and Buildings*, *231*, 110573. https://doi.org/10.1016/j.enbuild.2020.110573

Ciancio, V., Salata, F., Falasca, S., Curci, G., Golasi, I., & de Wilde, P. (2020). Energy demands of buildings in the framework of climate change: An investigation across Europe. *Sustainable Cities and Society*, *60*(March), 102213. https://doi.org/10.1016/j.scs.2020.102213

D'Agostino, D., Parker, D., Epifani, I., Crawley, D., & Lawrie, L. (2022). How will future climate impact the design and performance of nearly zero energy buildings (NZEBs)? *Energy*, *240*. https://doi.org/10.1016/j.energy.2021.122479

D'Agostino, D., Tzeiranaki, S. T., Zangheri, P., & Bertoldi, P. (2021). Assessing Nearly Zero Energy Buildings (NZEBs) development in Europe. *Energy Strategy Reviews*, *36*. https://doi.org/10.1016/j.esr.2021.100680

Deming, W. E. (1982). *Out of the Crisis*. Center for Advanced Engineering Study, Massachusetts Institute of Technology.

Di Giuseppe, E., Iannaccone, M., Telloni, M., D'Orazio, M., & Di Perna, C. (2017). Probabilistic life cycle costing of existing buildings retrofit interventions towards nZE target: Methodology and application example. *Energy and Buildings*, *144*, 416–432. https://doi.org/10.1016/j.enbuild.2017.03.055

Economidou, M., & Bertoldi, Paolo. (2014). *Financing building energy renovations : current experiences and ways forward*. European Commission. Joint Research Centre. Institute for the Protection and the Security of the Citizen. https://doi.org/10.2790/28141

Eliopoulou, E., & Mantziou, E. (2017). Architectural Energy Retrofit (AER): An alternative building's deep energy retrofit strategy. *Energy and Buildings*, *150*, 239–252. https://doi.org/10.1016/j.enbuild.2017.05.001

European Commission. (2023, August 21). *2030 climate & energy framework*. Https://Climate.Ec.Europa.Eu/Eu-Action/Climate-Strategies-Targets/2030-Climate-Energy-Framework_en#documentation.

European Environment Agency. (2023, August 21). *term: life cycle assessment*. Https://Www.Eea.Europa.Eu/Help/Glossary/Eea-Glossary/Life-Cycle-Assessment.

Ferreira, M., Almeida, M., & Rodrigues, A. (2017). Impact of co-benefits on the assessment of energy related building renovation with a nearly-

zero energy target. *Energy and Buildings*, *152*, 587–601. https://doi.org/10.1016/j.enbuild.2017.07.066

Fotopoulou, A., Semprini, G., Cattani, E., Schihin, Y., Weyer, J., Gulli, R., & Ferrante, A. (2018). Deep renovation in existing residential buildings through façade additions: A case study in a typical residential building of the 70s. *Energy and Buildings*, *166*, 258–270. https://doi.org/10.1016/j.enbuild.2018.01.056

Global Environmental Social and Governance Benchmark. (2022). *2022 Real Estate Assessment Results*. https://www.gresb.com/nl-en/2022-real-estate-results/

Guardigli, L., Bragadin, M. A., Della Fornace, F., Mazzoli, C., & Prati, D. (2018). Energy retrofit alternatives and cost-optimal analysis for large public housing stocks. *Energy and Buildings*, *166*, 48–59. https://doi.org/10.1016/j.enbuild.2018.02.003

Hamdy, M., Sirén, K., & Attia, S. (2017). Impact of financial assumptions on the cost optimality towards nearly zero energy buildings – A case study. *Energy and Buildings*, *153*, 421–438. https://doi.org/10.1016/j.enbuild.2017.08.018

International Energy Agency. (2020). *World Energy Statistics and Balances*.

International Energy Agency. (2022). *Energy Efficiency 2022*. www.iea.org

International Organization for Standardization. (2006). *Environmental management-Life cycle assessment-Principles and framework (ISO 14040)*. https://www.iso.org/standard/37456.html

Irulegi, O., Ruiz-Pardo, A., Serra, A., Salmerón, J. M., & Vega, R. (2017). Retrofit strategies towards Net Zero Energy Educational Buildings: A case study at the University of the Basque Country. *Energy and Buildings*, *144*(2017), 387–400. https://doi.org/10.1016/j.enbuild.2017.03.030

Jiménez-González, C., Kim, S., & Overcash, M. R. (2000). Methodology for Developing Gate-to-Gate Life Cycle Inventory Information. *The International Journal of Life Cycle Assessment*, *5*(3), 153–159. https://doi.org/10.1065/Ica2000.02.017

Landers, J. P. (1997). *Handbook of capillary electrophoresis* (J. P. Landers, Ed.; Second Edition). CRC Press.

Medved, S., Domjan, S., & Arkar, C. (2021). Contribution of energy storage to the transition from net zero to zero energy buildings. *Energy and Buildings*, *236*. https://doi.org/10.1016/j.enbuild.2021.110751

Momber, I., Gómez, T., Venkataramanan, G., Stadler, M., Beer, S., Lai, J., Marnay, C., & Battaglia, V. (2010). *Plug-in Electric Vehicle Interactions with a Small Office Building: An Economic Analysis using DER-CAM*. IEEE.

Official Journal of the European Union. (2012). *Commission Delegated Regulation No 244/2012 of 16 January 2012 supplementing Directive 2010/31/EU of the European Parliament and of the Council on the energy performance of buildings by establishing a comparative methodology framework for calculating cost-optimal levels of minimum energy performance requirements for buildings and building elements*.

Official Journal of the European Union. (2018). *DIRECTIVE (EU) 2018/844 of the European Parliament and of the Council of 30 May 2018 amending Directive 2010/31/EU on the energy performance of buildings and Directive 2012/27/EU on energy efficiency (Text with EEA relevance)*.

Republic of Türkiye Ministry of Environment Urbanization and Climate Change. (2020). *Kamu Binalarının Enerji Verimli Yenilenmesine Yönelik Rehber*. www.csb.gov.tr

Rinaldi, A., Schweiker, M., & Iannone, F. (2018). On uses of energy in buildings: Extracting influencing factors of occupant behaviour by means of a questionnaire survey. *Energy and Buildings*, *168*, 298–308. https://doi.org/10.1016/j.enbuild.2018.03.045

Rosso, F., Ciancio, V., Dell'Olmo, J., & Salata, F. (2020). Multi-objective optimization of building retrofit in the Mediterranean climate by means of genetic algorithm application. *Energy and Buildings*, *216*, 109945. https://doi.org/10.1016/j.enbuild.2020.109945

Salata, F., Ciancio, V., Dell'Olmo, J., Golasi, I., Palusci, O., & Coppi, M. (2020). Effects of local conditions on the multi-variable and multi-objective energy optimization of residential buildings using genetic algorithms. *Applied Energy*, *260*(August 2019), 114289. https://doi.org/10.1016/j.apenergy.2019.114289

Salvalai, G., Malighetti, L. E., Luchini, L., & Girola, S. (2017). Analysis of different energy conservation strategies on existing school buildings in a Pre-Alpine Region. *Energy and Buildings*, *145*, 92–106. https://doi.org/10.1016/j.enbuild.2017.03.058

Santangelo, A., & Tondelli, S. (2017). Occupant behaviour and building renovation of the social housing stock: Current and future challenges.

Energy and Buildings, *145*, 276–283. https://doi.org/10.1016/j.enbuild.2017.04.019

Semprini, G., Gulli, R., & Ferrante, A. (2017). Deep regeneration vs shallow renovation to achieve nearly Zero Energy in existing buildings: Energy saving and economic impact of design solutions in the housing stock of Bologna. *Energy and Buildings*, *156*, 327–342. https://doi.org/10.1016/j.enbuild.2017.09.044

Shnapp, S., Sitjà, R., & Laustsen, J. (2013). *What is a Deep Renovation Definition?*

Tagliabue, L. C., Di Giuda, G. M., Villa, V., De Angelis, E., & Ciribini, A. L. C. (2018). Techno-economical analysis based on a parametric computational evaluation for decision process on envelope technologies and configurations evaluation for decision process of envelope technologies and configurations. *Energy and Buildings*, *158*, 736–749. https://doi.org/10.1016/j.enbuild.2017.10.004

United Nation Environment Programme. (2022). *2022 Global Status Report for Buildings and Construction: Towards a Zero-emission, Efficient and Resilient Buildings and Construction Sector*. www.globalabc.org.

Wells, L., Rismanchi, B., & Aye, L. (2018). A review of Net Zero Energy Buildings with reflections on the Australian context. *Energy and Buildings*, *158*, 616–628. https://doi.org/10.1016/j.enbuild.2017.10.055

Yang, J. J., Santamouris, M., Lee, S. E., & Deb, C. (2016). Energy performance model development and occupancy number identification of institutional buildings. *ENERGY AND BUILDINGS*, *123*, 192–204. https://doi.org/10.1016/j.enbuild.2015.12.018

Yousefi, F., Gholipour, Y., & Yan, W. (2017). A study of the impact of occupant behaviors on energy performance of building envelopes using occupants' data. *Energy and Buildings*, *148*, 182–198. https://doi.org/10.1016/j.enbuild.2017.04.085

Zangheri, P., D'Agostino, D., Armani, R., & Bertoldi, P. (2022). Review of the Cost-Optimal Methodology Implementation in Member States in Compliance with the Energy Performance of Buildings Directive. *Buildings*, *12*(9). https://doi.org/10.3390/buildings12091482

CHAPTER 2

ADVANCE IN LITHIUM-ION BATTERIES: AN OVERVIEW

Dr. Çağrı ÜN[1]

DOI: https://dx.doi.org/10.5281/zenodo.8428647

”

[1] Davidson School of Chemical Engineering, Purdue University, West Lafayette, IN, USA
un0@purdue.edu. Orcid: 0000-0002-7925-5000

INTRODUCTION

Lithium-ion batteries (LIBs) are becoming inherent in contemporary society, integrated into everything from large-scale solar energy storage setups, hybrid, and electric vehicles, to more compact devices like laptops. They are being extensively utilized for high-powered portable purposes such as power tools, remote-controlled vehicles, lawn mowers, bicycles, and scooters. LIBs have emerged as the predominant energy storage solution, fundamentally transforming industries spanning from handheld electronics to electric cars and large-scale grid energy storage. Various configurations of lithium-ion batteries are vying as energy reservoirs for automotive applications. A variety of LIB types are being presented as energy storage options for the automobile sector.

The relentless march of battery technology progress and the seamless integration of electricity within the automotive domain have ushered in profound transformations within our evolving technological landscape. Today, we find ourselves immersed in a dynamic contest that spans a myriad of battery technologies, each vying for supremacy across an array of applications. In the grand scheme of this contest, victory will be bestowed upon those technologies that establish perfect resonance with the unique demands posed by each application, a harmonic interplay between battery technology/chemistry and the precise prerequisites set forth by the distinct spheres of application (Boukhalfa and Ravichandran, 2019).

At the core of the lithium-ion battery resides an intricate electrochemical arrangement. The functionality of the battery hinges on the reversible introduction and removal of lithium ions into and out of the cathode and anode substances as charge and discharge cycles take place (Goodenough and Park, 2013). Electrolytes, separators, and current collectors play a role in aiding ion movement between the dual electrodes. The effectiveness and comprehensive functionality of LIBs are intricately associated with the electrochemical speed, ionic movement, and durability of these constituents.

1. LIB TYPES AND PROPERTIES

Lithium-ion battery cells available for commercial use can be categorized according to their configuration and external appearance, delineating into cylindrical and prismatic cells. Cylindrical cells are encased in rigid shells, whereas prismatic cells encompass both rigid, rectangular prisms and soft, flexible pouch cells. A closer examination of the

manufacturing procedures for diverse lithium-ion battery cell designs, with a particular emphasis on the efficacy of the production cycle, has illuminated that the constraints of pick-and-place assembly are identified as the central hindrance in automotive manufacturing processes (Schröder et al., 2017). Figure 1 illustrates various cell types that are presently accessible in the market, along with their corresponding module configurations.

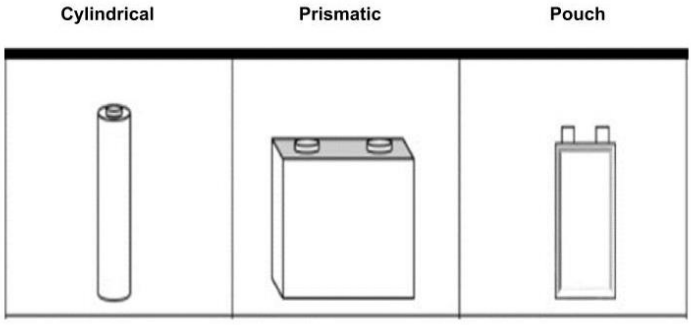

Figure 1. Various LIB Cell Types

A lithium-ion cell is composed of several components, including a cathode, an anode, a separator, and an electrolyte. The cathode and anode materials are coated onto current collectors made of copper and aluminum foil, respectively. The electrolyte serves as a medium for facilitating the movement of lithium ions between these electrodes. Positioned between the anode and cathode, the separator functions to prevent direct contact between the two electrodes, thereby averting short circuits, while still permitting the passage of ions.

In the course of the discharge reaction, lithium ions traverse from the anode and embed themselves into the vacant spaces within layers of cathode crystals—a phenomenon termed "intercalation." Upon recharging, the reverse occurs. Lithium ions migrate from the cathode positioned on the positive side of the battery and incorporate themselves into the anode (Tarascon and Armand, 2001). The components and processes of the lithium-ion battery (LiB) are visually depicted in Figure 2. The fundamental principle of the lithium-ion battery is presented, highlighting the intercalation process of lithium ions (depicted as yellow spheres) into the anode and cathode matrices during the charge and discharge cycles, respectively.

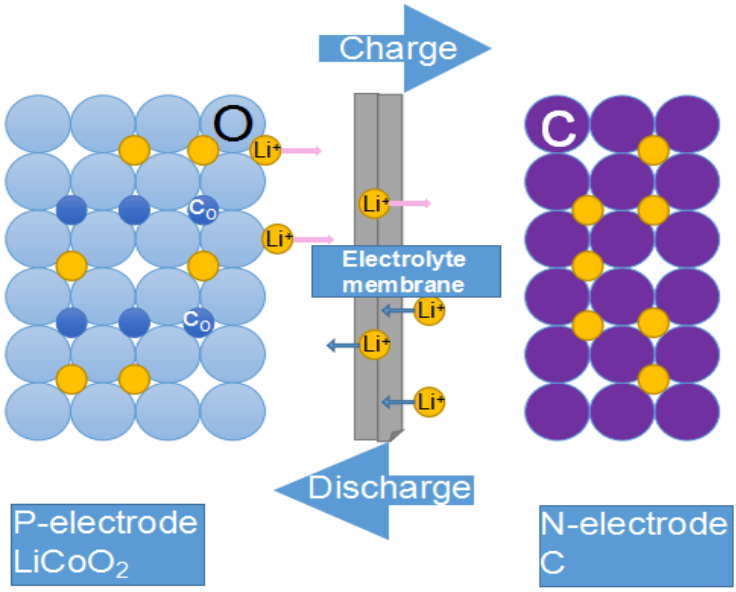

Figure 2. The components and processes of the LiB (URL-2)

The distinctive attributes of LiBs harnessed in the trials conducted as part of this study are elucidated below:

- ***Lithium Cobalt Oxide (LCO or $LiCoO_2$):*** LCO, a chemical compound, assumes a pivotal role as the positive electrode material in lithium-ion batteries. The performance of $LiCoO_2$ in battery applications hinges on the dimensions of its particles, prompting research and fabrication of particles spanning a spectrum from nanometer to micrometer scales. It's imperative to heed the C-rating when charging or discharging Li-cobalt. For instance, consider an 18650 cell endowed with a 2,400 mAh capacity, which should undergo charging and discharging at a rate no higher than 2,400 mA.
- ***Lithium Iron Phosphate (LFP or $LiFePO_4$):*** LFP, an inorganic compound available in various shades of gray, brown, red, or black in solid form, remains impervious to water solubility. LFP batteries operate at 3.3 V, boasting a charge density of 170 mAh/g. Noteworthy for its extended cycle life and resilience to elevated temperatures, LFP demonstrates robust stability.
- ***Lithium Nickel Cobalt Aluminum Oxide (NCA or***

$LiNiCoAlO_2$): NCA shares an affinity with nickel manganese cobalt oxide (NMC), renowned for its lofty specific energy and impressive longevity. NCA represents a notable stride forward from lithium nickel oxide.

- ***Lithium Nickel Manganese Cobalt Oxide ($LiNiMnCoO_2$ or NMC):*** NMC, a standout contender in the realm of Li-ion systems, harmoniously amalgamates a cathode triad encompassing nickel, manganese, and cobalt. In its formulation, NMC incorporates lithium nickel manganese cobalt oxide as the cathode counterpart and graphite as the anode. NMC's specific energy density spans the spectrum from 150 to 220 Wh/kg, while its thermal runaway threshold stands at 210°C (Un and Aydin, 2021).
- ***Lithium Titanate ($Li_4Ti_5O_{12}$ or LTO):*** Li-titanate claims a nominal cell voltage of 2.40 V. Its exceptional feature lies in its rapid charging capability, delivering a discharge current that is a substantial tenfold of its rated capacity. Li-titanate distinguishes itself with commendable discharge characteristics even at lower temperatures and stands out for its exemplary safety profile (URL-3).

Progressions in electrode materials are of paramount importance in augmenting the performance of lithium-ion batteries (LIBs). The trajectory from initial designs featuring graphite and lithium cobalt oxide ($LiCoO_2$) has led to the emergence of advanced cathodes like nickel cobalt manganese (NCM) and nickel cobalt aluminum (NCA), marking significant advancements (Lu et al. 2013). Additionally, the integration of silicon-based anodes into the equation has intensified the pursuit of superior energy densities, extended cycle lifetimes, and expedited charge/discharge rates. This pursuit has catalyzed the creation of innovative materials and composite architectures. This section accentuates the most recent strides in electrode materials, underscoring their profound influence on battery efficiency.

An NMC battery stands out with its remarkable attributes, including an extended cycle life, heightened stability, and a superior energy density when pitted against lithium cobalt oxide (LCO) and lithium iron phosphate (LFP) batteries. Flourishing within a temperature spectrum spanning from -4.4 °C to 70 °C, LFP batteries exhibit an exceptional resilience to temperature

fluctuations, outshining other chemistries in this aspect. LFP batteries also hold a distinct advantage in terms of their reduced susceptibility to thermal runaways, a virtue attributed to their lack of reliance on cobalt. Nonetheless, these benefits are counterbalanced by certain drawbacks, such as a relatively lower energy density and a shorter operational lifespan in comparison to their NMC and NCA counterparts. Lithium iron nano phosphate (LiFePO4) batteries find their niche in a multitude of applications, including electric and hybrid vehicles, as well as renewable energy generation.

LCO batteries lay claim to a significant current capacity and an extended calendar lifespan. Beyond these attributes, they offer an elevated energy density and an increased level of safety when juxtaposed with NMC batteries. LCO batteries function at heightened voltage levels compared to LFP batteries. Notably, the thermal runaway threshold for LCO stands at 250 °C, a mark that stands relatively higher in comparison to NMC and NCA batteries, thus bolstering their safety profile. However, LMO batteries are marked by a notably abbreviated lifespan, spanning a range of 300 to 700 cycles. Furthermore, their rapid charging characteristics can potentially trigger thermal runaway, while their performance deteriorates precipitously at elevated temperatures (Boukhalfa and Ravichandran, 2019).

Figure 3 shows the different various graph representation of LIB's.

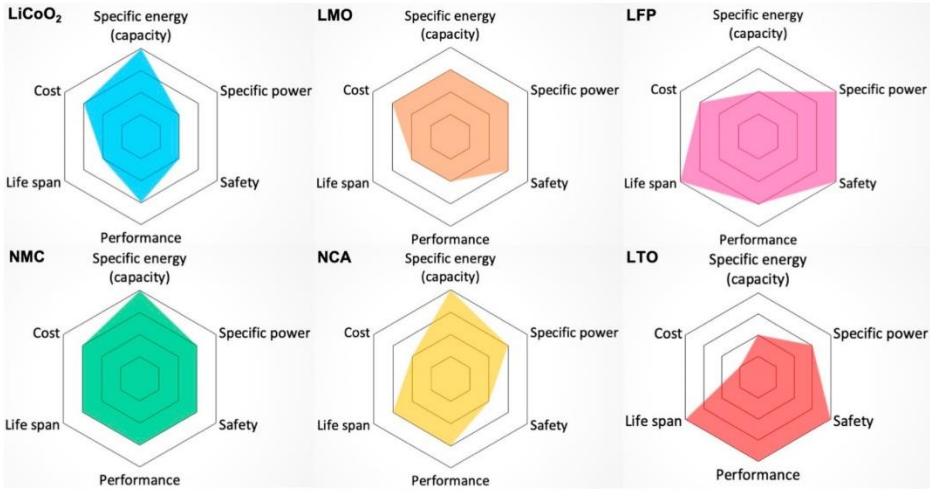

Figure 3. The comparison plots of LIB's

2. LIB MARKET

The demand for automotive LIBs experienced a substantial rise of approximately 65% to reach 550 GWh in 2022, up from about 330 GWh in 2021. This growth was predominantly spurred by the expansion in sales of electric passenger cars, which saw new registrations surge by 55% in 2022 compared to the previous year. In China, the demand for batteries used in vehicles witnessed an impressive increase of over 70%, coupled with an 80% rise in electric car sales during 2022 when contrasted with 2021. However, the growth in battery demand was slightly moderated by a growing proportion of Plug-in Hybrid Electric Vehicles (PHEVs). Conversely, battery demand for vehicles in the United States surged by approximately 80%, despite electric car sales experiencing a more moderate uptick of around 55% in 2022. Although the average battery size for battery electric cars in the United States expanded by roughly 7% throughout 2022, this average size continues to remain about 40% higher than the global average. This can be attributed in part to the greater prevalence of SUVs in the U.S. electric car market compared to other major markets. Additionally, manufacturers' strategic moves to offer extended all-electric driving ranges also contribute to this phenomenon. Notably, global sales of Battery Electric Vehicles (BEVs) and Plug-in Hybrid Electric Vehicles (PHEVs) are surpassing the sales of Hybrid Electric Vehicles (HEVs). Given that BEV and PHEV battery sizes tend to be larger, this trend further propels the demand for batteries (IEA, 2023).

As of 2022, lithium nickel manganese cobalt oxide (NMC) has successfully maintained its dominant position as the primary battery chemistry, boasting a commanding market share of 60%. Trailing behind is lithium iron phosphate (LFP), capturing a market share just below 30%, while nickel cobalt aluminum oxide (NCA) occupies a relatively modest share of approximately 8%. A noteworthy trend in the battery landscape is the ascendancy of lithium iron phosphate (LFP) cathode compositions, marking their highest market share in the past decade. This surge can be largely attributed to the preferences of Chinese Original Equipment Manufacturers (OEMs). Impressively, a substantial 95% of LFP batteries found their home in electric Light Duty Vehicles (LDVs) manufactured in China. Notably, BYD has taken the lead in this demand, accounting for an impressive 50%, with Tesla contributing 15%. Interestingly, Tesla's adoption of LFP batteries surged from 20% in 2021 to an impressive 30% in 2022. Among the vehicles featuring LFP batteries by Tesla, a substantial 85% were manufactured in

China, while the remainder were produced in the United States using cells imported from China. On the contrary, the United States only produced approximately 3% of electric vehicles incorporating LFP batteries in 2022 that rely on nickel, manganese, and cobalt, such as NCA and NMC batteries. However, LFP batteries are met with the challenge of lower energy density in comparison to NMC batteries. Additionally, LFP batteries contain phosphorus, an essential element in food production.

If LFP batteries were to dominate the battery landscape, their mass use could account for nearly 1% of the current agricultural phosphorus demand, signaling a potential clash between battery requirements and agricultural needs.

In recent years, alternatives to traditional Li-ion batteries have emerged, and sodium-ion (Na-ion) batteries stand as a prominent example. This chemistry boasts a distinct advantage: it leverages more cost-effective materials, thereby enabling the production of economical batteries. Furthermore, Na-ion batteries entirely circumvent the necessity for critical minerals, setting them apart as the only feasible chemistry devoid of lithium. A significant stride in this direction is China's CATL, which has developed a Na-ion battery projected to cost 30% less than an LFP battery. However, Na-ion batteries fall short of the energy density offered by Li-ion counterparts, presenting 75 to 160 Wh/kg compared to 120 to 260 Wh/kg. This distinctive feature positions Na-ion batteries as promising candidates for urban vehicles with shorter ranges or stationary storage, but their viability might be challenged in regions prioritizing extended range autonomy or facing limitations in charging infrastructure. Notably, China is at the forefront of Na-ion battery production, boasting nearly 30 operational, planned, or under-construction manufacturing plants with a combined capacity exceeding 100 GWh. To provide context, the current manufacturing capacity of Li-ion batteries stands at approximately 1,500 GWh. Several automakers have already unveiled plans for Na-ion electric vehicles. For instance, BYD's Seagull offers an impressive range of 300 km, accompanied by a price tag of USD 11,600 (with the possibility of discounts that could potentially bring the price down to $9,500). Another notable entrant is the Sehol EX10, a product of the VW-JAC collaboration, boasting a range of 250 km. While these initial models might slightly exceed the cost of the most affordable small Battery Electric Vehicle (BEV) models in China, such as the Wuling Mini BEV available for a modest USD 5,000 to 6,500. They still maintain a cost

advantage over analogous options with comparable driving ranges. For context, the Wuling Mini BEV provides a range of 170 km, while BYD's Dolphin BEV, the second-best-selling small BEV in China in 2022, with a similar range to the announced Na-ion cars, can command a price exceeding USD 15,000. Notably, BYD is strategically poised to progressively integrate Na-ion batteries into all models priced below USD 29,000 as battery production scales up. These promising announcements hint at the imminent availability and operation of Na-ion-powered electric vehicles between 2023 and 2024, symbolizing the attainment of a Technological Readiness Level (TRL) of 8-9, signifying preparedness for commercial application. This transition is particularly remarkable considering its prior TRL 6 (full-scale prototype) assessment in the IEA Clean Technology Guide in 2022, underscoring the swift pace of technological evolution (IEA, 2023).

The global hunger for batteries is poised to undergo a seismic shift, surging from a modest 185 GWh in 2020 to a staggering projection that eclipses 2,000 GWh by the year 2030. While the landscape of 2020 was dominated by the prevalence of consumer electronics, the relatively restrained energy capacities exhibited by devices like phones naturally resulted in a corresponding demand that was less formidable in the gigawatt scale. However, the crux of this remarkable escalation is intricately tied to the sweeping electrification of the transportation sector, a phenomenon that is set to define the lion's share of battery requisites come 2030, manifesting in a palpable surge in overall energy storage capacity.

This palpable wave of change has reverberated across the global stage, with numerous nations bearing witness to a resounding uptick in electric vehicle sales. At the vanguard of this transformative movement stands China, an exemplar of electric vehicle adoption, having already triumphantly recorded the sale of over 430,000 units in the inaugural half of 2019 alone. China's ascendancy in this arena is not ephemeral; it is rooted in a grander vision that envisages the deployment of approximately 532,000 electric buses within the realm of public transportation by the year 2022.

A chorus of nations, resolute in their commitment to adopting more ecologically sound lifestyles, is coalescing around a transformative aspiration—the widescale embrace of electric vehicles. This movement, at the intersection of mobility and sustainability, is poised to yield a profound ripple effect, potentially signaling a momentous reduction in the consumption of gasoline within the automotive domain. In the wake of this astounding

momentum achieved by the burgeoning e-mobility technologies, the global demand for batteries stands on the precipice of substantial expansion, a transformation poised to carve the contours of our energy future. Figure 4 shows the global battery demand forecast from 2020 to 2030

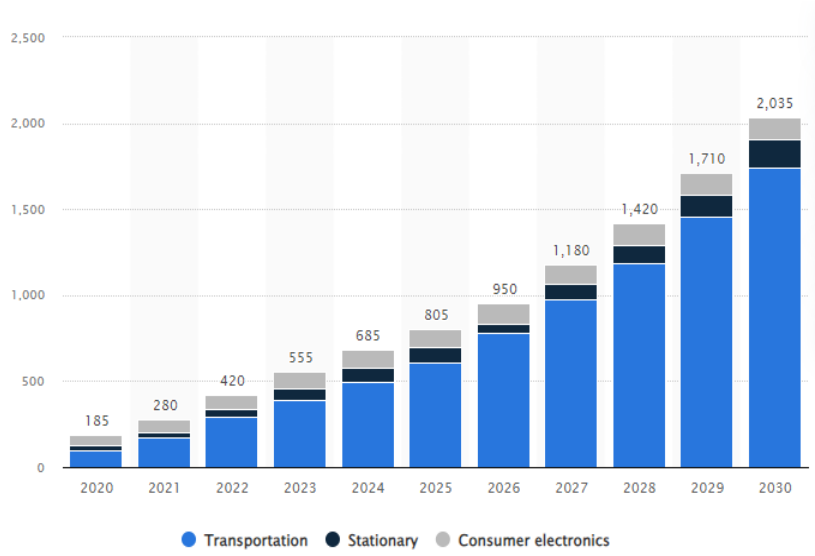

Figure 4. Global Battery Demand Forecast (URL-1)

3. ENERGY EFFICIENCY OF LIB's

Lithium-ion batteries are widely used energy storage devices that have become essential in various applications such as consumer electronics, electric vehicles (EVs), and renewable energy systems. Energy efficiency is an important aspect of these batteries, as it affects their overall performance and contributes to their economic and environmental viability.

Here's some information on lithium-ion battery energy efficiency:

- *Coulombic Efficiency:* Coulombic efficiency refers to the ratio of the actual amount of charge stored in the battery during discharge to the theoretical amount of charge that should have been stored based on the charge applied during charging. It represents the efficiency of the electrochemical reactions within the battery. Generally, lithium-ion batteries have high coulombic efficiencies, often exceeding 95% or more.

- *Round-Trip Efficiency:* Round-trip efficiency is a broader measure of battery energy efficiency, taking into account both charging and discharging losses. It considers not only the electrochemical losses within the battery but also factors like thermal losses during charging and discharging. Round-trip efficiency typically ranges from 80% to 90% for most commercial lithium-ion batteries.
- *Peukert's Law:* This law states that the capacity of a battery decreases as the discharge rate increases. This means that at higher discharge rates, the usable capacity of the battery is reduced, leading to lower energy efficiency. Manufacturers often provide discharge rate-dependent efficiency curves to help users understand the battery's performance under different loads.
- *Temperature Dependence:* Lithium-ion battery efficiency is influenced by temperature. Operating the battery at extreme temperatures (either very high or very low) can reduce its efficiency. Charging at high temperatures can lead to capacity loss, while low temperatures can increase internal resistance, reducing the available capacity and overall efficiency.
- Over the course of multiple charge-discharge cycles, lithium-ion batteries might experience capacity fade due to electrode degradation, solid electrolyte interphase (SEI) formation, and other factors. This can lead to a decrease in energy efficiency as the battery ages.
- *State of Charge (SoC) Range:* The efficiency of a lithium-ion battery can also vary depending on the state of charge. Operating the battery within certain optimal SoC ranges can improve its efficiency. Discharging a battery too deeply or charging it to extremely high levels can lead to reduced efficiency.
- *Energy-Dense vs. Power-Dense Designs:* Lithium-ion batteries can be designed for either high energy density (more energy storage) or high power density (rapid energy release). The efficiency might vary between these two design types due to differences in electrode materials and internal structure.

- *Improvements in Battery Chemistry:* Research and development efforts are ongoing to improve lithium-ion battery energy efficiency. This includes developing advanced electrode materials, optimizing manufacturing processes, and enhancing the overall design to minimize losses.
- *Application-Specific Considerations:* Energy efficiency requirements can vary depending on the application. For example, in EVs, high energy efficiency is crucial to maximize driving range, while in renewable energy storage, efficiency might influence the economics of storing and retrieving energy.
- *Battery Management Systems (BMS):* Effective battery management systems play a significant role in optimizing the performance and efficiency of lithium-ion batteries. BMS monitors battery health, state of charge, temperature, and other parameters to ensure safe and efficient operation.

It's important to note that while lithium-ion batteries are generally efficient, actual efficiency can vary based on factors such as battery chemistry, design, usage patterns, and operating conditions. Manufacturers often provide efficiency specifications for their specific battery models, so it's recommended to refer to those specifications for more accurate information. These efficiency values are approximations and can vary based on the exact battery chemistry, design, and operating conditions. Additionally, advancements in technology and manufacturing can lead to improvements in efficiency over time (URL-4). Table 1. shows the efficiency factors and ranges in lithium-ion battery performance.

Table 1. Efficiency Factors and Ranges in Lithium-Ion Battery Performance

Aspect	Efficiency Range	Assumptions and Notes
Coulombic Efficiency	95% - 99%	High efficiency due to controlled electrochemical reactions.
Round-Trip Efficiency	80% - 90%	Includes charging, discharging, and thermal losses.
Peukert's Law Efficiency	70% - 95%	Efficiency decreases at higher discharge rates due to internal resistance. Assumes discharge rates from C/5 to 2C.
Temperature Dependence	70% - 95%	Efficiency decreases at extreme temperatures (below -10°C or above 40°C). Assumes standard operating range between 0°C and 35°C.
Cycle Efficiency	90% - 98%	Efficiency might degrade by a few percentage points over 500 cycles. Assumes a typical lithium-ion battery chemistry.
Energy-Dense Design	95% - 98%	Slightly higher efficiency due to optimized electrode materials for energy density.
Power-Dense Design	80% - 90%	Slightly lower efficiency due to higher discharge rates for power density.
Application-Specific	Variable	Efficiency varies based on specific application (EVs, consumer electronics, renewable energy storage).
Battery Management System	95% - 99%	An efficient BMS can optimize charging and discharging, contributing to overall efficiency.

4. ADVANTAGES AND DISADVANTAGES OF LITHIUM-ION BATTERIES

Exploring the advantages and disadvantages of lithium-ion batteries is essential to understanding their role in modern energy storage solutions. These power-packed batteries have revolutionized various industries, yet they also come with their own set of challenges.

4.1. Advantages of Lithium-ion Batteries

- *High Voltage:* Single-cell operating voltage is notably high, ranging around 3.7-3.8V (3.2V for lithium iron phosphate). This voltage is three times that of Ni-Cd and Ni-MH batteries.
- *Large Specific Energy:* Actual specific energy is approximately 555 Wh/kg, yielding a specific capacity of over 150 mAh/g. This is 3-4 times greater than Ni-Cd and 2-3 times greater than Ni-MH, approaching 88% of its theoretical value.
- Lithium-ion batteries generally endure more than 500 charge cycles, and even surpass 1000 in some cases. Lithium iron phosphate variants can exceed 2000 cycles.
- *Small Self-Discharge:* At room temperature, a fully charged Li-ion battery retains a self-discharge rate of about 2% after one month, substantially lower than Ni-Cd (25-30%) and Ni-MH (30-35%).
- *Fast Charge:* A battery charged at a 1C rate can achieve over 80% of its nominal capacity in just 30 minutes. Lithium iron phosphate batteries can reach 90% capacity within 10 minutes.
- *Wide Working Temperature Range:* Li-ion batteries are functional within a temperature range of -25 to 45 °C, with potential to extend to -40 to 70 °C with improvements in electrolyte and cathode technology.

4.2. Disadvantages of Lithium-ion Batteries:

- *Aging:* Lithium-ion battery capacity diminishes over time, depending on usage frequency and temperature. High temperatures can expedite this decline, particularly noticeable in products with high operational currents.
- *Vulnerability to Overcharge:* Overcharging leads to irreversible

embedding of excess lithium ions in the lattice, resulting in a compromised battery life.

- *Sensitivity to Over Discharge:* Over discharge triggers excessive removal of lithium ions from the electrode, causing structural damage to the lattice and reducing battery longevity.
- *Safety Concerns:* The use of organic electrolytes in lithium-ion batteries can lead to safety hazards like overheating, fires, or even explosions (URL-2).

5. ENVIRONMENTAL BACKGROUND OF LITHIUM-ION BATTERIES:

Lithium-ion batteries consistently allure us with their unforeseen attributes and applications. As we embrace these unexpected revelations, they challenge preconceived limitations, igniting inventive resolutions for our energy landscape. However, it's essential to recognize that the life cycle of lithium-ion batteries, spanning production, utilization, and disposal phases, bears significant environmental consequences. The extraction of crucial raw materials, particularly lithium and cobalt, can trigger habitat disturbance and water pollution, highlighting the intricacies involved in ensuring their sustainability (Gruber et al., 2011). Furthermore, the energy-intensive nature of the manufacturing process adds to carbon emissions and exacerbates resource depletion. In this context, this section delves into the comprehensive life cycle assessment of lithium-ion batteries (LIBs), encompassing aspects like their carbon footprint, the viability of material recovery, and the prospects for efficient recycling.

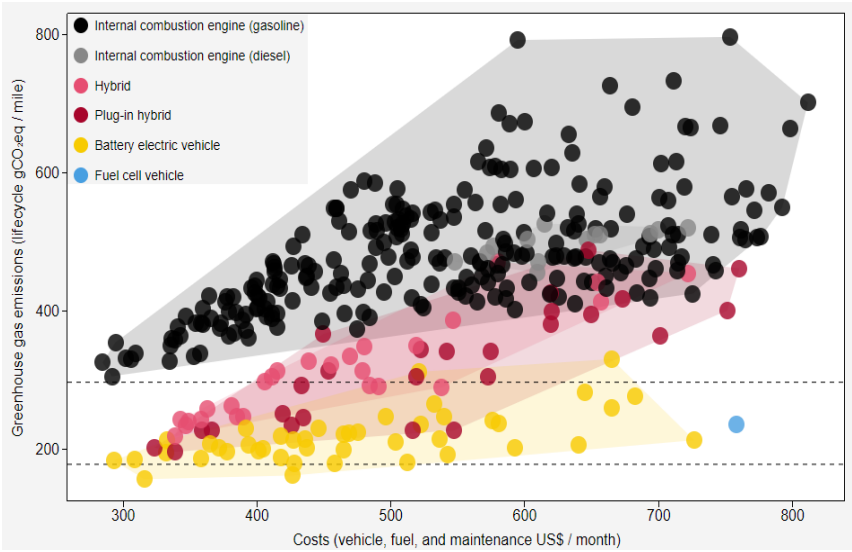

Figure 5. Vehicles Evaluated Against Climate Targets (URL-5)

Lithium-ion batteries stand as a pivotal foundation for achieving a fossil fuel-free economy, witnessing exponential growth in applications such as electric vehicles and stationary energy storage. This expansion can be attributed to technological strides and notable price drops. While their adoption in electric vehicles and stationary storage systems has undeniably curbed greenhouse gas emissions by replacing internal combustion engines, their optimal contribution to a fossil fuel-free economy hinges on recharging them exclusively with renewable energy sources. Policies designed to promote the adoption of lithium-ion batteries while upholding environmental considerations should encompass incentives throughout the battery value chain, encompassing closed-loop recycling systems. In the quest to counteract climate change and cultivate a fossil fuel-free economy, the global consensus is to promptly and substantially curtail greenhouse gas emissions. The Paris Agreement, for instance, lays out an ambitious plan to reduce global emissions. Human activities have been responsible for releasing approximately 50 billion tons of greenhouse gases (GHGs) in terms of CO_2 equivalent on a global scale each year since the mid-2010s. The electricity and heat sector assume the foremost role as the principal emitter, followed by the transport, manufacturing, and agricultural sectors. In this context, Li-ion batteries emerge as a promising and eco-friendly technology, poised to supplant conventional fossil-fuel powered devices. Notably, batteries have assumed exceptional significance in the two sectors primarily accountable for

GHG emissions; electricity generation and transportation.

Particular significance is the interplay between these sectors, wherein advancements in one sector yield synergistic improvements in the other, establishing a virtuous cycle characterized by decreased costs, heightened production, and escalated demand. In the realm of electricity generation, the cost-effectiveness of LIBs facilitates the integration of greater renewable energy capacity through solar and wind sources into power grids. An acknowledged drawback of solar and wind energy is their inherent variability in power generation. Solar energy is dependent on sunlight availability, while wind energy relies on consistent wind patterns. To address these fluctuations, batteries store surplus energy during periods of high generation and distribute stored energy during times of deficiency.

Furthermore, the substantial energy storage capacity of batteries enables a reduction in the maximum capacity requisite for power plants. This diminishes associated construction expenses, a significant factor given that power plants are designed to accommodate peak demands, such as during exceptionally hot summer days when air conditioning usage surges (Kawamura et al., 2021).

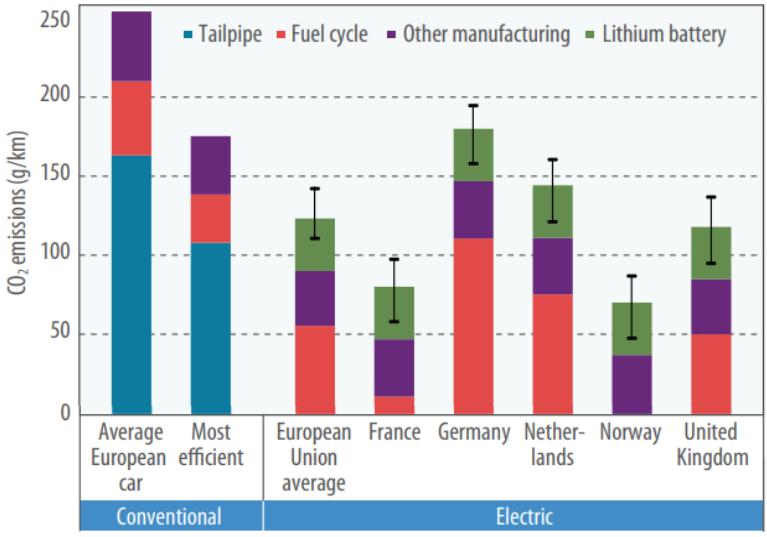

Figure 6. Comparison of lifecycle carbon dioxide emissions in traditional, electrified, and plug-in hybrid automobiles across diverse European regions (Hall and Lutsey, 2018)

6. CONCLUSIONS

The quest for advanced LIBs is a journey fraught with challenges that beckon innovative solutions. Among these hurdles, the specter of capacity degradation, constrained lifespan, and the looming scarcity of crucial resources stand out, demanding inventive strategies to steer the technology forward. In response to these challenges, the horizon shines with promising avenues. One such path entails the evolution of solid-state electrolytes, offering the tantalizing prospect of enhanced performance and safety. Complementing this trajectory are the strides made in smart battery management systems, which promise to optimize energy usage, enhance longevity, and streamline charging patterns. Moreover, addressing the pressing need for sustainable practices, the development of sophisticated recycling technologies paves the way for responsible disposal and resource recovery.

As researchers and engineers navigate these challenges, they also delve into the realm of alternative electrode materials and groundbreaking designs. Notably, the realm of lithium-sulfur and lithium-air batteries emerge as a realm of untapped potential, where creative material innovations hold the key to overcoming the current limitations faced by traditional LIBs.

In the larger context, the role of lithium-ion batteries transcends mere technological advancement. LIBs have played a pivotal role in catalyzing a paradigm shift in energy storage and utilization, facilitating a seamless transition towards a more ecologically balanced and electrified future. Yet, as the march towards sustainability continues, driven by the crescendo of demand for energy storage solutions that are both high-performing and environmentally conscious, the imperative of ongoing research and development in LIB technology becomes even more pronounced. This overview offers an all-encompassing overview of the contemporary landscape, carefully delineating the challenges encountered and illuminating potential avenues for innovation in lithium-ion batteries. It serves as a resounding testament to their essential role in shaping the intricate tapestry of the energy landscape that awaits in the days ahead.

REFERENCES

Boukhalfa, S., Ravichandran, K. (2019). State of the electric vehicle lithium-ion battery market report, PreScouter Publications.

Goodenough, J.B., Park, K.S. (2013). The Li-ion rechargeable battery: A perspective. Journal of the American Chemical Society, 135(4), pp. 1167-1176.

Gruber, P.W., Medina, P.A., Keoleian, G.A., Kesler, S.E., Everson, M.P., Wallington, T.J., Nassar, N.T. (2011). Global lithium availability: A constraint for electric vehicles. Journal of Industrial Ecology, 15(5), pp.760-775.

Hall, D., Lutsey, N. (2018). Effects of battery manufacturing on electric vehicle life-cycle greenhouse gas emissions, International Council on Clean Transportation Publications.

International Energy Agency (IEA), Global Electric Vehicle Outlook, 2023

Kawamura, H., Lafleur, M., Iversen, K., Cheng, H.W.J. (2021). Lithium-Ion Batteries: A Pillar For A Fossil Fuel-Free Economy, Frontier Technology Issues, United Nations.

Lu, L., Han, X., Li, J., Hua, J., Ouyang, M. (2013). A review on the key issues for lithium-ion battery management in electric vehicles. Journal of Power Sources, 226, pp.272-288.

Miao, Y., Hynan, P., Von Jouanne, A., Yokochi, A. (2019). Current Li-Ion Battery Technologies in Electric Vehicles and Opportunities for Advancements. Energies, 12, 1074.

Schröder, R., Aydemir, M., Seliger, G. (2017). Comparatively assessing different shapes of lithium-ion battery cells, Procedia Manufacturing Journal, 8, pp. 104-111.

Tarascon, J.M., Armand, M. (2001). Issues and challenges facing rechargeable lithium batteries, Nature. 414, pp. 359–367.

Un, C., Aydin, K. (2021). Thermal Runaway and Fire Suppression Applications for Different Types of Lithium Ion Batteries, Vehicles, 3, pp. 480-497.

URL-1: https://www.statista.com/statistics/1103218/global-battery-demand-forecast/

URL-2: https://insightsolutionsglobal.com/how-does-a-lithium-ion-battery-work/

URL-3:https://www.techsciresearch.com/blog/manufacturing-lithium-ion-batteries/29.html (accessed February 14, 2021).

URL-4:https://batteryuniversity.com/article/bu-1003a-battery-aging-in-an-electric-vehicle-ev
URL-5: https://www.carboncounter.com/#!/explore

CHAPTER 3

FUEL INJECTION STRATEGIES TO IMPROVE AFTER-TREATMENT THERMAL MANAGEMENT IN DIESEL ENGINE SYSTEMS: A REVIEW

Assist. Prof. Hasan Üstün BAŞARAN[1]

DOI: https://dx.doi.org/10.5281/zenodo.8428506

[1] Izmir Katip Celebi University, Faculty of Naval Architecture and Maritime, Naval Architecture and Marine Engineering Department, Izmir, TURKEY. hustun.basaran@ikcu.edu.tr, 0000-0002-1491-0465.

INTRODUCTION

Today, modern heavy-duty (HD) vehicles are dominantly driven via use of diesel engines. The reason behind this widespread use is mostly due to high thermal efficiency, improved fuel economy, and reliability of compression-ignition (CI) engines. Customers may prefer gasoline-fueled cars for their private vehicles due to the low cost. However, when it comes to commercial use, particularly mass transportation of goods and people, diesel engines are the leading driving force. Many serious analyses project that this prevailing force is unlikely to go through a significant change at least for several decades to come [Kalghatgi (2018), Lešnik et al. (2020)]. A total replacement of current technology with electric vehicles is not seen to be achieved before overcoming the high cost, inadequate infrastructure, and too long battery charging time, which are significant and technically difficult setbacks for fully electric transportation [Ajanovic & Haas (2018)]. Instead of electric vehicles, hybrid vehicles are expected to be more favorable for the not too distant future, as they do not depend on battery power alone for operation. However, those vehicles partially use internal combustion engines and thus, need the improvement of diesel engines for next generation reliable transportation [Reitz et al. (2020)]. Therefore, the search for improved, more efficient diesel engines should continue in order to secure future transportation.

One significant and continuing development for diesel engine is to improve its environmentally unfriendly emission rates [Joshi (2022)]. Although the thermal efficiency is enhanced up to 50% in some engines, the unhealthy nitrogen oxide (NOx) and the cancer-causing particulate matter (PM) are current and will probably be future paramount concerns for diesel engines to keep its leading role in transportation [Conway et al. (2021)]. Since this problem directly concerns human health, environmental organizations immediately issue some strict regulations on diesel emission rates. One reputable environmental body, European Union (EU), is highly determined to limit tailpipe harmful emission rates. Table 1 demonstrates the evolution of stringent emission rates for HD diesel engines due to EU [Dieselnet, EU standards (2023)]. It also shows how much EU is decisive to keep emission rates as low as possible.

Table 1: EU emission standards for heavy-duty CI (diesel) engines: Steady-state testing [Dieselnet, EU standards (2023)]

Stage	Date	Test	CO	HC	NOx	PM	PN	Smoke
			g/kWh				1/kWh	1/m
Euro I	1992, ≤ 85 kW	ECE R-49	4.5	1.1	8.0	0.612		
	1992, > 85 kW		4.5	1.1	8.0	0.36		
Euro II	1996.10		4.0	1.1	7.0	0.25		
	1998.10		4.0	1.1	7.0	0.15		
Euro III	*1999.10 EEV only*	ESC & ELR	*1.5*	*0.25*	*2.0*	*0.02*		*0.15*
	2000.10		2.1	0.66	5.0	0.10[a]		0.8
Euro IV	2005.10		1.5	0.46	3.5	0.02		0.5
Euro V	2008.10		1.5	0.46	2.0	0.02		0.5
Euro VI	2013.01	WHSC	1.5	0.13	0.40	0.01	8.0×10^{11}	

[a] PM = 0.13 g/kWh for engines < 0.75 dm^3 swept volume per cylinder and a rated power speed > 3000 min^{-1}

It stands out in Table 1 that the restrictions for all emission rates become tighter and tighter since 1992. While the limits for NOx and PM in 1992 are 8.0 and 0.612 g/kWh, respectively, current Euro VI regulation issued in 2013 states that NOx should remain below 0.40 g/kWh and PM cannot exceed 0.01 g/kWh. Those numbers are noticeably low compared to the initial standards and thus, are technically very difficult to overcome. Also, a possible more stringent Euro VII regulation, which is likely considering the previous 6 regulations, can be even a greater threat for HD diesel engines.

Faced with the all-time-low emission limits in Table 1, both diesel manufacturers and academicians are in an ongoing search for innovative techniques to reduce diesel emission rates [Fayyazbakhsh et al. (2022)]. One effective method to improve emission rates is to maintain low temperature combustion (LTC) [Imtenan et al. (2014)]. Since emission rates such as NOx and PM are more or less related to in-cylinder temperature, techniques such as RCCI, HCCI and PCCI are experimentally shown to provide LTC and thus, minimized NOx & PM rates [Agarwal et al. (2017)]. Another widely utilized approach is to provide exhaust gas recirculation (EGR) during the operation. A positive effect of EGR on the reduction of especially NOx rates comes from the fact that it can bring down the in-cylinder temperature through redirected engine-out exhaust gas [Agarwal et al. (2011), Millo et al. (2012)].

In addition to EGR, different types of non-diesel fuels are examined to limit the emission rates. Hydrogen has a significant potential to meet emission regulations for next generation diesel engines [Onorati et al. (2022)]. LNG, dimethyl ether, and methanol are seen as potential promising alternatives for diesel fuel for improved emission rates as well [Chen et al. (2018)]. Apart from non-traditional fuels, there is also a significant trend towards the use of battery as the energy source in vehicles, which can minimize inner-city emission rates [Goyal & Jain (2020)]. However, some studies state that electric vehicles can cause significant CO_2 rise due to battery production and thus, are not that emission-free as most researchers think [Zimakowska-Laskowska & Laskowski (2022)]. Therefore, an overall transition of electric vehicles in highway transportation is not possible before a general consensus on emission rates is determined by producers and researchers.

Those advanced strategies have high potential to diminish emission rates. However, not all cases in vehicles can attain low rates using these techniques alone. Therefore, manufacturers particularly implement an exhaust after-treatment (EAT) unit to fulfill strict emission norms. EAT is mostly put in the system right before the exhaust release. The intention is to clean the engine-out gas before its flow into the environment. The cleaning process, in other words, the reduction of NOx and PM rates at engine-exit flow, is maintained via some particular catalysts placed inside the EAT system [Votsmeier et al. (2009), Martinovic et al. (2021)].

EAT units mostly succeed to decrease harmful contaminants in diesel vehicles. However, producers are faced with a serious drawback while using these units in engine systems. These devices are heavily temperature-dependent and are affected negatively particularly at low catalyst temperatures, as seen in Figure 1 [Li et al. (2021)]. At high temperatures (mainly above 250^oC), catalyst inside the SCR unit is sufficiently warm to keep chemical reactions in a fast and well-performed manner. However, as the temperature remains especially below 200^oC, the SCR system is prone to operate with a poor conversion efficiency. This causes a serious problem for diesel vehicles at low loads since exhaust temperature is highly inadequate (below 200^oC) to achieve high conversion efficiency and reduce NOx rates.

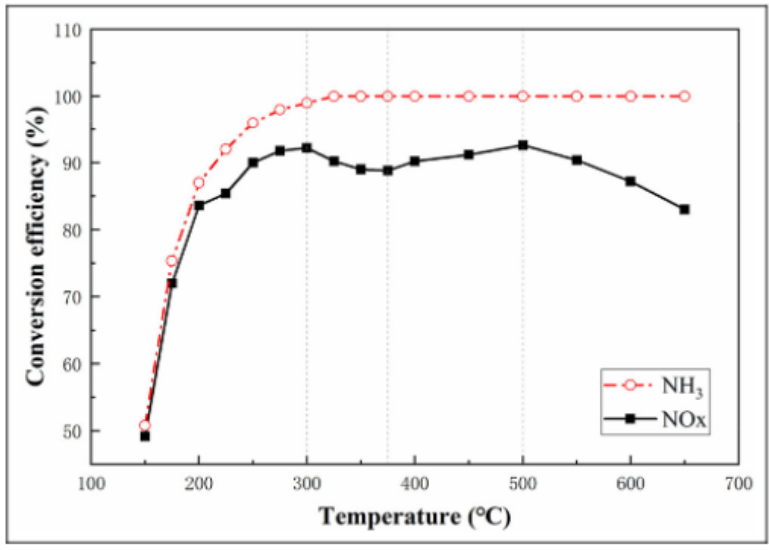

Figure 1: Impact of catalyst temperature on NH_3 and NOx conversion efficiency of a SCR unit [Li et al. (2021)]

Not only does SCR need high temperature (250°C – 450°C) in a conventional EAT system, but also DPF requires temperatures above 500°C to achieve high oxidation efficiency and minimize soot emissions, as seen in Figure 2 [Goldenberg (1983)]. Elevated exhaust temperature can help reduce diesel soot rates via improved DPF unit.

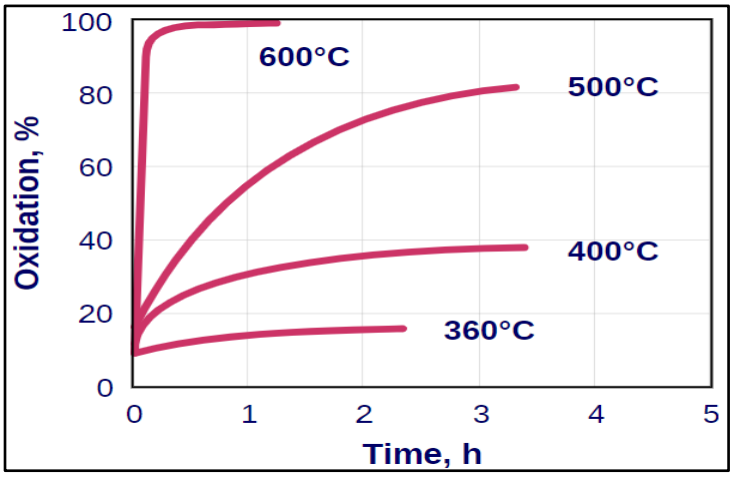

Figure 2: Effect of temperature on soot oxidation of DPF unit [Goldenberg (1983)]

This work concentrates on fuel-based inner-engine methods to improve EAT thermal management in diesel vehicles. The advantage of preferring those strategies is that there is no requirement of any external device to be placed and to be controlled on the engine system while exhaust thermal management (ETM) is improved and EAT is operated effectively. However, those methods also have the disadvantage of degrading combustion and thus, mostly result in fuel inefficiency. In the following part, some general effects of those methods are introduced. After this concise overview, previous works utilizing those techniques to achieve high exhaust temperature are separately explained. Each approach has its own positive and negative impacts on engine performance and thus, one can be more useful than the other depending on the operation condition of a vehicle. In order to overcome the negative effects and achieve low-fuel-penalty operation, those methods can also be combined with airflow-based ETM techniques.

1. AN OVERVIEW OF FUEL-BASED ETM TECHNIQUES

In general, engine-base strategies for enhanced EAT management are classified as air-dependent and fuel-dependent techniques. Airflow-base approaches such as intake throttling, variable valve timing (VVT) [Basaran (2017)], and cylinder deactivation (CDA) are examined extensively in a previous work [Basaran (2023)]. The aim of this work is to explore the fuel-based strategies to improve diesel EAT thermal management. For the following subsections, some general features of those techniques are briefly mentioned. Then in the next section, each technique is explained in a detailed manner.

1.1. Delayed Fuel Injection and Ignition Timing

An easy method to modulate the combustion in diesel engines is to sweep the fuel injection timing later than the nominal timing. The same is valid for gasoline engines as well through delaying the ignition timing. As long as the combustion occurs far from the top dead center (TDC), in-cylinder temperature is kept at high levels through the exhaust phase, and thus, engine-out temperature increases. The method is easy-to-implement in both diesel and gasoline engines as it only needs the reasonable control of injection or ignition timing. It does not need any outer engine component as well. However, modulating the combustion process generally worsens the thermal efficiency. Therefore, delayed injection timing mostly needs extra fuel injection to maintain constant engine load in the system. The technique seems

to be appropriate to use when a relatively low exhaust temperature rise is needed to achieve 250^{o}C or above [Cavina et al. (2013)].

1.2. Close and Late Post-Fuel Injection

In addition to the main injection, fuel can also be injected into the combustion medium as a post-fuel injection (PFI). PFI can be applied as close or late, depending on the injection timing near or far from the main injection process. Close PFI is generally implemented between 20 to 60 degrees after TDC. The aim of close PFI, similar to delayed fuel injection, is to boost exhaust temperature through keeping in-cylinder temperature at high levels before the exhaust phase. Not only injection timing but also quantity of PFI is significant to determine the engine-out temperature in diesel engines [Wu et al. (2021)].

Different from close PFI, late PFI is applied mostly at timings higher than 60 degrees after TDC and is not directly related to the increase of in-cylinder temperature. At late timings, not a significant amount of fuel is combusted and thus, the temperature in the medium is not noticeably elevated. Late PFI, unlike close PFI, provides high HC rates inside the cylinder before exhaust gas flows through the DOC. Those high HC rates within the flow can be oxidized inside the DOC unit and thus, generates increased exhaust temperatures at DOC-exit, which is useful for DPF and SCR units in diesel engines [Wang et al. (2020)]. Similar to close PFI, quantity of injected fuel (in addition to injection timing) is important in late PFI method to maintain high DOC-out temperature.

2. FUEL PATH STRATEGIES TO IMPROVE EXHAUST THERMAL MANAGEMENT

Exhaust energy is critical in HD diesel vehicles at low loads unless an external device such as a heat storage unit is placed to warm up the EAT unit [Hamedi et al. (2019)]. Without outer tools, only exhaust heat provides the required heat transfer to EAT system and keeps it at efficient levels. Thus, high exhaust temperature is necessary to ensure improved EAT thermal management and low emission rates [Gao et al. (2019)]. This section attempts to introduce typical fuel path techniques used to achieve this purpose in diesel vehicles.

2.1. Delayed Fuel Injection Timing

Retarding the timing of the fuel injection is one of the effective fuel path techniques to accelerate EAT heat up. As mentioned earlier, combustion is highly sensitive to fuel injection timing in diesel engines. Therefore, when nominal injection timing is swept forward or backward, combustion is inevitably altered. A modified combustion process directly influences the in-cylinder temperature and thus, exhaust-out temperature. Bai et al. searched in a 6-cylinder diesel engine the effect of delayed fuel injection timing on fuel consumption and exhaust temperature [Bai et al. (2017)], as shown in Figure 3.

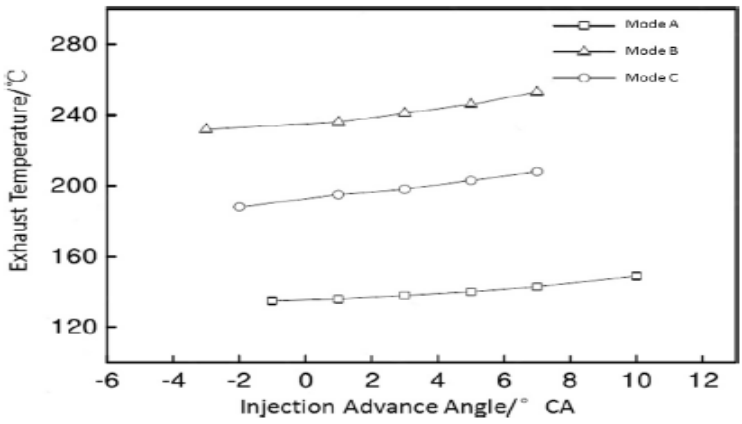

(a)

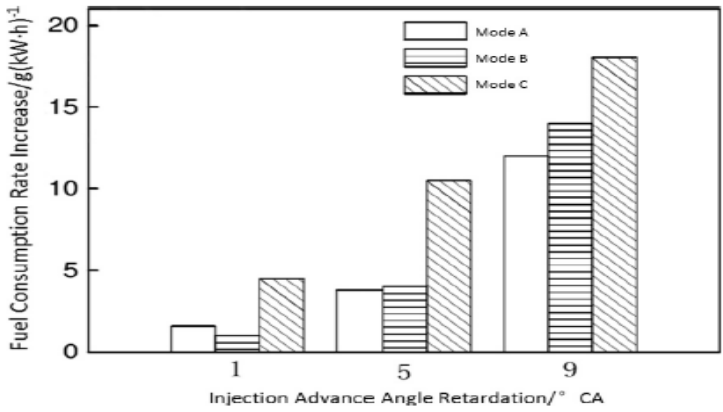

(b)

Figure 3: The impact of delayed injection timing on **(a)** Exhaust temperature **(b)** Rise on fuel consumption rate [Bai et al. (2017)]

The modes (A, B & C) on Figure 3 denote the operating conditions of the engine. The speeds and torques for A, B, and C are 1100 RPM with 100 Nm, 1200 RPM with 200 Nm, and 1300 RPM with 300 Nm, respectively. Late fuel injection raises the exhaust temperature in all aforementioned engine loading cases. However, temperature rise is not very high in this method. For instance, in mode C, close to 28^{o}C exhaust temperature rise is obtained (exhaust temperature can barely reach 253^{o}C) even though the injection timing is retarded 10 ^{o}CA degrees from the nominal condition.

One other important effect of retarded fuel injection is that it requires high fuel inefficiency as seen in Figure 3. Fuel consumption needs to be increased more than 10 g/kWh (close to 20 g/kWh in Mode C) as injection timing is delayed 9 ^{o}CA degrees from the baseline timing. Overall, late fuel injection timing is definitely useful to rise engine-out temperature. However, considering the high thermal inefficiency shown in Figure 3 (b), it is derived that it is mostly beneficial when the system needs a slight temperature rise to achieve an exhaust temperature of 250^{o}C and above.

Similar works examined the potential of late fuel injection timing at different loads in diesel engines [Lapuerta et al. (2014), Wu et al. (2021), Basaran (2022)]. General conclusion from those studies is that this technique can be helpful to improve exhaust temperature, but it should be combined with other techniques, particularly at low loads, to attain desirable high exhaust temperatures.

2.2. Delayed Ignition Timing

Delayed fuel injection timing is applied in diesel engines as fuel is indeed injected at a specific timing into the high pressure charge in those engines. Gasoline engines do not have injection timing, but ignition timing since air-fuel mixture is compressed in those engines. Retarding the ignition timing in a spark-ignition engine can be as successful as DFI to increase exhaust temperature [Kessels et al. (2010)]. Therefore, the method has a potential to achieve effective ETM in gasoline engines. Kim and Cho explored the impact of ignition retard in a 4-cylinder inline spark-ignition engine [Kim and Cho (2005)]. As demonstrated in Figure 4, spark timing of the engine is delayed through the TDC to improve the engine-out temperature.

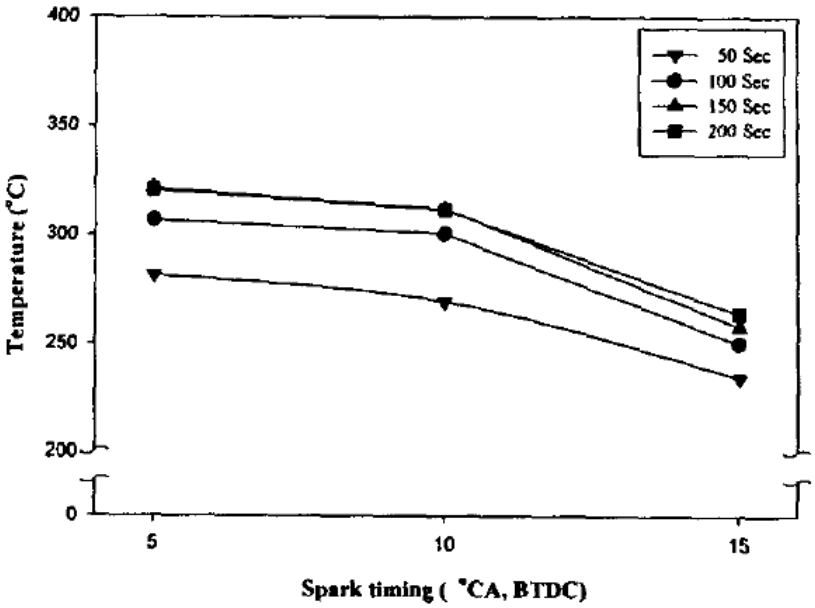

Figure 4: The impact of ignition timing on exhaust temperature [Kim and Cho (2005)]

It is explicitly seen that late spark timing boosts the exhaust temperature in the gasoline engine. The timings on the upper right of the plot shows the seconds past after the engine start. The measurements for late spark timing are achieved for 4 different cases: 50, 100, 150, and 200 seconds after the engine start. In all those cases, exhaust temperature gets higher values as long as spark timing is actuated from 15 ^{o}CA degrees BTDC to 5 ^{o}CA degrees BTDC ($T_{exhaust}$ is above 250^{o}C for the latest timing in all conditions). It is stated that as the start of combustion is retarded, in-cylinder flame endures a longer time before the exhaust is opened and thus, hot exhaust gas is allowed to flow in delayed spark timing mode in the engine [Kim and Cho (2005)]. Obviously, as a certain timing is reached after the engine start (~ 100 sec), more temperature rise can be yielded and thus, exhaust temperature can be maintained above 300^{o}C, which is noticeably helpful, particularly during engine start, to enhance EAT and curb emission rates.

2.3. Close Post-injection

Apart from delayed fuel injection timing and late ignition timing, close post-injection (CPI) can be adopted as an effective means to rise engine-out temperature in diesel engines [Ozel et al. (2018)]. In a traditional fuel injection technique, the main injection has the highest injection rate and is

applied the longest duration compared to other pre-, close post- and late post-injections, as indicated in Figure 5 [Hu et al. (2023)].

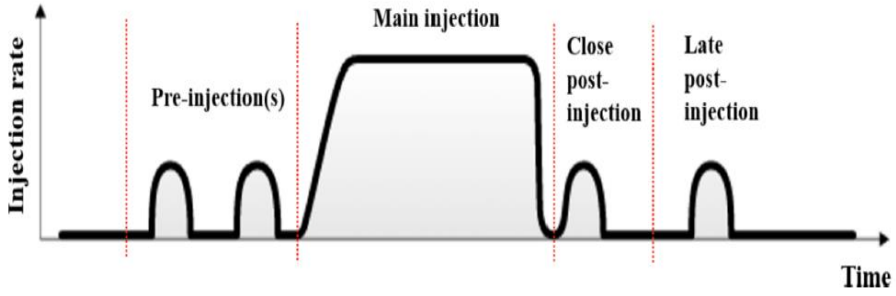

Figure 5: The traditional fuel injection technique [Hu et al. (2023)]

CPI is applied with a lower injection rate and with a shorter duration relative to the main injection. Pre-injection and late post-injection rates are also low compared to the main injection rate. Pre-injection is not directly related to the exhaust temperature improvement. Instead, it is applied to enhance the in-cylinder combustion and thermal efficiency. Unlike CPI, late post-injection is implemented far from the main injection timing. Therefore, it is generally effective on post-DOC temperature, rather than directly on exhaust port-out temperature. Unlike late post-injection, CPI occurs at a position where in-cylinder pressure and temperature remain still at high levels. In other words, it is placed at a timing appropriate for another combustion process (other than main combustion). Thus, it is certainly effective on the improvement of in-cylinder and engine-out temperature.

Tan et al. quantified the impact of CPI on exhaust temperature and total hydrocarbon (THC) rates in an inline 6-cylinders, intercooled and turbocharged diesel engine, as seen in Figures 6&7 [Tan et al. (2020)].

CPI is provided in the fuel injection system with different fuel injection timings (10^{o}CA, 20^{o}CA, 30^{o}CA, and 40^{o}CA ATDC, respectively) and with different injection quantities (4, 8, 12, and 16 mm^3 per cycle, respectively) in the plots below. The technique is applied at 100 RPM speed and at a torque of 100 Nm where exhaust temperature is 115^{o}C (much below the threshold temperature of 250^{o}C). As demonstrated in Figure 6, delaying the injection timing and increasing the injection quantity are both highly helpful to elevate exhaust gas temperature. Nominal exhaust temperature can be raised above 200^{o}C through an injection timing of 20^{o}CA ATDC and an

injection quantity of 12 mm^3 per cycle. More importantly, CPI achieves to reach 250^oC (an exhaust temperature rise of 135^oC) via an injection timing of 30^oCA ATDC and an injection quantity of 16 mm^3, which is a considerable improvement for EAT effectiveness. Overall, CPI has a notable potential to rise the temperature at EAT inlet.

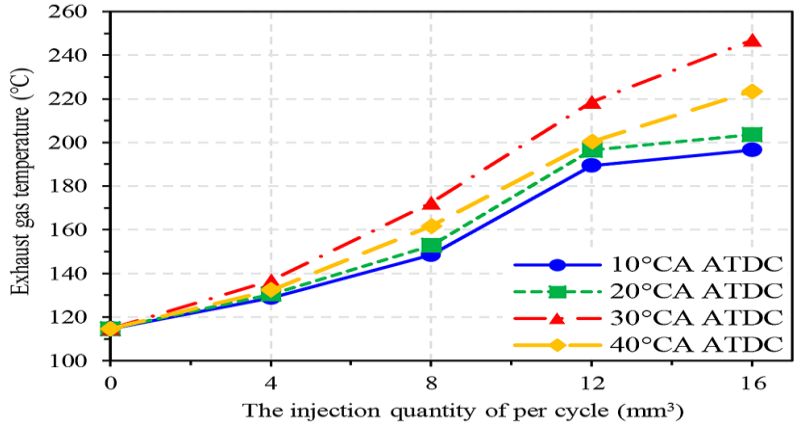

Figure 6: The impact of CPI timing and quantity on exhaust temperature [Tan et al. (2020)]

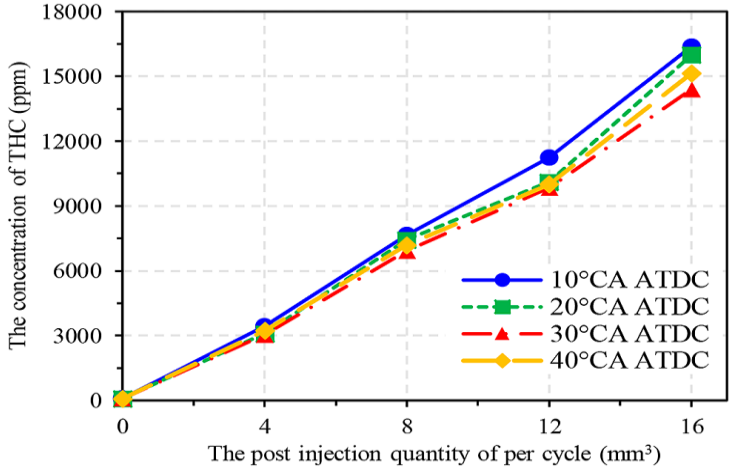

Figure 7: The impact of CPI timing and quantity on THC rates [Tan et al. (2020)]

CPI increases the in-cylinder and engine-out temperature since it allows an extra combustion inside the cylinder. Although the pressure starts to decrease as injection timing is further delayed from the TDC, the in-cylinder medium is still warm for an additional combustion. Not all the fuel injected is

combusted, but even partial combustion is useful to maintain high combustion chamber temperature. Thus, those extra injections provide added heat and maintain high in-cylinder temperature before the expansion and exhaust phases of the engine.

The impact of CPI on HC rates is significant as well, as shown in Figure 7. As mentioned earlier, the combustion in CPI mode is not complete since the in-cylinder medium is not as hot as the one in the main injection mode. Therefore, some part of the fuel remains unburnt inside the cylinder and rises the HC rates of the in-cylinder charge before flowing through the DOC in the system. As the oxidation of HC is possible inside the DOC, more HC rates in CPI mode correspond to high DOC-out temperature and thus, is beneficial for DPF and SCR units. THC rates tend to increase in Figure 7 in all injection timings as more fuel is injected into the system. The rise can be attributed to ineffective combustion of the fuel, leading to higher THC rates due to higher unburnt amount of fuel at high injection quantities. The injection timing does not seem to be affecting THC rates in a noteworthy manner. However, as pointed out in Figure 6, not all injection timings attain to improve exhaust above 200^{o}C or even 250^{o}C. Therefore, using slightly delayed post-injection instead of highly delayed post-injection is generally preferred when the system does not necessitate a significant exhaust temperature rise to maintain EAT unit above 250^{o}C. In some cases, an optimization between injection timing and quantity can be needed since high exhaust temperature at DPF & SCR inlet can be obtained at moderately delayed post-injection timings if the THC rates are raised adequately to improve DOC-exit temperature in the system.

CPI proves to be an effective method to sustain high exhaust temperature in diesel engines [Anbarasu and Ramani (2022)]. However, as stated formerly, it deteriorates the combustion and thus, generally increases the fuel consumption. Nie et al. analyzed the effect of CPI on BSFC in a 4-cylinder direct injection diesel engine [Nie et al. (2022)]. It is seen in Figure 8 that both quantity and timing of post-injection worsen the BSFC. The main reason for increased fuel penalty is the incomplete combustion of additional fuel injection. The study examines the effect of altitude in Figure 8 as well. Using post-injection particularly at high altitudes needs more BSFC than sea level condition due to low airflow and inadequate combustion at those levels. Thus, reasonable control of CPI is a must to keep fuel penalty at low levels.

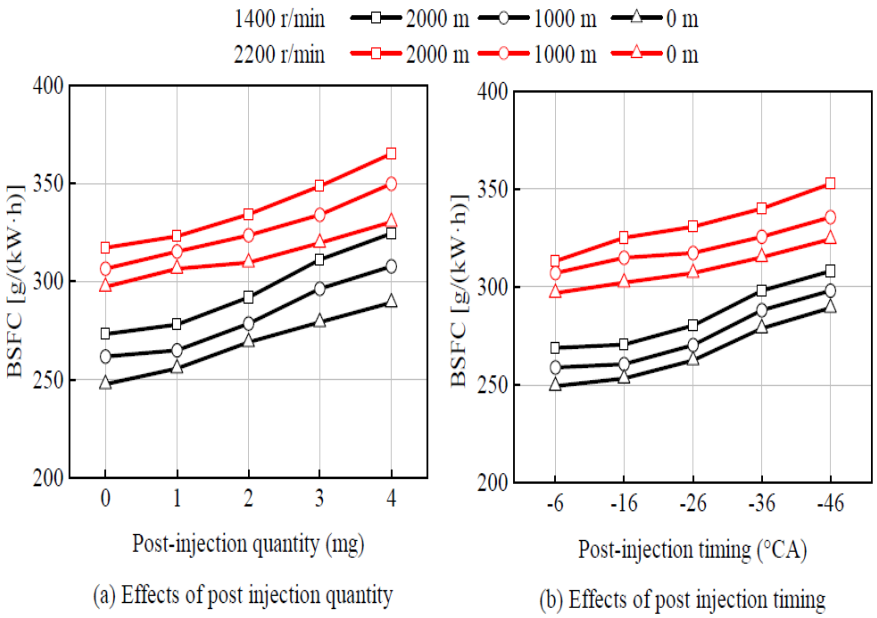

Figure 8: The impact of post-injection quantity and post-injection timing on BSFC at different engine speeds and at different altitudes [Nie et al. (2022)]

2.4. Late Post-injection

Close post-injection is one way to boost turbine-out exhaust temperature in engine systems [Subramanian and Rothamer (2023)]. Post-injection does not have to be used close to main injection timing all the time. It can also be implemented far from the main injection timing, namely, late post-injection (LPI), as demonstrated previously in Figure 5.

LPI generally refers to fuel injection at the second half of the expansion phase or close to the exhaust phase in diesel engines. Unlike CPI, which mainly aims to rise temperature at DOC inlet [Honardar et al. (2011)], LPI particularly aims to improve the temperature at DOC outlet [Tan et al. (2020)].

Sun et al. examined the impact of LPI on exhaust temperature and HC rates in a 4-cylinder common rail compression-ignition engine working at 1400 RPM speed [Sun et al. (2020)]. The effect of LPI on exhaust temperature at the entrance and exit of DOC unit for different load ratios is shown in Figure 9.

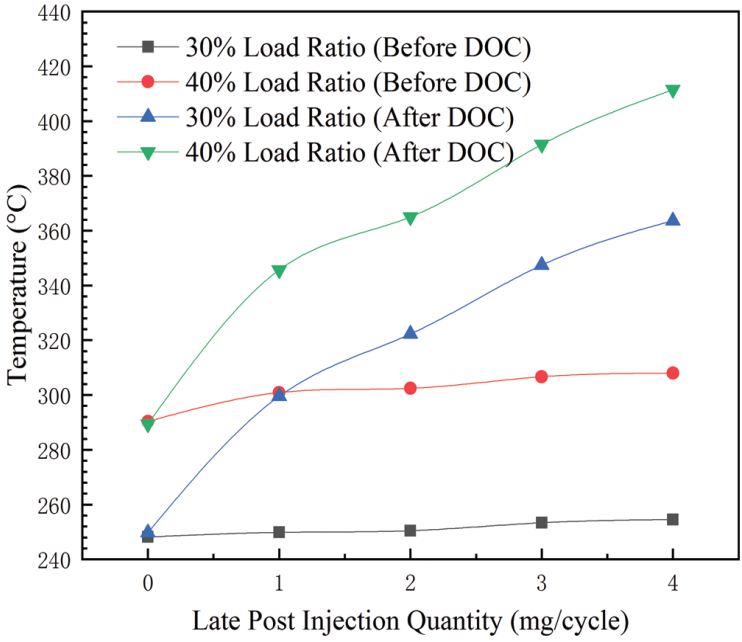

Figure 9: Effect of LPI quantity on exhaust temperature at inlet and outlet of DOC unit [Sun et al. (2020)]

In the analysis, timing of the post-injection is fixed at 140°CA after TDC and only the fuel quantity is changed from 1 to 4 mg/cycle. As explicitly shown in Figure 9, even at different loads, the quantity does not affect the temperature at DOC inlet significantly. However, a significant temperature rise (more than 100°C) is observed at DOC exit. High loads require more fuel consumption and thus, the temperature is maintained at higher levels in 40% Load ratio compared to 30% Load ratio. The benefit of LPI on particularly inlet and outlet of DOC unit can be better seen in Figure 10 [Sun et al. (2020)].

At baseline position in Figure 10, without LPI, HC rate is low at DOC inlet, which makes it difficult to rise the temperature at DOC exit, as seen in Figure 9. Also, HC conversion efficiency is relatively low (close to % 80) at this condition. However, as LPI is applied and the quantity of injected fuel is increased, more HC can be oxidized within the DOC unit and thus, both HC conversion efficiency (above % 90) and temperature at DOC exit (above 400°C) are significantly improved.

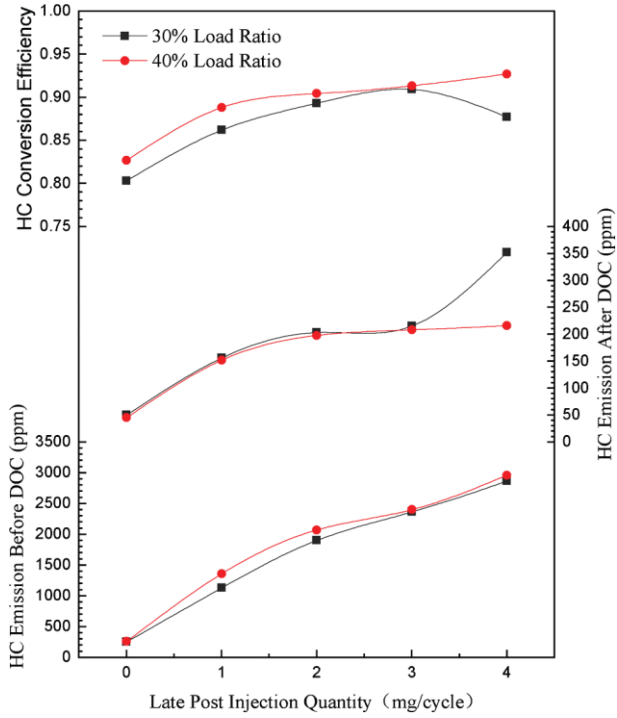

Figure 10: Effect of LPI quantity on DOC conversion efficiency and HC emission at inlet and outlet of DOC unit [Sun et al. (2020)]

It should also be noted that the DOC unit has a capacity to oxidize a certain amount of HC emission. As seen in Figure 10, after a certain quantity rise, conversion efficiency is not enhanced noticeably and HC rate at DOC exit starts to rise, which is not desirable. Therefore, the quantity rise should be adjusted in the system considering the adequate temperature rise in Figure 9 and the sufficient conversion efficiency improvement in Figure 10. The optimum quantity can be the best solution for the lowest emission rates at engine exit. In a similar experimental work arranged with a 6-cylinder DI diesel engine, Wu et al. particularly emphasized the need to control the quantity and timing of post-injection in order to generate the possible minimum tailpipe soot and NOx rates [Wu et al. (2019)].

LPI is definitely effective at increasing the temperature at DOC-out through enabling higher HC oxidation inside the DOC [Chen et al. (2014)]. However, its effect on engine torque and engine-out emission rates should also be considered so as to understand the overall advantage or disadvantage of the technique. Wang et al. quantified the impact of post-injecting timing on

exhaust temperature and emission rates of a 4-cylinder turbocharged diesel engine at 3200 RPM speed and at different loads [Wang et al. (2022)]. The effect of post-injection timing on torque and exhaust gas temperature (EGT) are illustrated in Figure 11. While CPI generally improves the torque compared to no-post condition, LPI either keeps it similar at high loads (50% and 80% loads) or reduces it at low loads (20% load), which is disadvantageous since higher fuel consumption is needed in LPI mode to keep torque constant in the system.

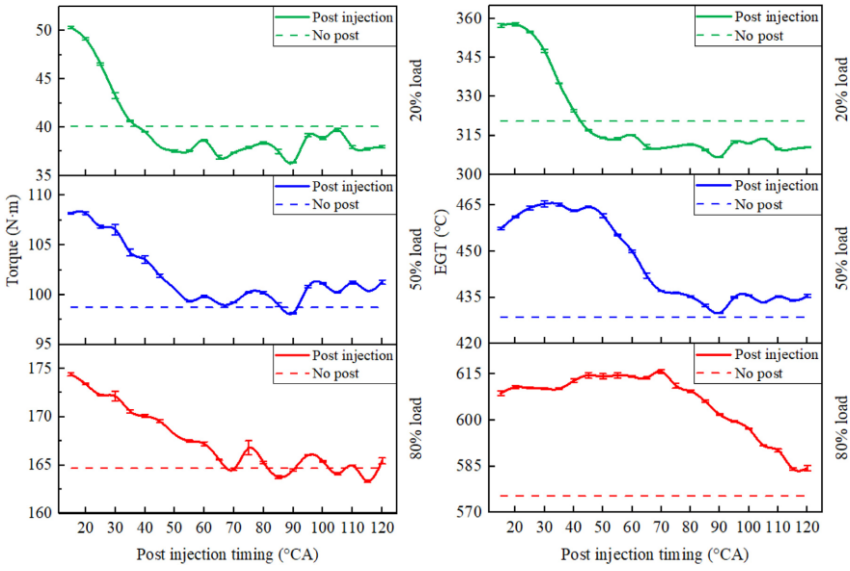

Figure 11: Impact of post-injection timing on **(a)** Torque and **(b)** EGT [Wang et al. (2022)]

Also, CPI causes a meaningful rise in EGT at all loads in Figure 11. However, LPI seems to be slightly or moderately effective at high loads and even has a negative effect on EGT at low load (20% load). This result is in fact consistent with the previous study examined in Figure 9 [Sun et al. (2020)]. Unlike CPI, the objective of LPI is not to boost EGT but to increase the DOC-out temperature via elevating the HC rates in the system. The reduction in EGT in extremely delayed post-injection timings may be due to highly lowered oxygen levels and thus, highly ineffective combustion at those timings.

The effect of post-injection on emission rates was investigated in the same work as well [Wang et al. (2022)]. The variation of NOx & soot rates with different post-injection timings are shown in Figure 12.

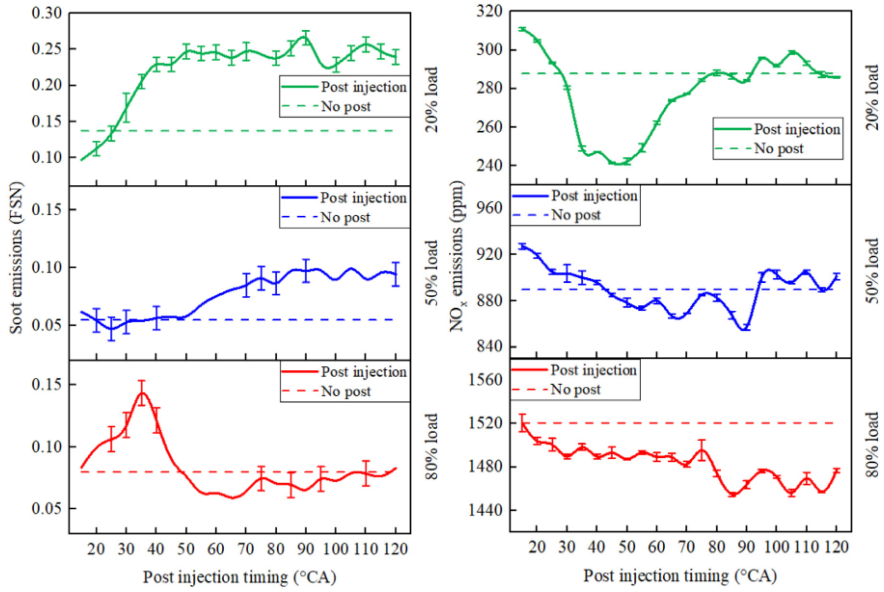

Figure 12: Impact of post-injection timing on **(a)** soot and **(b)** NO_x emissions [Wang et al. (2022)]

CPI affects soot emission negatively at high load (80% load). The soot emission is comparable at medium load (50% load) and is reduced at low load (20% load) at low injection timings. Thus, CPI is preferable technique for improved ETM at low-to-moderate loads as it elevates EGT (in Figure 11) without any rise in soot rates. Unlike CPI, LPI causes a negative effect in soot rates in almost all loads in Figure 12. In-cylinder combustion degrades as post-injection is implemented at highly delayed timings (particularly further than 60 ^{o}CA). Most of the fuel in LPI mode cannot go through the combustion process. However, the in-cylinder medium is still warm for the evaporation of the fuel and thus, there is an unavoidable soot rise, especially in low and medium loads. At high load (80% load) there is not a significant rise in soot levels. This is because in-cylinder temperature is hotter at retarded injection timings in this condition compared to other loads. Therefore, the combustion process is not as ineffective as it is in other loads. Also, EGT is kept above 550^{o}C (close to 600^{o}C) at this load, which is sufficient for active regeneration

of DPF unit. Thus, the soot rates can be reduced before the exhaust gas completely leaves the system.

CPI has a comparable NOx rate at high load (80% load) and higher NOx rates relative to no-post condition in Figure 12. The main reason of NOx rise is that CPI increases the in-cylinder temperature in almost all loads, which is proportional with NOx formation inside the cylinders. However, despite the NOx rise, CPI is effective to improve both EGT and soot rates. Therefore, considering the SCR unit operates more effectively under increased EGT and is more likely to reduce NOx rates, CPI is still a good option to use for enhanced ETM in diesel engine. LPI does not affect NOx rates significantly at low-to-moderate loads since in-cylinder temperature is not altered noticeably in LPI mode. At high load (80% load), NOx rate is decreased via LPI application. This is attributed to low air-to-fuel ratio and reduced oxygen level at this condition, which does not allow a rise in NOx rate.

Overall, both CPI and LPI are capable of boosting diesel EGT or DOC-exit temperature at different engine loads. Nevertheless, these techniques generally need fuel penalty and at some engine loads, rise the emission rates to undesirable levels. Therefore, it can be more useful to combine those methods with other techniques such as EGR and Miller cycle to achieve ETM improvement with relatively lower fuel penalty [Guan et al. (2020)].

CONCLUSIONS

This work overviews the fuel injection methods to improve the diesel EAT thermal management in highway vehicles. Fuel injection strategies are generally seen to be effective at achieving high EGT (above 250^{o}C) in diesel engines.

Delaying the main injection timing is found to be slightly or in some cases (highly delayed cases) moderately effective to elevate EGT. Similarly, retarded ignition timing in gasoline engines can directly improve EGT at low loads. However, those two techniques mostly necessitate high fuel penalty (above %10) for a relatively mild temperature rise (up to 30^{o}C) and a relatively low efficiency improvement in EAT unit. Thus, they are not preferred primarily at low loads. Those methods are normally combined with other inner-engine techniques such as Miller cycle to yield high EGT rise (50^{o}C or more) with an acceptable (below %10) fuel consumption penalty,

which maintains NOx and soot rates at low levels.

Unlike retarded injection timing, CPI and LPI enhance EGT more (100^{o}C or more) with a similar fuel consumption penalty. While CPI boosts directly EGT at exhaust port, LPI particularly improves DOC exit temperature through more HC oxidation inside the DOC unit. Both CPI & LPI induce thermal inefficiency due to ineffective combustion of the additional fuel injected at a low-pressure medium. Incomplete combustion in CPI & LPI modes cause high soot rates, which is undesirable. However, LPI can enable reduced NOx rates at particularly moderate-to-high loads while EGT at DPF and SCR inlet is highly improved. The system is generally faced with a trade-off between EGT and fuel penalty or EGT and soot rates as post-injection techniques are applied. Therefore, post-injection needs further research such as comparing diesel and non-diesel fuel injection, combining post-injection with EGR or electrical heating or with other effective airflow-based ETM methods. Those advanced works can be helpful to minimize fuel penalty and emission rates while EAT thermal management is improved in diesel engine systems.

REFERENCES

Agarwal, D., Singh, S. K., & Agarwal, A. K. (2011). Effect of Exhaust Gas Recirculation (EGR) on performance, emissions, deposits and durability of a constant speed compression ignition engine. Applied energy, Vol. 88(8), pp. 2900-2907.

Agarwal, A. K., Singh, A. P., & Maurya, R. K. (2017). Evolution, challenges and path forward for low temperature combustion engines. Progress in energy and combustion science, Vol. 61, pp. 1-56.

Ajanovic, A. & Haas, R. (2018). Electric vehicles: solution or new problem?. Environment, Development and Sustainability, Vol. 20, pp. 7-22.

Anbarasu, M. & Ramani, V. S. (2022). Improvement of SCR thermal management system and emissions reduction through combustion optimization. SAE Technical Paper No. 2022-28-0482, doi:10.4271/2022-28-0482.

Bai, S., Chen, G., Sun, Q., Wang, G. and Li, G. X. (2017). Influence of active control strategies on exhaust thermal management for diesel particular filter active regeneration. Applied Thermal Engineering, Vol. 119, pp. 297-303.

Basaran, H. U. & Ozsoysal, O. A. (2017). Effects of application of variable valve timing on the exhaust gas temperature improvement in a low-loaded diesel engine. Applied Thermal Engineering, Vol. 122, pp. 758-767.

Basaran, H. U. (2022). Late Fuel Injection Combined with Retarded Intake Valve Closure for Improved Exhaust System Warm-up in Diesel Automotive Vehicles. Sustainability of Natural Resources' Efficiency, pp. 33-60.

Basaran, H. U. (2023). An Overview of Airflow-based Measures to Improve Exhaust After-treatment Thermal Management to Reduce Emission Rates in Diesel-driven Vehicles. Multidisciplinary Insights: Geothermal Wells, Preservation, Engineering, and Chemical Processes, pp. 61-87.

Cavina, N., Mancini, G., Corti, E., Moro, D., De Cesare, M. and Stola, F. (2013). Thermal management strategies for SCR after treatment systems. SAE Technical Paper No. 2013-24-0153.

Chen, P., Ibrahim, U. and Wang, J. (2014). Experimental investigation of diesel and biodiesel post injections during active diesel particulate filter regenerations. Fuel. Vol. 130, pp. 286-295.

Chen, Y., Ma, J., Han, B., Zhang, P., Hua, H., Chen, H. and Su, X. (2018). Emissions of automobiles fueled with alternative fuels based on engine technology: A review. Journal of Traffic and Transportation Engineering (English Edition). Vol. 5(4), pp. 318-334.

Conway, G., Joshi, A., Leach, F., Garcia, A. & Senecal, P. K. (2021). A review of current and future powertrain technologies and trends in 2020. Transportation Engineering, Vol. 5, p. 100080.

Dieselnet, EU standards. http://www.dieselnet.com/standards/eu/hd.php#stds (Retrieved: 30.09.2023)

Fayyazbakhsh, A., Bell, M. L., Zhu, X., Mei, X., Koutny, M., Hajinajaf, N. & Zhang, Y. (2022). Engine emissions with air pollutants and greenhouse gases and their control technologies. Journal of Cleaner Production, p. 134260.

Goldenberg, H. & Jain, P. (1983). Depollution des gaz d'echappement des moteurs Diesel au moyen de pots catalytiques. Revue Inst. Franc. du Petrole, Vol. 38, pp. 793-805.

Goyal, H. & Jain, P. (2020). A Comprehensive Review of Electric Vehicles. Journal of Green Engineering, Vol. 10, pp. 12627-12647.

Guan, W., Pedrozo, V. B., Zhao, H., Ban, Z. & Lin, T. (2020). Miller cycle combined with exhaust gas recirculation and post-fuel injection for emissions and exhaust gas temperature control of a heavy-duty diesel engine. International Journal of Engine Research, Vol. 21(8), pp. 1381-1397.

Hamedi, M. R., Doustdar, O., Tsolakis, A. and Hartland, J. (2019). Thermal energy storage system for efficient diesel exhaust aftertreatment at low temperatures. Applied Energy, Vol. 235, p. 874-887.

Honardar, S., Busch, H., Schnorbus, T., Severin, C., Kolbeck, A. F. & Korfer, T. (2011). Exhaust temperature management for diesel engines assessment of engine concepts and calibration strategies with regard to fuel penalty. SAE Technical Paper No. 2011-24-0176.

Hu, J., Wu, Y., Liao, J., Cai, Z. & Yu, Q. (2023). Heating and storage: A review on exhaust thermal management applications for a better trade-off between environment and economy in ICEs. Applied Thermal Engineering, Vol. 220, 119782.

Imtenan, S., Varman, M., Masjuki, H. H., Kalam, M. A., Sajjad, H., Arbab, M. I. & Fattah, I. R. (2014). Impact of low temperature combustion attaining strategies on diesel engine emissions for diesel and

biodiesels: A review. Energy Conversion and Management, Vol. 80, pp. 329-356.

Joshi, A. (2022). A Review of Emissions Control Technologies for On-Road Vehicles. Engines and Fuels for Future Transport, pp. 39-56.

Kalghatgi, G. (2018). Is it really the end of internal combustion engines and petroleum in transport?. Applied Energy, Vol. (225), pp. 965-974.

Kessels, J. T. B. A., Foster, D. I and Bleuanus, W. A. J. (2010). Fuel penalty comparison for (electrically) heated catalyst technology comparison. Oil Gas Sci. Technol., Vol. 65, pp. 47-54.

Kim, D. S. and Cho, Y. S. (2005). Effects of cam phase and spark retard to increase exhaust gas temperature in the cold start period of an SI engine. International Journal of Automotive Technology, Vol. 6(6), pp. 585-590.

Lapuerta, M., Hernandez, J. J. and Oliva, F. (2014). Strategies for active diesel particulate filter regeneration based on late injection and exhaust recirculation with different fuels. International Journal of Engine Research, Vol. 15(2), pp. 209-221.

Lešnik, L., Kegl, B., Torres-Jimenez, E. and Cruz-Peragon, F. (2020). Why we should invest further in the development of internal combustion engines for road applications. Oil & Gas Science and Technology-Revue d'IFP Energies nouvelles, Vol. 75, p. 56.

Li, S., Zhang, C., Zhou, A., Li, Y., Yin, P., Mu, C. and Xu, J. (2021). Experimental and kinetic modeling study for N2O formation of NH3-SCR over commercial Cu-zeolite catalyst. Advances in Mechanical Engineering, Vol. 13(4), p. 16878140211010648.

Marathe, N. V., Walke, N. H., Juttu, S., Chaudhari, H. B., Dev, S. & Samant, M. P. (2022). Introduction to Thermal Management Techniques. Handbook of Thermal Management of Engines, pp. 3-27.

Martinovic, F., Castoldi, L. and Deorsola, F. A. (2021). Aftertreatment technologies for diesel engines: An overview of the combined systems, Vol. 11(6), pp. 653.

Millo, F., Giacominetto, P. F., & Bernardi, M. G. (2012). Analysis of different exhaust gas recirculation architectures for passenger car Diesel engines. Applied Energy, Vol. 98, pp. 79-91.

Nie, X., Bi, Y., Liu, S., Shen, L. & Wan, M. (2022). Impacts of different exhaust thermal management methods on diesel engine and SCR performance at different altitude levels. Fuel, Vol. 324, p. 124747.

Onorati, A. et al. (2022). The role of hydrogen for future internal combustion engines. International Journal of Engine Research, Vol. 23(4), pp. 529-540.

Ozel, C., Hall, M. J. & Matthews, R. (2018). Increasing Exhaust Temperature of an Idling Light-Duty Diesel Engine through Post-Injection and Intake Throttling. SAE Technical Paper No. 2018-01-0223.

Reitz, R. D., Ogawa, H., Payri, R., Fansler, T., Kokjohn, S., Moriyoshi, Y., Agarwal, A. K., Arcoumanis, D. Assanis, D., Bae, C. & Boulouchos, K. (2020). IJER editorial: The future of the internal combustion engine, Vol. 21(1), pp. 3-10.

Subramanian, S. and Rothamer, D. (2023). Exploration of fuel property impacts on the combustion of late port injections using binary blends and high-reactivity ether bioblendstocks. SAE Technical Paper No. 2023-01-0264, doi:10.4271/2023-01-0264.

Sun, K., Li, D., Liu, H. and Bai, S. (2020). Influence of diesel engine intake throttle and late post injection process on the rise of temperature in the diesel oxidation catalyst. Fluid Dynamics & Materials Processing, Vol. 16(3), pp. 573-584, DOI:10.32604/fdmp.2020.09591.

Tan, P., Duan, L., Li, E., Hu, Z. and Lou, D. (2020). Experimental study on thermal management strategy of the exhaust gas of a heavy-duty diesel engine based on in-cylinder injection parameters SAE Technical Paper No. 2020-01-0621, doi:10.4271/2020-01-0621.

Votsmeier, M., Kreuzer, T., Gieshoff, J. & Lepperhoff, G. (2009). Automobile exhaust control. Ullmann's Encyclopedia of Industrial Chemistry, Vol. 4, pp. 407-424.

Wang, J., Wang, B. and Cao, Z. (2020). Experimental research on exhaust thermal management control strategy for diesel particular filter active regeneration. International Journal of Automotive Technology, Vol. 21, p. 1185-1194.

Wang, Z., Shen, L., Lei, J., Yao, G. and Wang, G. (2022). Impact characteristics of post injection on exhaust temperature and hydrocarbon emissions of a diesel engine. Energy Reports, Vol. 8, p. 4332-4343.

Wu, Y., Wang, P., Farhan, S. M., Yi, J. and Lei, L. (2019). Effect of post-injection on combustion and exhaust emissions in DI diesel engine. Fuel, Vol. 258, p. 116131.

Wu, B., Jia, Z., guo Li, Z., yi Liu, G. & lin Zhong, X. (2021). Different exhaust temperature management technologies for heavy-duty diesel

engines with regard to thermal efficiency. Applied Thermal Engineering, Vol. 186, p. 116495

Zhang, X., Zhu, J., Zhang, Z. & Bai, S. (2022). Study on the Effect of Exhaust Thermal Management on SCR of Euro VI Diesel Engine, FEB – Fresenius Environmental Bulletin, 11678.

Zimakowska-Laskowska, M. & Laskowski, P. (2022). Emission from internal combustion engines and battery electric vehicles: Case study for Poland, Atmosphere, 13(3), p. 401.

CHAPTER 4

TRIBOLOGICAL EFFECTS OF COBALT AND BORON ON COPPER-BASED COMPOSITES

Merve HORLU[1]

Gamze ISPIRLIOGLU KARA[2]

Cevher Kursat MACIT[3]

Dr. Burak TANYERI[4]

Prof. Bunyamin AKSAKAL [5]

Ersoy YILMAZ[6]

DOI: https://dx.doi.org/10.5281/zenodo.8428666

[1]Aisin Automotive Industry Trade Inc. Tuzla, İstanbul. mervehorlu@gmail.com.Orcid No: 0000-0003-0775-2849

[2] Ataturk University, Faculty of Engineering, Department of Mechanical Engineering, Erzurum, Turkey.gamze.ispirlioglu@atauni.edu.tr.Orcid No: 0000-0001-9968-1739

[3] Firat University, Faculty of Engineering, Department of Mechanical Engineering, Elazıg, Turkey.macitkursatcevher@gmail.com.Orcid No: 0000-0003-0466-7788

[4] Firat University, School of Aviation, Aircraft Airframe-Engine Maintenance, Elazıg, Turkey.btanyeri@firat.edu.tr.Orcid No: 0000-0002-3517-9755

[5] Firat University, School of Aviation, Aircraft Airframe-Engine Maintenance, Elazıg, Turkey.baksakal@firat.edu.tr.Orcid No: 0000-0003-4844-9387

[6]Aisin Automotive Industry Trade Inc. Tuzla, İstanbul.eyilmaz@aisin.com.tr

INTRODUCTION

Composite materials can be produced in different ways (Kirik et al., 2013; Wang et al., 2010). One of these methods is powder metallurgy (Yalcin & Varol, 2008). Powder metallurgy involves the production of materials by pressing powdered products and sintering them at high temperatures (Zheng et al., 2008). Pure metals, plastics, ceramics and fine powdered alloys can be mixed in specific proportions and formed under pressure (Uzun & Usca, 2018). These products are then sintered at a temperature below the melting temperature of the matrix material, creating a strong bond between the contact surfaces of the powdered particles. Complex and small parts can be easily produced with this method. Compared to other methods, material waste is less and a certain degree of porosity and permeability is achieved. The dime0nsional accuracy and excellent surface quality achieved in most materials produced by powder metallurgy eliminates the need for further processing (Sap, 2021). Uygur produced Fe-Cu-Mn-C-based steel by powder metallurgy and found that it increased hardness, tensile strength and reduced porosity (Uygur, 2007). Ozgun and Akbulut found significant increases in relative density values by adding Fe and B reinforcement to Stellite 6 super alloy matrix material with the same method (Ozgun & Akbulut, 2017).

Copper (Cu) is widely used in engineering and electronics applications due to its excellent electrical and thermal conductivity and good ductility, and studies continue to increase (Jiang et al., 2018; Schubert et al., 2008). Due to its unique properties, copper is expected to be an outstanding material for manufacturing parts in industries linked to water supply and electrical and thermal industries. It has wide applications in gas turbine nozzles, rocket engines, electrical switches, combustion chamber wall linings and electronics (Lu et al., 2013). However, there are some circumstances that affect the more widespread use of Cu. Copper is not preferred for structural applications due to its low mechanical properties at high temperatures (Nazeer et al., 2019). The poor mechanical and tribological properties of Cu limit its use. To increase the use of Cu and Cu alloys, it is necessary to add reinforcing elements (Chundru et al., 2019).

Cobalt (Co) has been widely researched in recent years due to its unique properties (Barekat et al., 2016; Ozgün & Dinler, 2018). It is resistant to abrasion and corrosion and has biocompatible properties (Xia et al., 2013). Cobalt also has a high melting point and hardness (Baco-Carles et al., 2008). It is frequently used in many industrial fields such as cutting tools, magnets,

rechargeable batteries (Cabrol et al., 2019).

Boron (B) is a corrosion resistant element and has very low solubility in metals at room temperature (Uzunsoy, 2010). The use of boron in powder metallurgy applications has been found to be quite limited. Boron-reinforced copper matrix composites can have properties such as high stiffness, high strength and thermal stability (Ma & Zhang, 2016; Zepon et al., 2015). In addition, boron's antimicrobial properties may also make it preferable for in-body applications (Li et al., 2018).

In this study, a new hybrid blend was made by adding 1% Co and 1% B to pure Cu powder. When the literature studies were examined, it was seen that a hybrid blend was not made using the reinforcing elements used in this study to Cu powders. It is aimed to improve the tribological properties of the Cu matrix composite with the addition of reinforcing elements used in the study. Microstructure (SEM, EDX and XRD), hardness and wear tests under 10N load in dry conditions were carried out to characterize the composites. The fabrication, characterization and tribological experiments of the prepared hybrid composites are described in detail in the Method section.

METHOD

In the method section, the preparation of the powders, the preparation of the prepared hybrid powders into test specimens with the powder metallurgy process steps, the metallographic preparation and characterization of the hybrid composites, and finally the tribological tests will be explained in detail.

Materials Used, Preparation of Powders and Production Scheme

Powders with physical properties of 44 (μm) particle size and 99.9% purity were used in the study. Table 1 shows the amount of samples used by weight in the powders produced and the nomenclature of the composites. The sample preparation scheme is shown in Figure 1. In the preparation of the composites, the matrix material was adjusted to be copper and mixed with the reinforcing elements whose weight percentages are given in Table 1. Before the compounding process, the materials were weighed on a balance with a sensitivity of 10^{-4} in the ratios in Table 1 with a total weight of 3 grams. The prepared powders were mixed in a magnetic grinder for 2.5 hours at 250 rpm by adding ethyl alcohol and citric acid. The resulting solution was then dried in an oven at 90 °C for 6 hours without exposure to air. After drying, the

mixture was poured into a mold lubricated with zinc stearate ($Zn(C_{18}H_{35}O_2)_2$) and test specimens were prepared in a hydraulic press at a pressure of 35 MPa.

Table 1. Nomenclature of powders and amount of additives by weight

Sample Name	Cu	B	Co
Cu	%100	-	-
Cu-B	%99	%1	-
Cu-Co	%99	-	%1
Cu-Co-B	%98	%1	%1

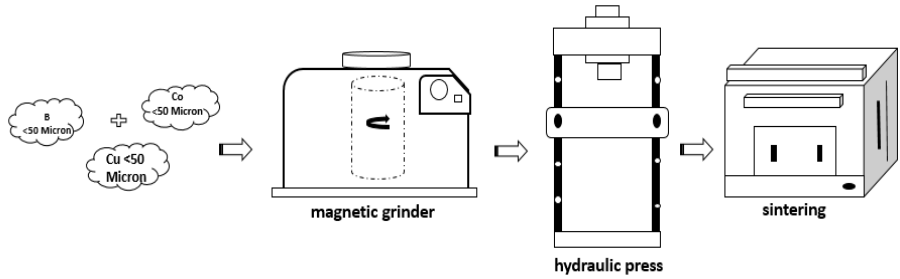

Figure 1. Preparation scheme of copper-based composites

Microstructure, Hardness, Tribology and Characterization

Figure 2 shows the process steps to be applied in microstructure, hardness, tribology and characterization of hybrid samples.

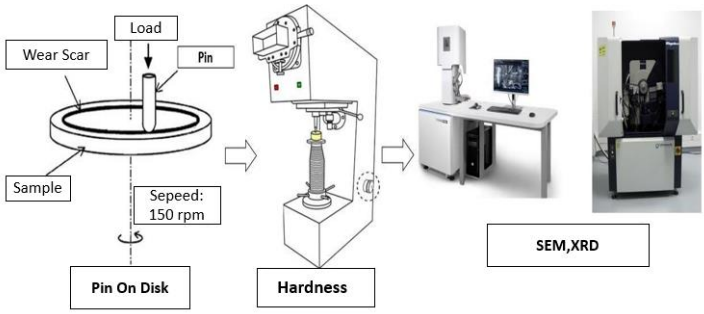

Figure 2. Flowchart

Microstructure

The microstructures of the samples, which were produced, pressed, sintered, bakelite, sanded and polished and metallographically analyzed, were examined by X-Ray Diffraction (XRD) for the determination of the reinforcing element particles distributed in the Cu matrix structure and the distribution of the powders by Scanning Electron Microscope (SEM) and Energy Dispersive X-Ray Spectrometer (EDX) analysis.

Hardness

In hardness tests, measurements were taken from 5 different points at load values between 1-10,000 g with a hardness tester and the average hardness of the composites was determined by averaging these values. The average hardness value was found in Vickers.

Tribology

Wear tests were performed with a pin-on-disk wear tester at constant load (10 N), sliding distance (1000 m) and sliding speed (150 rpm). The weight loss of the composites as a result of abrasion was measured on a balance with a sensitivity value of 10^{-4}. The measured values were recorded and weight loss graphs and coefficient of friction graphs were created for each sample according to the distance.

Characterization

As a result of the wear tests of the samples, the wear marks that occurred as a result of wear were examined and interpreted in detail in SEM analysis.

RESEARCH AND FINDINGS

The research and findings section of the hybrid composites, in which the production, characterization and tests carried out are mentioned in detail in the method section, includes the examination of the data obtained in the characterization results (XRD, SEM and EDX), the results of the hardness and wear tests of the hybrid composites and the SEM images of the wear depths occurring on the wear surfaces after wear.

XRD Results

X-ray diffraction is a non-destructive analysis method that can be used to determine the crystallographic properties of materials and the phases

they contain. As a result of X-ray diffraction applied to powder samples, properties such as grain size, primary orientation and crystal structure can be determined. The XRD diffraction patterns of the composites produced are shown in Figure 4. XRD analyses showed that each sample retained its characteristic peaks and these characteristic peaks are consistent with literature studies. After mixing, Cu and B formed the compound CuB_{24} among themselves. With the addition of reinforcing elements, the intensities of the characteristic peaks of copper changed.

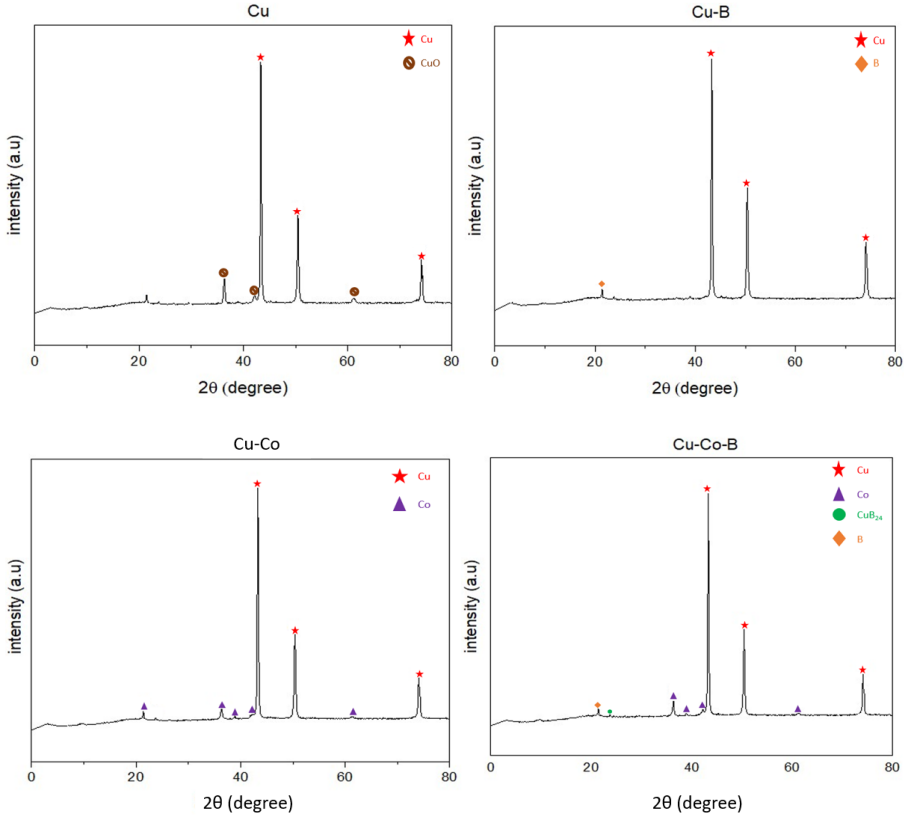

Figure 4. XRD diffraction patterns of the samples

SEM Images and EDX Analysis

SEM and EDX analysis results of the prepared hybrid composite are shown in Figure 5. In SEM images, it is seen that the reinforcing elements are homogeneously distributed on the copper matrix structure. EDX analysis also shows the formation of Co and B powders on the matrix structure.

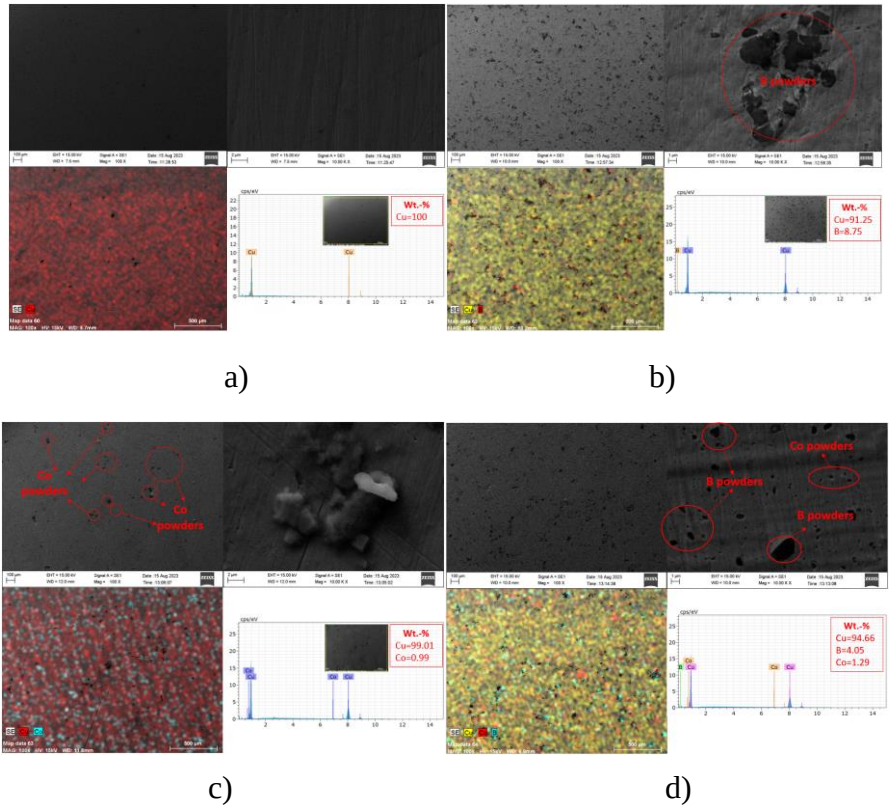

Figure 5. SEM images and EDX analysis result a) Cu, b) Cu-B, c) Cu-Co, d) Cu-Co-B

Hardness and Tribology

Oxide layers were also observed on the surfaces of the samples. In order to prevent these oxide layers from reducing the values to be obtained in tribological tests, the surfaces of the hybrid composites were prepared by sanding and polishing again. When the hardness values of the hybrid composites are examined, the average hardness values taken from 5 different points are shown in Figure 6. In hardness values, the highest hardness value was observed in Cu-B composite. In the hardness results, much higher hardness results were observed with the addition of reinforcing elements compared to pure copper composites. B and Co doping is also observed to positively affect the hardness results in literature studies. (Baco-Carles et al., 2008; Barekat et al., 2016; Cabrol et al., 2019; Li et al., 2018; Ma & Zhang, 2016; Ozgun & Dinler, 2018; Uzunsoy, 2010; Xia et al., 2013; Zepon et al., 2015). The change in weight loss and coefficient of friction values of the

hybrid composites at a total sliding distance of 1000 meters are shown in Figures (7-9). Similar results to the hardness values were observed in the wear tests. The lowest weight loss in the samples was observed in the Cu-B sample, while the reinforcement elements increased the wear resistance. Co and B additives increased the friction resistance of copper matrix specimens and decreased the average friction coefficient values (Baco-Carles et al., 2008; Barekat et al., 2016; Cabrol et al., 2019; Li et al., 2018; Ma & Zhang, 2016; Ozgun & Dinler, 2018; Uzunsoy, 2010; Xia et al., 2013; Zepon et al., 2015).

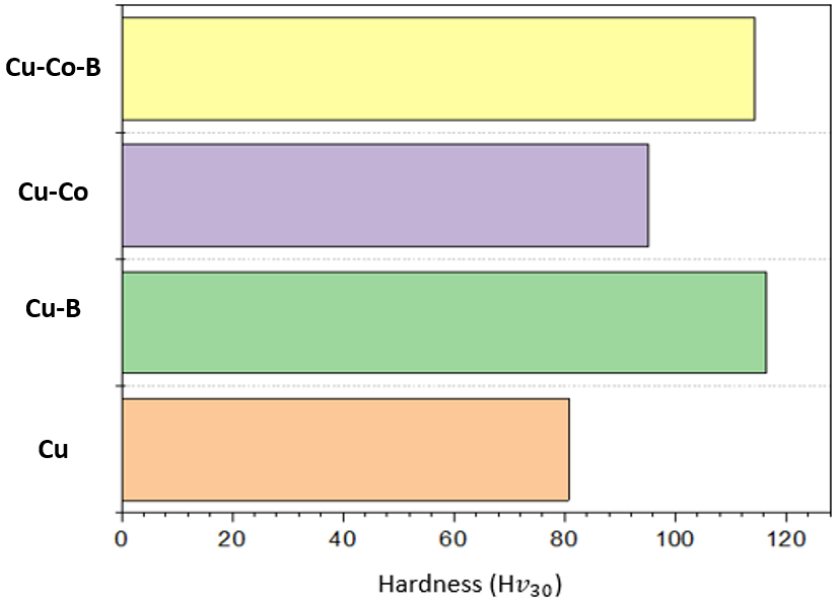

Figure 6. Hardness results

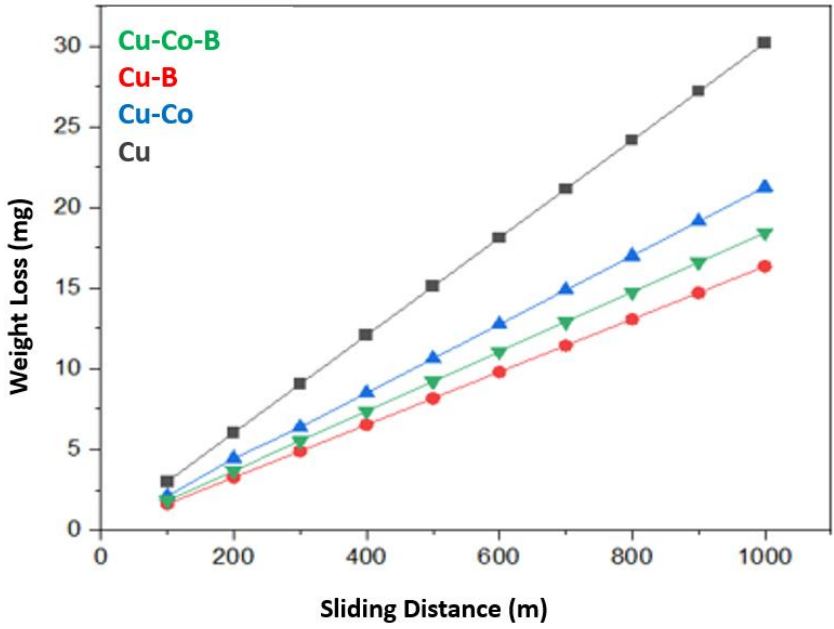

Figure 7. Wear weight loss results

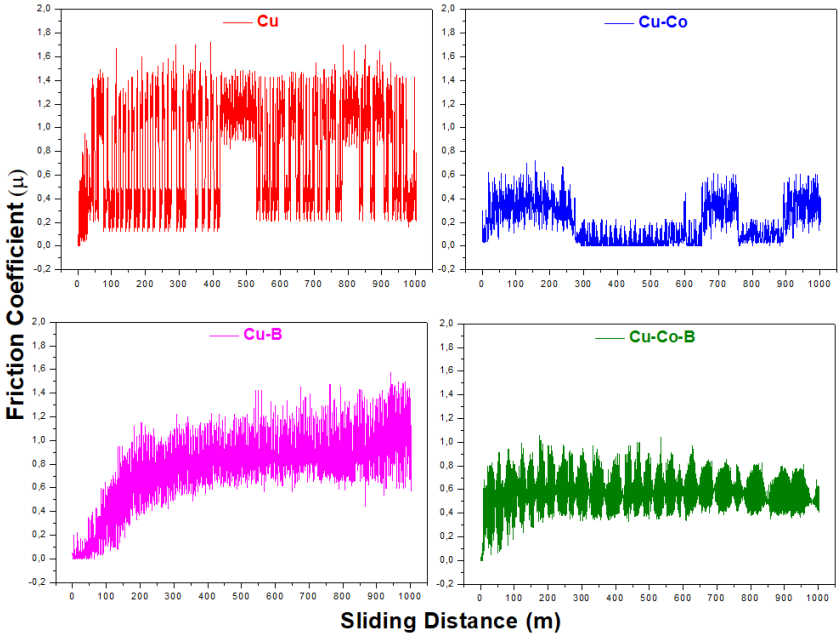

Figure 8. Coefficient of friction values

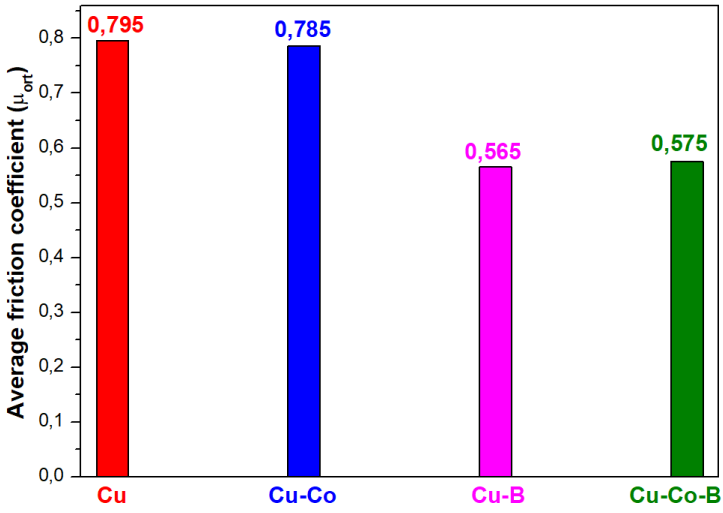

Figure 9. Average coefficient of friction values

SEM Images After Wear

SEM images of the friction coefficient values of the composites after wear are shown in Figure 10. In the wear images, it was observed that deep cracks and scars were formed on the pure Cu sample after wear. Adhesive wear mechanism was observed with the formation of deep craters in the pure Cu sample and deformation of the wear surface. With the addition of B and Co, a decrease in the wear scars and depths and a significant increase in the wear resistance of Cu-B and Cu-Co-B samples were observed. It was clearly observed in the total weight loss, friction coefficient value and SEM images after wear that the reinforcing elements significantly increased the wear of Cu matrix composites. (Baco-Carles et al., 2008; Barekat et al., 2016; Cabrol et al., 2019; Özgün & Dinler, 2018; Xia et al., 2013). Wear resistance was improved by the doping of B particles (Li et al., 2018; Ma & Zhang, 2016; Uzunsoy, 2010; Zepon et al., 2015). The best wear resistance was observed in Cu-B sample. It was observed that B reinforcement of Cu matrix composites formed a tribo layer between the wear pin and the wear sample during wear and the lubricity of B increased the resistance to wear.

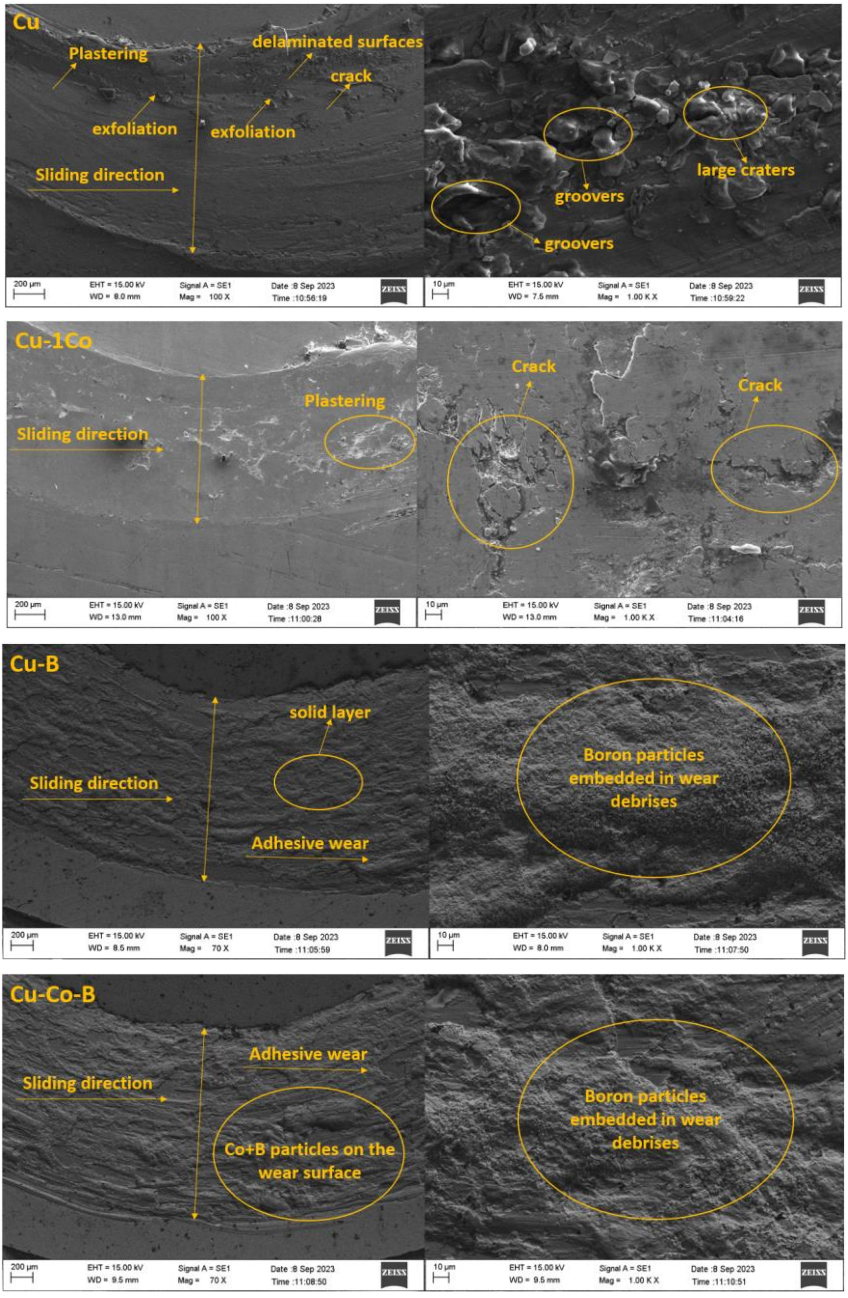

Figure 10. SEM images after wear

RESULTS

Different composites (Cu, Cu-B, Cu-1Co and Cu-Co-B) were produced by powder metallurgy production method. When the results obtained in the study are analyzed;

- XRD diffraction patterns show that the matrix material and reinforcements retain their characteristic peaks.

- SEM images and EDX results show that the powders are homogeneously distributed.

- In the hardness tests applied to the composites, 30% (Cu-B), 15% (Cu- 1Co) and 29% (Cu-Co-B) better results were obtained compared to pure Cu, respectively. The highest hardness value was observed in Cu-B composite.

- In the wear test, Co and B additives increased the wear resistance of the Cu matrix material and better results were obtained in terms of weight loss in total sliding distance and friction coefficient values.

- As a result of the tests, it was seen that studies can continue with different reinforcing elements to improve tribological properties in copper matrix composites.

REFERENCES

Baco-Carles, V., Arnal, A., Poquillon, D., & Tailhades, P. (2008). Correlation between the morphology of cobalt oxalate precursors and the microstructure of metal cobalt powders and compacts. *Powder Technology*, *185*(3), 231–238.

Barekat, M., Razavi, R. S., & Ghasemi, A. (2016). Nd: YAG laser cladding of Co–Cr–Mo alloy on γ-TiAl substrate. *Optics & Laser Technology*, *80*, 145–152.

Cabrol, E., Boher, C., Vidal, V., Rezai-Aria, F., & Touratier, F. (2019). A correlation between tribological behavior and crystal structure of cobalt-based hardfacings. *Wear*, *426*, 996–1007.

Chundru, V. R., Koona, R., & Pujari, S. R. (2019). Surface modification of Ti6Al4V alloy using EDMed electrode made with nano-and micron-sized TiC/Cu powder particles. *Arabian Journal for Science and Engineering*, *44*, 1425–1436.

Jiang, X., Liu, W., Li, Y., Shao, Z., Luo, Z., Zhu, D., & Zhu, M. (2018). Microstructures and mechanical properties of Cu/Ti3SiC2/C/graphene nanocomposites prepared by vacuum hot-pressing sintering and hot isostatic pressing. *Composites Part B: Engineering*, *141*, 203–213.

Kirik, I., Ozdemir, N., & Caligulu, U. (2013). Effect of particle size and volume fraction of the reinforcement on the microstructure and mechanical properties of friction welded MMC to AA 6061 aluminum alloy. *Kovove Mater*, *51*(4), 221–227.

Li, J., Gan, L., Liu, Y., Mateti, S., Lei, W., Chen, Y., & Yang, J. (2018). Boron nitride nanosheets reinforced waterborne polyurethane coatings for improving corrosion resistance and antifriction properties. *European Polymer Journal*, *104*, 57–63.

Lu, Y., Sagara, K., Matsuda, Y., Hao, L., Jin, Y. R., & Yoshida, H. (2013). Effect of Cu powder addition on thermoelectric properties of Cu/TiO2− x composites. *Ceramics International*, *39*(6), 6689–6694.

Ma, S., & Zhang, J. (2016). Wear resistant high boron cast alloy-A review. *Rev. Adv. Mater. Sci*, *44*(1), 54–62.

Nazeer, F., Ma, Z., Gao, L., Wang, F., Khan, M. A., & Malik, A. (2019). Thermal and mechanical properties of copper-graphite and copper-reduced graphene oxide composites. *Composites Part B: Engineering*, *163*, 77–85.

Özgün, Ö., & Akbulut, Ö. F. (2017). The Effect of element additions on the

microstructure and the mechanical properties of cobalt based superalloys produced via powder metallurgy technique. *Sakarya University Journal of Science*, *21*(2), 223–231.

Özgün, Ö., & Dinler, İ. (2018). Production and characterization of WC-reinforced Co-based superalloy matrix composites. *Metallurgical and Materials Transactions A*, *49*, 2977–2989.

Sap, E. (2021). Microstructure and mechanical effects of Co–Ti powder particles on Cu matrix composites. *Russian Journal of Non-Ferrous Metals*, *62*, 107–118.

Schubert, T., Trindade, B., Weißgärber, T., & Kieback, B. (2008). Interfacial design of Cu-based composites prepared by powder metallurgy for heat sink applications. *Materials Science and Engineering: A*, *475*(1–2), 39–44.

Uygur, I. (2007). Fe-Cu-C çeliklerine mangan ilavesinin mekanik özelliklere etkisi. *Gazi Üniversitesi Mühendislik Mimarlık Fakültesi Dergisi*, *22*(3).

Uzun, M., & Usca, U. A. (2018). Effect of Cr particulate reinforcements in different ratios on wear performance and mechanical properties of Cu matrix composites. *Journal of the Brazilian Society of Mechanical Sciences and Engineering*, *40*, 1–9.

Uzunsoy, D. (2010). Investigation of dry sliding wear properties of boron doped powder metallurgy 316L stainless steel. *Materials & Design*, *31*(8), 3896–3900.

Wang, H., Fang, Z. Z., & Sun, P. (2010). A critical review of mechanical properties of powder metallurgy titanium. *International Journal of Powder Metallurgy*, *46*(5), 45–57.

Xia, Y., Yu, P., Schaffer, G. B., & Qian, M. (2013). Cobalt-doped Ti–48Al–2Cr–2Nb alloy fabricated by cold compaction and pressureless sintering. *Materials Science and Engineering: A*, *574*, 176–185.

Yalcin, B., & Varol, R. (2008). Production of Ti-6Al-4V and Ti-5-Al-2.5 Fe Alloys Via Powder Metalurgy Method and Investigation of its Some Mechanical Properties. *JOURNAL OF POLYTECHNIC-POLITEKNIK DERGISI*, *11*(3), 235–241.

Zepon, G., Nascimento, A. R. C., Kasama, A. H., Nogueira, R. P., Kiminami, C. S., Botta, W. J., & Bolfarini, C. (2015). Design of wear resistant boron-modified supermartensitic stainless steel by spray forming process. *Materials & Design*, *83*, 214–223.

Zheng, H. X., Mentz, J., Bram, M., Buchkremer, H. P., & Stöver, D. (2008).

Powder metallurgical production of TiNiNb and TiNiCu shape memory alloys by combination of pre-alloyed and elemental powders. *Journal of Alloys and Compounds*, *463*(1–2), 250–256.

BÖLÜM 5

EXPLORING THE INTERPLAY OF STRUCTURAL AND MAGNETIC PROPERTIES IN TECHNOLOGICALLY ENHANCED Eu-DOPED $GdMnO_3$ MATERIALS

Dr. Jamal Eldin Fadoul Mohammed IBRAHIM[1]
DOI: https://dx.doi.org/10.5281/zenodo.8428496

[1] University of Miskolc, Doctoral School of Material Science and Technology, Institute of Ceramic and Polymer Engineering, Faculty of Material Science and Engineering, Miskolc, Hungary (Macaristan). jamalfadoul@gmail.com, ORCID ID: 0000-0003-2479-5955

1. INTRODUCTION

Rare earth manganese compounds with a perovskite structure have remained a subject of intensive exploration and investigation within the scientific community for several years. Their unique combination of ferroelectric and ferromagnetic properties has rendered them objects of great interest, with the potential for groundbreaking applications. At the forefront of this field is the compound $REMnO_3$, which exhibits the ability to crystallize in two distinct perovskite structures: hexagonal and orthorhombic. Among these, the orthorhombic structure holds particular significance as it contributes to the formation of a remarkable class of materials known as magnetoelectric multiferroics, a category characterized by the simultaneous presence of ferroelectric and ferromagnetic orders. Looking more closely at these compounds, two noteworthy structures, $HoMnO_3$ and $GdMnO_3$, have garnered substantial attention due to their remarkable behavior at low temperatures. These materials exhibit intriguing properties that can be further enhanced and tailored through the application of an external electric field. This unique characteristic bestows upon them the distinction of being magnetoelectric materials, where the interplay between electrical and magnetic phenomena can be harnessed for a range of potential applications (Cheng and Mostovoy, 2007; Wang, Liu and Ren, 2009; Goto et al., 2004).

The ability to modify the properties of $HoMnO_3$ and $GdMnO_3$ structures through the application of an electric field underscores the immense potential of magnetoelectric materials. This manipulation provides a means to control and fine-tune their behavior, paving the way for advancements in diverse fields such as electronics, data storage, and sensing technologies. By exploiting the interplay between ferroelectric and ferromagnetic orders, researchers aim to unlock novel ways to harness and utilize the fundamental forces of nature for practical applications (Ibrahim, 2015).

Beyond their considerable potential within the realm of advanced science, multiferroic materials have garnered significant attention owing to their distinctive ability to display a robust interplay between ferroelectric ordering and magnetic polarization. This captivating characteristic has not only elevated their prospects for groundbreaking applications but has also piqued the fundamental curiosity of the research community.

A ferroic substance essentially demonstrates either ferromagnetic, ferroelectric, or ferroelastic orders, and its distinctiveness often manifests

through the clear presence of a well-defined hysteresis loop when subjected to electric, magnetic, or mechanical forces. (Ibrahim, 2015; Ibrahim, Mergen, Sahin and Basheer, 2017). "Multiferroic" refers to a substance that encompasses multiple foundational ferroic behavior mechanisms, such as ferroelectricity, ferromagnetism, and ferroelasticity, within a singular phase (Schmid, 1994). With the consideration of the antiferroic concept, the term "multiferroic" has been broadened to encompass any material capable of presenting the simultaneous occurrence of diverse sequences, including magnetic, electric, and ferroelectric phenomena, all within a solitary phase (Pandu, 2014).

Multiferroic materials serve as an exemplary illustration of a cutting-edge class of smart materials, adept at seamlessly integrating multiple attributes within a unified phase. (Ederer and Spaldin, 2004).

Lately, the classification of multiferroic materials has bifurcated into two primary categories: single-phase multiferroics and multiferroic composites. Single-phase multiferroics, as recognized by researchers like Wang, Hu, Lin, and Nan (2010), represent materials that seamlessly bridge the realms of ferroelectricity and ferromagnetism within a singular phase. Notably, these materials exhibit relatively modest polarization magnitudes and weak degrees of magnetoelectric coupling. A diligent pursuit of knowledge and development in the realm of single-phase multiferroics has yielded substantial contributions across diverse fields (Wang et al., 2010).

In contrast, the domain of multiferroic composites entails an indirect fusion of ferroelectric and ferromagnetic attributes, orchestrated through the intricate cross-interaction between distinct sequences present within the composite material, facilitated by mechanical strain. This unique amalgamation instigates a remarkable coupling between the two phases, harnessing their combined potential for magnetic-piezoelectric interfaces, while individually each phase might lack the ability to establish magnetoelectric coupling. The manifestation of the magnetoelectric effect in composites is intricately hinged on the intricate microstructure of the composite and the intricate interplay of magnetic-piezoelectric interfaces, a phenomenon explored in depth by Nan et al., (Nan et al., 2008).

Further discernment reveals that single-phase multiferroics can be delineated into discrete typologies based on their crystallographic orientation and chemical composition. Noteworthy categories encompass the perovskite

structure, rare earth manganites exemplified by $REMnO_3$ (with RE denoting elements such as Ho, Lu, Y, Gd, and Sc), $BaMF_4$ compounds where M encapsulates elements such as Mg, Mn, Fe, Co, Ni, Zn, and the $REMn_2O_5$ compounds (with RE embodying elements like Y, Tb, Dy, and Ho). This multifaceted classification framework provides a comprehensive panorama of the diverse landscape of single-phase multiferroics, elucidating the multifarious pathways through which these materials manifest their captivating properties.

The potential future applications of multiferroic materials stem from their unique coexistence of ferroelectric and (anti)ferromagnetic orders, paving the way for an array of innovative technical uses. Notably, these materials offer prospects in emerging multi-state memory technologies, where they can serve as both conventional magnetic data storage tools and pioneers of transformative methods. Traditionally, data writing involves the application of magnetic fields, whereby the electromagnet's high leakage field in the write head controls the magnetization direction of each data bit. This conventional process can be enhanced through the utilization of the magnetoelectric effect, allowing the manipulation of magnetization using electric fields. This breakthrough not only presents the opportunity for high-density, low-power data storage devices but also unlocks novel avenues for future memory technologies (Gerhard et al., 2010). Furthermore, the magnetoelectric properties intrinsic to multiferroic materials hold significant potential for integration within an assortment of sensing applications, particularly in the realms of integrated optics and fiber optic communication. Through the incorporation of multiferroic materials, sensors utilizing magnetoelectric properties can be engineered to facilitate advanced functionalities in film waveguides. These innovative developments align with the work of Venevtsev, Gagulin, and Zhitomirsky (1987) and showcase the broader scope of possibilities for harnessing the magnetoelectric properties of multiferroic materials in diverse sensor applications (Venevtsev et al., 1987).

In essence, the symbiotic fusion of ferroelectric and (anti)ferromagnetic attributes in multiferroic materials lays the foundation for a future brimming with technological advancements across data storage, sensing technologies, and integrated optics, thereby epitomizing the multifaceted potential inherent in these remarkable substances.

Enhanced electrical and magnetic attributes within the $REMnO_3$ compound can be achieved through strategic doping with suitable elements.

This deliberate introduction of dopants into either the hexagonal or orthorhombic regions of $REMnO_3$ has been proven to induce disruption within the Mn-O network. This disruption has a profound impact on not only the compound's magnetic, electric, and multiferroic properties but also its structural characteristics.

Gaining comprehensive insights into the internal arrangement of materials holds paramount importance in the development and application of advanced materials. This research endeavors to create a singular-phase compound by substituting Eu for Gd in $Gd_{1-x}Eu_xMnO_3$ compositions with designated values of x, specifically 0.2 and 0.8. The preparation of samples involves the solid-state reaction method. Employing X-ray diffraction (XRD) and scanning electron microscopy (SEM) enables the investigation of the resolution limit associated with each contribution of Eu. Additionally, the magnetic properties are assessed through employment of the VSM device. This study meticulously delves into the influence of doping on both the crystal structure and magnetic attributes, revealing compelling insights (Ibrahim, 2015).

The profound implications of these multiferroic ceramic materials extend to novel functionalities and promising applications in a multitude of domains, including microelectronics, information technology, sensors, memories, converters, and data storage devices for radar systems, among others. The synthesis of such high-tech materials stands poised to significantly bolster the technological foundation of nations, yielding substantial contributions to their overall infrastructural advancements.

2. MATERIALS AND METHODS

In this section, technique used to synthesize Eu doped $GdMnO_3$ ceramics is explanined. Eu doped to Gd in $GdMnO_3$ through $Gd_{1-x}Eu_xMnO_3$ compositions. Characterization techniques used structural identification of doped samples will also be described in this section.

2.1 Synthesis of $Gd_{1-x}Eu_xMnO_3$

The synthesis of single-phase doped $Gd_{1-x}Eu_xMnO_3$ (with x values of 0.2 and 0.8) ceramic powders followed the conventional solid-state reaction route, as depicted in Figure 1. The starting materials consisted of high-purity Gd_2O_3 (99.9%; Alfa Aesar), Mn_2O_3 (98%; Alfa Aesar), and Eu_2O_3 (99.9%; Alfa Aesar) powders, all commercially available and of analytical purity. Precise amounts of these compounds were meticulously weighed to achieve

the desired $Gd_{1-x}Eu_xMnO_3$ compositions (x=0.2 and 0.8), and the mixture was thoroughly blended in ethyl alcohol for a duration of 6 hours, employing zirconium balls within a plastic container. Subsequently, the obtained slurry was subjected to drying in an oven at 95°C for 24 hours, followed by calcination at 600°C for 10 hours. The calcined powder, agate in nature, was further crushed and ground into a fine powder. To explore phase development, this powdered material underwent heat treatment at various temperatures ranging from 1000 to 1350°C, utilizing a heating and cooling rate of 300°C/hour over a duration of 10 hours.

Cylindrical pellets, featuring dimensions of 10 mm in diameter and 2 mm in thickness, were meticulously prepared utilizing a uniaxial pressing device exerting a pressure of 10 MPa. The sintering process was carried out at 1350°C for a duration of 20 hours, employing a heating and cooling rate of 120°C/hr. These sintering operations were executed using a high-temperature programmable furnace.

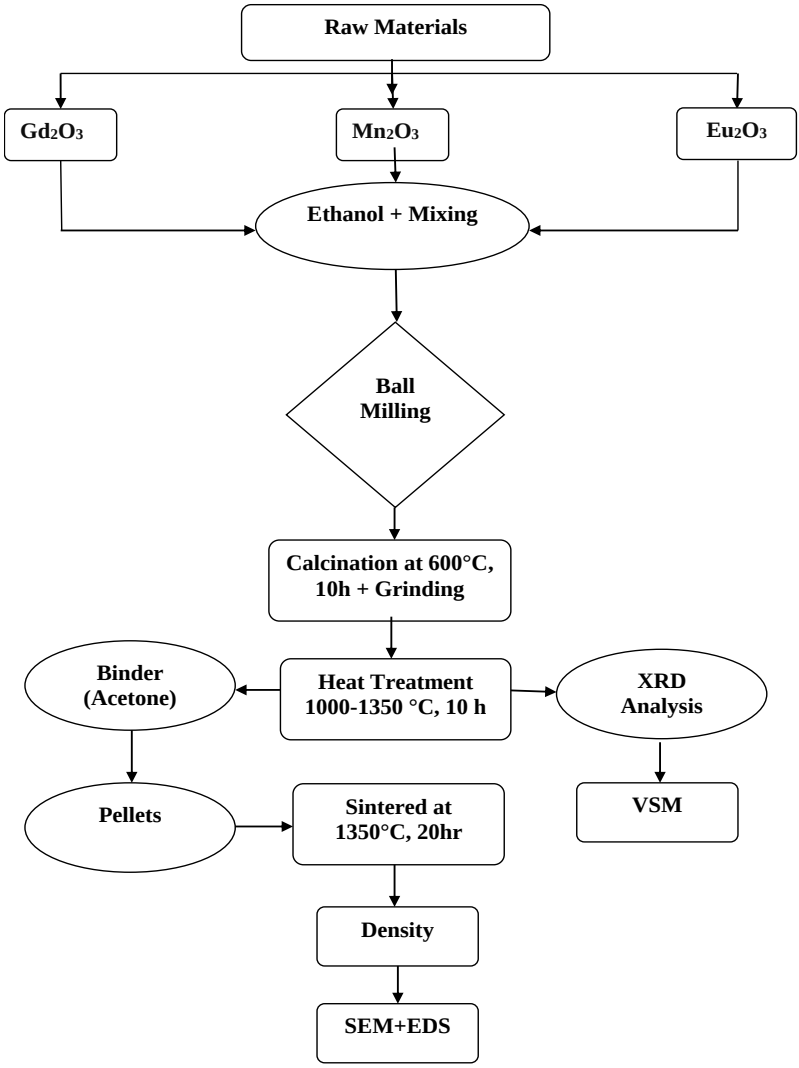

Figure 1: Diagram of the process for synthesis of $Gd_{1-x}Eu_xMnO_3$ material (Ibrahim, 2015).

Following the sintering process, the resulting samples underwent characterization through X-ray diffraction (XRD) and scanning electron microscopy (SEM). Additionally, the magnetic hysteresis behavior of the Eu-doped $GdMnO_3$ samples ($Gd_{1-x}Eu_xMnO_3$) was investigated at low temperatures using magnetic hysteresis measurements conducted with a Vibrating Sample Magnetometer (VSM).

2.2. Characterization

In this investigation, the characterization of sintered ceramic materials doped with Eu in $GdMnO_3$ was carried out utilizing X-ray diffractometry (XRD) and scanning electron microscopy (SEM) which were integral in comprehending the material's structural properties and composition (Qasrawi, Sahin, Abed and Emek, 2021; Qasrawi, Sahin, Emek, Kartal and Kargin, 2019; Şahin, Emek, Ibrahim et al., 2023). X-ray diffraction (XRD) analysis is a potent method employed for the identification of crystalline phases present within a sample, while also furnishing insights into phase concentration, the extent of non-crystalline components, crystal size, and ultimately, chemical composition (Şahin and Emek, et al., 2023; Şahin, 2022; Şahin, et. al., 2023). In the process of sample measurement, the sintered pellets undergo comminution in an agate mortar, transforming them into fine powder. Subsequently, the resulting powder is loaded into a sample holder and subjected to thorough characterization using the Bruker D2 PHASER X-ray diffractometer (XRD). The samples are subjected to a scanning range spanning 2θ: 10-70°, employing a scanning speed of 1°/min and a step size of 0.01016°. The employed Cu-Kα radiation (λ=1.54184 Å) facilitates this analytical procedure. The primary objective of this analysis is twofold: to ascertain the solubility limit of each introduced additive within the sintered pellet and to discern the possible formation of any secondary phases. The comprehensive analysis is conducted utilizing the FullProf software, enabling computer-based evaluation.

To delve into surface characteristics, scanning electron microscopy (SEM) is harnessed, employing the JEOL5910 LV instrument. The SEM device facilitated the detection of even trace amounts of potential secondary phases. Moreover, it facilitated the examination of microstructures and morphological features (Qasrawi et al., 2021; Qasrawi et al., 2019; Şahin et al., 2023). As a preliminary step to SEM examination, the fractured surfaces of the pellets undergo gold coating through the SC7680 Super Coater. With these preparations in place, the fractured surfaces of the manufactured samples undergo meticulous investigation at varying magnifications utilizing secondary and backscattered electrons.

Furthermore, an exploration of the low-temperature (10 K) magnetic properties of the Eu-doped $GdMnO_3$ samples ($Gd_{1-x}Eu_xMnO_3$) is conducted through the application of a vibrating sample magnetometer (VSM) (Şahin et al., 2023). The VSM device, as employed by Şahin, Emek, Ibrahim (2023),

conducted magnetic hysteresis measurements utilizing a Cryogenic Limited PPMS (Physical Properties Measurement System) setup.

This device, meticulously calibrated with certified reference materials like nickel and palladium, employs a closed circuit Helium system to attain extremely low temperatures, starting from room temperature (Ibrahim, 2015; Bayrak, 2012), allowing for thorough magnetic and electrical characterization of dust samples under magnetic fields as high as 5 Tesla. The resultant magnetization of the sample, as a function of the applied magnetic field (M-H), is meticulously obtained through this investigation. This comprehensive approach encompasses a multi-faceted analysis, combining XRD, SEM, and VSM techniques, to unravel the intricate characteristics and behaviors of the Eu-doped $GdMnO_3$ ceramic samples.

3. RESULTS AND DISCUSSION

The necessary characterizations of the new doped material have been carried out in this section, by controlling the microstructure of the new material, the desired properties are tried to be achieved.

3.1. XRD Analysis of Eu doped $GdMnO_3$

Figure 2 depicts the X-ray diffraction (XRD) pattern of both undoped and A site-doped $Gd_{1-x}Eu_xMnO_3$ ceramics (with x values of 0.2 and 0.8), subjected to heat treatment at 1350°C for 24 hours. It is evident from all the samples' XRD patterns that a singular perovskite structure prevails, evidenced by the precise concordance between the observed peaks and the anticipated positions. Notably, no additional peaks indicative of secondary phase formation are discernible, signifying a monophasic composition (Figure 2). This observation underscores the successful integration of Eu, even in higher concentrations (x=0.8), within the lattice, resulting in a seamless incorporation into the solid solution.

Upon scrutinizing the peaks more closely, a subtle leftward shift in peak positions becomes apparent with the elevation of doping concentration. This shift is attributed to the expansion of the lattice parameter, resulting in an augmented volume of the unit cell.

This expansion is a direct consequence of the replacement of Gd with Eu, where the ionic radius of Eu (2.65 Å) surpasses that of Gd (2.54 Å). The incremental increase in unit cell parameters due to doping concentration

increment can lead to a slight perturbation in the lattice, potentially inducing alterations in the crystal structure.

This modulation holds the potential to significantly influence the material's magnetic properties, establishing a crucial connection between lattice changes and magnetism. The calculation of lattice parameters and unit cell volume is performed using the FullProf program, with the resultant values presented in Table 1.

This meticulous analysis not only reaffirms the structural integrity of the doped ceramics but also elucidates the intricate interplay between doping, lattice parameters, and resulting material properties.

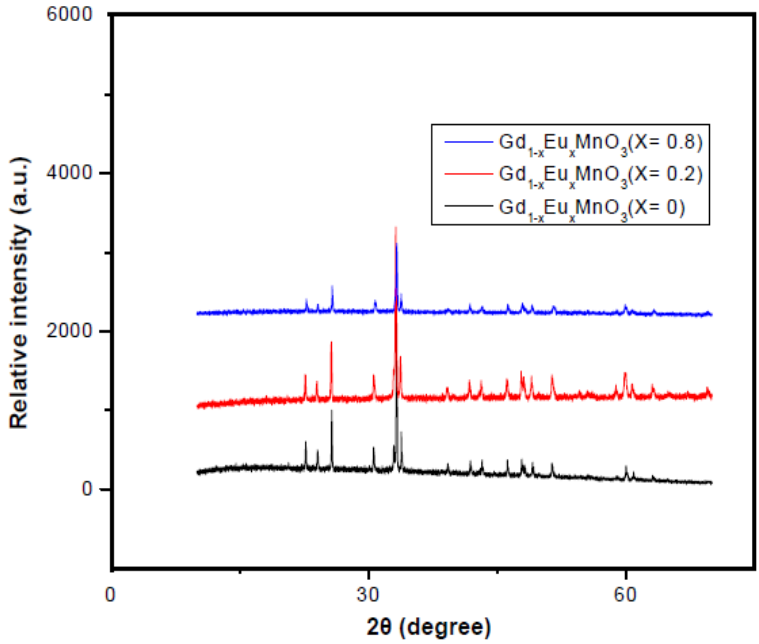

Figure 2: XRD patterns of $Gd_{1-x}Eu_xMnO_3$ ceramic compounds (x=0, 0.2, 0.8) at room temperature after a 24 hour heat treatment.

The undoped $GdMnO_3$ specimen demonstrates a lattice parameter in close proximity to the anticipated theoretical value, as gleaned from the PDF reference file (PDF No: 25-337). Concurrently, an elevation in Eu concentration leads to a corresponding increase in the lattice parameter, a consequence of the larger ionic radius of Eu (2.56 Å) relative to that of Gd (2.54 Å).

Furthermore, for instances of diminished Eu content (x=0.2), the X-ray diffraction (XRD) pattern aligns with that of $GdMnO_3$. In contrast, the XRD pattern corresponding to higher concentrations of Eu-doped $GdMnO_3$ (x=0.8) demonstrates a notable concordance with $EuMnO_3$ (PDF No: 25-335). This compelling observation substantiates a significant shift, wherein as the content of Eu increases, the compounds undergo a transition to $EuMnO_3$ instead of remaining as $GdMnO_3$.

In summary, this progression underscores a distinct transformation in the compounds, indicating their conversion to $EuMnO_3$ from $GdMnO_3$, a shift directly linked to the augmenting concentration of Eu within the composition. This insight provides valuable implications for comprehending the intricate interplay between composition and crystalline structure in these materials.

Tablo 1. Determined lattice characteristics of Eu doped $GdMnO_3$ samples ($Gd_{1-x}Eu_xMnO_3$ ceramics where x= 0.2 and 0.8 heat treated at 1350°C for 24 h) by utilizing FullProf

Composition	a (Å)	b (Å)	c (Å)	Volume $(Å)^3$	Space group	Crystal type
$GdMnO_3$	5.31	5.84	7.43	230.41	Pnma	orthorhombic
$Gd_{0.8}Eu_{0.2}MnO_3$	5.3141	5.8432	7.4219	230.46	Pnma	orthorhombic
$Gd_{0.2}Eu_{0.8}MnO_3$	5.3366	5.842	7.453	232.33	Pnma	orthorhombic

3.2. SEM Analysis of Eu doped $GdMnO_3$

The scanning electron microscope (SEM) serves as a versatile apparatus, effectively unveiling topographical attributes, morphological characteristics, and phase distribution across the sample surface.

As a potent magnification tool, the SEM employs two distinct imaging modalities: secondary electrons (SE) and backscattered electrons (BSE), both instrumental in material imaging and analysis.

As illustrated in Figure 3, the secondary and backscattered electron micrographs of $Gd_{0.8}Eu_{0.2}MnO_3$ and $Gd_{0.2}Eu_{0.8}MnO_3$ (comprising the $Gd_{1-x}Eu_xMnO_3$ compound with doping concentrations x=0.2 and x=0.8) demonstrate the microstructural features.

The SEM micrographs affirm the absence of secondary phases or impurities, corroborating findings from X-ray diffraction (XRD) analyses.

Notably, the backscattered electrons do not reveal any discernible phase contrast.

The grain sizes evident in samples with x values of 0.2 and 0.8 fall within the range of 4 to 11 micrometers and 5 to 12 micrometers, respectively.

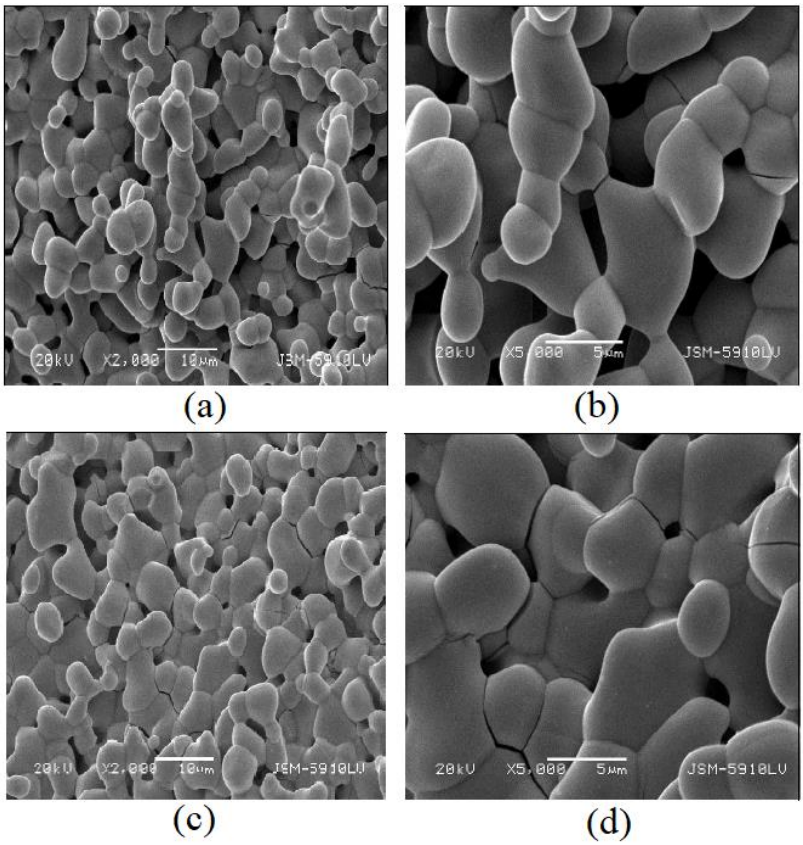

Figure 3: SEM micrographs of Eu doped $GdMnO_3$, ($Gd_{1-x}Eu_xMnO_3$ ceramic where x= 0.2 and x= 0.8 sintered at 1350°C for 24h). a) specimen at ×2000 SEI of $Gd_{0.8}Eu_{0.2}MnO_3$, b) specimen at x5000 SE of $Gd_{0.8}Eu_{0.2}MnO_3$, c) specimen at x2000 SEI of $Gd_{0.2}Eu_{0.8}MnO_3$, d) specimen at x5000 SEI of $Gd_{0.2}Eu_{0.8}MnO_3$.

This observation underscores a consistent grain size across both compositions, indicating that doping does not induce significant alterations in grain dimensions.

This consistent grain size distribution contributes valuable insights into the influence of doping on the material's microstructure.

3.3. Magnetic Characteristics of Eu doped $GdMnO_3$

The assessment of magnetic hysteresis involves the utilization of a Cryogenic Limited PPMS (Physical Properties Measurement System) device. Employing the Vibrating Sample Magnetometer (VSM) measurement technique, this assessment entails the determination of magnetic properties within a designated magnetic field range, either at room temperature or at a specific temperature setting (Şahin et al., 2023; İbrahim, 2015). The Vibrating Sample Magnetometer (VSM) serves as a pivotal tool for magnetic material characterization.

To comprehensively explore the impact of Eu additives on magnetic characteristics, the magnetic evaluation of Eu-doped samples is conducted at an exceptionally low temperature, specifically 10 K.

This meticulous approach enables an in-depth understanding of the intricate relationship between the introduction of Eu and the resultant alterations in the material's magnetic behavior.

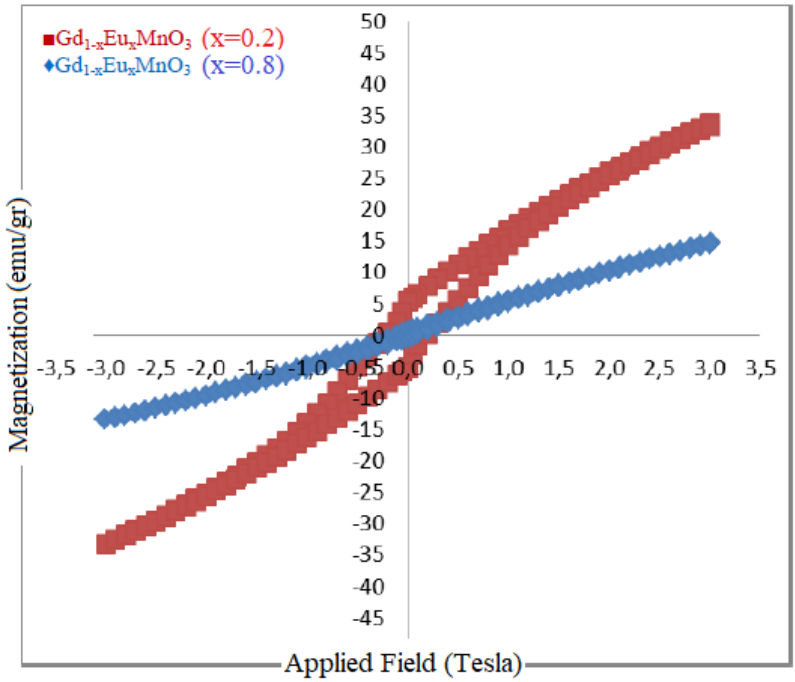

Figure 4: $Gd_{1-x}Eu_xMnO_3$ ceramic material magnetic hysteresis loops after a 24 hour heat treatment at 1350°C (x=0.2 and 0.8).

Figure 4 illustrates the magnetization response of the $Gd_{1-x}Eu_xMnO_3$ material, specifically for x values of 0.2 and 0.8, with respect to a varying magnetic field (M-H) at a notably low temperature of 10 K. The results present a striking ferromagnetic phenomenon within the x=0.2 sample, evidenced by a saturation magnetization (Ms) of 35 emu/g. However, a discernible shift in magnetic behavior occurs with a dopant concentration of x=0.8, leading to a marked reduction in Ms to approximately 14 emu/g. This pronounced shift marks a significant transition from ferromagnetic to paramagnetic behavior, exemplifying the sensitivity of magnetic properties to dopant concentration.

The superior ferromagnetic behavior apparent in the x=0.2 sample can be attributed to the beneficial substitution of Eu, which effectively suppresses spiral spin modulation, thereby promoting a more coherent and robust ferromagnetic state (Uniyal, 2009). Conversely, as x exceeds the threshold of 0.2, the structural perturbations introduced by higher dopant concentrations disrupt the intricate spin regulation mechanism, consequently distorting the ferromagnetic behavior and precipitating a measurable decrease in Ms (Uniyal, 2009). These findings provide valuable insights into the interplay between dopant concentration, crystal structure, and resulting magnetic behaviors, shedding light on the underlying mechanisms that govern the material's magnetic response.

4. CONCLUSION

This study delved into the influence of Eu doping on the structural and magnetic attributes of $GdMnO_3$ multiferroic ceramics. Employing the conventional solid-state reaction method, an array of orthorhombic $Gd_{1-x}Eu_xMnO_3$ powder specimens was meticulously generated. By varying the reaction conditions, particularly the heat treatment temperature, the resulting samples exhibited diverse morphologies, structures, and compositions. Noteworthy alterations were observed within these perovskite-based multiferroic ceramics, emphasizing the profound effects of Eu doping and controlled manipulation.

Thorough characterization encompassed X-ray diffraction (XRD), scanning electron microscopy (SEM), and Vibrating Sample Magnetometer (VSM) analyses. The strategic incorporation of Eu into the A-sites exerted a

discernible influence on crystal structures, primarily attributed to variations in atomic dimensions of the doped elements. Magnetic evaluation of Eu-doped samples, conducted at ultra-low temperatures down to 10 K, unveiled a compelling interplay between ferromagnetic and antiferromagnetic ordering. Notably, $GdMnO_3$ samples doped with Eu showcased intriguing ferromagnetic tendencies at specific doping concentrations, potentially stemming from subtle structural perturbations within the lattice.

The emerging Eu-doped $GdMnO_3$ systems exhibit significant shifts in magnetic properties, stemming from the induced structural modifications. This observation underscores the potential of these materials for multiferroic applications, presenting enhanced ferromagnetic characteristics. As a result of these magnetic and structural adjustments, considering alternative doping strategies may offer avenues to further tailor and amplify the multiferroic attributes of orthorhombic $Gd_{1-x}Eu_xMnO_3$. This investigation advances our comprehension of Eu doping as a potent avenue for harnessing desirable properties in multiferroic ceramics, paving the way for innovative applications and tailored material design.

5. ACKNOWLEDGE

This study was dedicated to memory of Prof. Dr. Ayhan Mergen. My master’s degree data was used in the study. I would also like to thank Prof. Dr. Ayhan Mergen's doctoral student Dr. Ethem İlhan ŞAHİN for their help.

REFERENCES

Bayrak, A. (2012). *Manyetik nano parçacıkların (MNP) kontrollü sentezi ve yüzey modifikasyonu ile polimerleşme tepkimelerinde kullanımları*. İnönü Üniversitesi Fen Bilimler Enstitüsü Kimya Anabilim Dalı, Malatya.

Cheong, S. W., Mostovoy, M. (2007). Multiferroics: a magnetic twist for ferroelectricity. *Journal of Nature materials*, 6, 13-20.

Ederer, C. and Spaldin, N. A. (2004). A new route to magnetic ferroelectrics. *Nature Materials*, 3, 849-851.

Gerhard, L., Yamada, T. K., Balashov, T., Takacs, A. F., Wesselink, R. J. H., Däne, M., Fechner, M., Ostanin, S. A., Ernst, A., Mertig, I. and Wulfhekel. W. (2010). Magnetoelectric coupling at metal surfaces. *Nature nanotechnology*, 5(11), 792-797.

Goto, T., Kimura, T., Lawes, G., Ramirez, A. P., Tokura, Y. (2004). Ferroelectricity and giant magnetocapacitance in perovskite rare-earth manganites. *Journal of Physical Review Letters*, 92(25), 257201.

Ibrahim, J. F. M., Mergen, A., Sahin, E. İ., Basheer, H. S. (2017). The effect of europium doping on the structural and magnetic properties of $GdMnO_3$ multiferroic ceramics. *Advanced Ceramics Progress*, 3(4), 1-5.

Ibrahim, J. E. (2015). *Enhancement of Structural and Magnetic Properties of Eu and Fe Doped $GdMnO_3$ and Cr Doped $HoMnO_3$ Multiferroic Ceramics*, Master Thesis, Marmara University Institute For Graduate Sturdies In Pure and Applied Sciences, İstanbul-Turkey.

Nan, Ce-Wen, Bichurin, M. I., Dong, S., Viehland, D., Srinivasan, G. (2008). Multiferroic magnetoelectric composites: historical perspective, status, and future directions. *Journal of Applied Physics*, 103, 031101.

Pandu, R. (2014). $CrFe_2O_4$–$BiFeO_3$ perovskite multiferroic nanocomposites–A Review. *Material Science Research India*, 11(2), 128-145.

Qasrawi, A. F., Sahin, E. İ., Abed, T. Y., Emek, M. (2021). Structural and dielectric properties of $Ba_{1-x}La_x(Zn_{1/3}Nb_{2/3})O_3$ solid solutions. *Phys. Status Solidi B*, 258, 2000419-2000436.

Qasrawi, A. F., Sahin, E. İ, Emek, M., Kartal, M. and Kargin, S. (2019). Structural and dielectric performance of the $Ba(Zn_{1/3}Nb_{2/3-x}Sb_x)O_3$ perovskite ceramics. *Materials Research Express*, 6, 095095.

Schmid, H. (1994). Multi-ferroic magnetoelectrics. *Ferroelectrics*, 162(1), 317-338.

Şahin, E. İ., Emek, M., Ibrahim, J. E. F. M. *et al.* (2023). Shielding effectiveness performance of polyaniline-$NiFe_2O_4$:Cu composites for sub-8 GHz applications. *Optical and Quantum Electronics,* 55, 500.

Şahin E. İ. (2022). Microwave electromagnetic shielding effectiveness of $ZnNb_2O_6$-chopped strands composites for radar and wideband (6.5-18 GHz) applications. *Lithuanian Journal of Physics*, 62(3), 161-170.

Şahin, E. İ., Emek, M., Ibrahim, J. E. F. M. (2023). *Instrumental measurements laboratory* (1st ed.). Iksad Publishing House.

Uniyal, P., Yadav, K. L. (2009). Room temperature multiferroic properties of Eu doped $BiFeO_3$. *Journal of Applied Physics*, 105, 07D914.

Venevtsev, Y. N., Gagulin, V. V., Zhitomirsky, I. D. (1987). Material science aspects of seignette-magnetism problem, *Ferroelectrics*, 73(1), 221-248.

Wang, K. F., Liu, J. M., Ren, Z. F. (2009). Multiferroicity: the coupling between magnetic and polarization orders. *Journal of Advances in Physics*, 58, 321-448.

Wang, Y., Hu, J., Lin, Y., Nan, C.-W. (2010). Multiferroic magnetoelectric composite nanostructures. *NPG Asia Materials*, 2, 61-68.

CHAPTER 6

ROCKET MOTOR THRUST ANALYSIS WITH CFD

Assist. Prof. Dr. Feridun KARAKOÇ[1]

Fatih Enes ALP[2]

Res. Assist. Dr. Melih CANLIDİNÇ[3]

Res. Assist. Ahmet DAYANÇ[4]

DOI: https://dx.doi.org/10.5281/zenodo.8428569

[1] Assist. Prof.; Kutahya Dumlupinar University Faculty of Engineering Department of Mechanical Engineering. feridun.karakoc@dpu.edu.tr ORCID No: 0000-0002-6210-4070

[2] Student; Kutahya Dumlupinar University Faculty of Engineering Department of Mechanical Engineering. fatih.alp@ogr.dpu.edu.tr

[3] Kutahya Dumlupinar University Faculty of Engineering Department of Mechanical Engineering. melih.canlidinc@dpu.edu.tr ORCID No: 0000-0002-4011-9490

[4] Kutahya Dumlupinar University Faculty of Engineering Department of Mechanical Engineering. ahmet.dayanc@dpu.edu.tr ORCID No: 0000-0002-5214-9021

INTRODUCTION

Rockets operate based on Newton's laws of motion. Simply put, rocket engines eject high-pressure and high-temperature gases resulting from the combustion of fuel through a nozzle. The rapid expulsion of gases from the nozzle propels the rocket forward. This principle is, in fact, based on Newton's third law of motion, which states that "for every action, there is an equal and opposite reaction".

Considered a pioneer of rocket science, an American physicist and engineer Robert H. Goddard successfully launched the first liquid-fueled rocket in 1926, which is regarded as the foundation of modern rockets. This rocket is acknowledged as a step towards physical space travel and Goddard's rocket reached a speed of 60 miles per hour and a height of 12.5 meters, burning fuel for only 2.5 seconds. This rocket set the precedent for the development of multi-stage rockets and other rocket engines that would later be used in space research. Goddard later worked on both liquid fuel rocket engines and solid fuel rocket engines. He also made significant advancements in rocket fuel systems, guidance systems, and other rocket technologies (Center, 2004).

One of the most important developments in rocket engines is the V2 rocket developed by Wernher von Braun and his team at the Army Research Center in Peenemünde, Germany, during World War II (V-2 Rocket - Wikipedia, 2023). The V-2 rocket was the first long-range ballistic missile used by Nazi Germany during World War II. It is also the first vehicle that allowed a man-made object to reach space. As shown in Figure 1, this rocket used a liquid-fueled rocket engine with the capacity to reach space and is considered a precursor of ballistic missiles (Rocket - Liquid Fuel, Propulsion, Engines | Britannica, 2023). The technical specifications of the rocket can be listed as follows: length - 14 m, diameter - 1.65 m, range - 320 km, speed - 5760 km/h, altitude - 189 km, and weight - 12.5 tons.

After World War II, rocket engines continued to evolve, signaling the dawn of space exploration. The 1950s and 1960s were a period of significant advancements in rocket engine technology, especially during the "space race" between the United States and the Soviet Union.

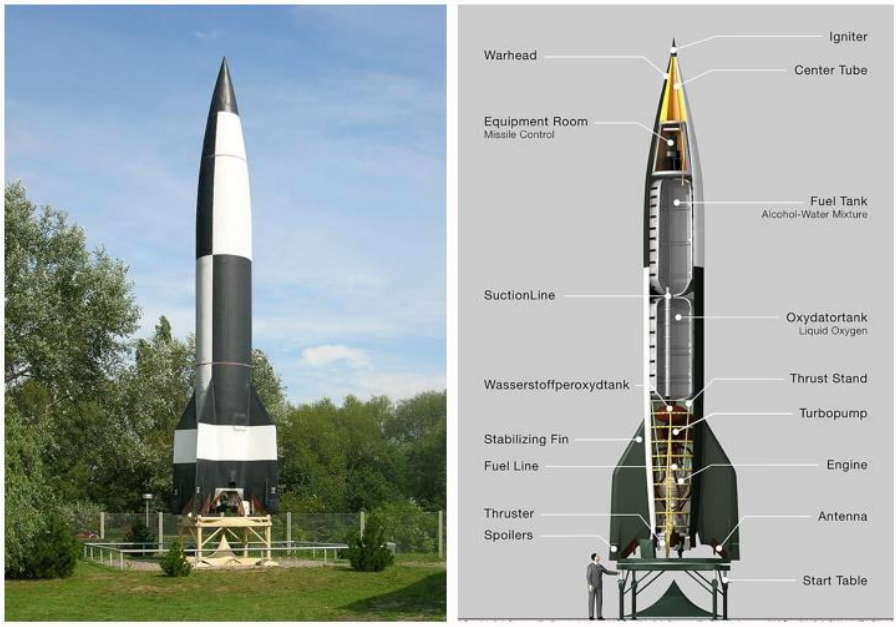

Figure 1: V-2 Rocket and Schematic View

The rocket engines developed during this time were used in the Apollo programs, as shown in Figure 2, particularly by NASA between 1961 and 1975 to carry out manned missions to the Moon (Gisler & Sornette, 2009). The Apollo spacecraft comprised a three-person cabin, a missile, and a propulsive capsule.

Figure 2: Apollo Programs

The foundation of this program, the Saturn V, as seen in Figure 3, was used to launch the first American space station, Skylab (Bilstein, 1999). Saturn V was launched 13 times from the Kennedy Space Center in Florida and has a payload capacity of 140,000 kg to low Earth orbit. This three-stage rocket used high-energy fuels such as liquid hydrogen and liquid oxygen and employed the F-1, the most powerful single-chamber liquid-fueled rocket engine ever developed, in its first stage (Young, 2008). Furthermore, as of 2021, this rocket is the only launch vehicle to have transported humans beyond low Earth orbit.

Figure 3: Saturn V Rocket

Recently, the rocket engines developed by SpaceX, as shown in Figure 4, offer significant improvements over previous generations. SpaceX is an American private space transportation company based in Hawthorne, California, founded by Elon Musk in 2002. The primary goals of the company are to reduce the cost of space transportation and establish a human colony on Mars. Chronologically, SpaceX was the first private company to reach and return a spacecraft from the International Space Station (ISS) in 2010. In 2012, the Dragon spacecraft became the first private vehicle to deliver cargo to the ISS. By 2020, SpaceX became the first private company to transport NASA astronauts to the ISS. SpaceX has developed and manufactured the

Falcon and Starship rocket families, but the Starship is designed for long-distance flights between Mars and other planets (Reddy, 2018).

Figure 4: SpaceX's Raptor Engine

SpaceX's Raptor engine provides high efficiency and reusability by using liquid methane (CH4) and liquid oxygen (O2). This engine has a "staged combustion" cycle, as shown in Figure 5, which redirects the exhaust from the gas generator back to the combustion chamber, increasing the engine's efficiency. Additionally, the Raptor engine follows the "full-flow" principle, which means that both components are completely directed to the combustion chamber, enabling the engine to produce more thrust. SpaceX uses the Raptor engine in both the Falcon rocket family and the Starship vehicle (Seedhouse, 2022).

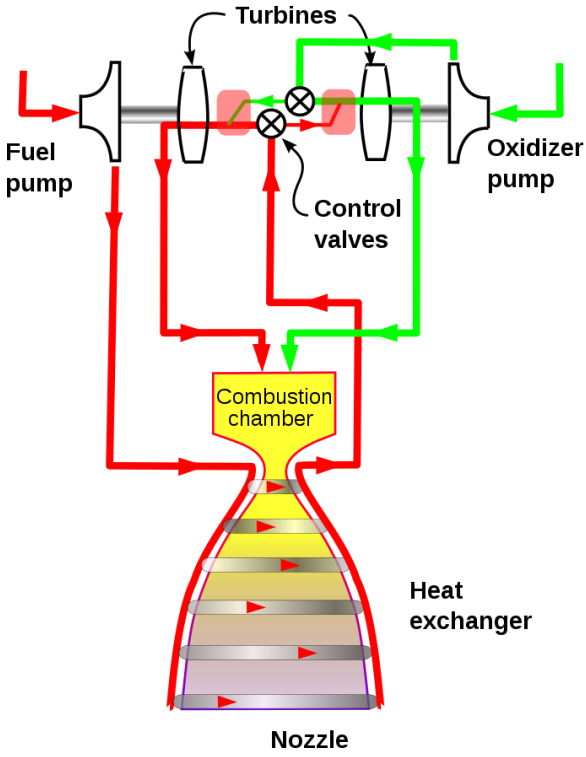

Figure 5: Full-Flow "Staged Combustion" Diagram

In our Computational Fluid Dynamics (CFD) analysis to understand the effect of the staged combustion cycle, we removed the intermediate stage where the exhaust gas is redirected back to the combustion chamber, as shown in Figure 6. Thus, we obtained less thrust force at the nozzle exit than the values explained on Nasaspaceflight, revealing how efficient the process of redirecting exhaust gas is.

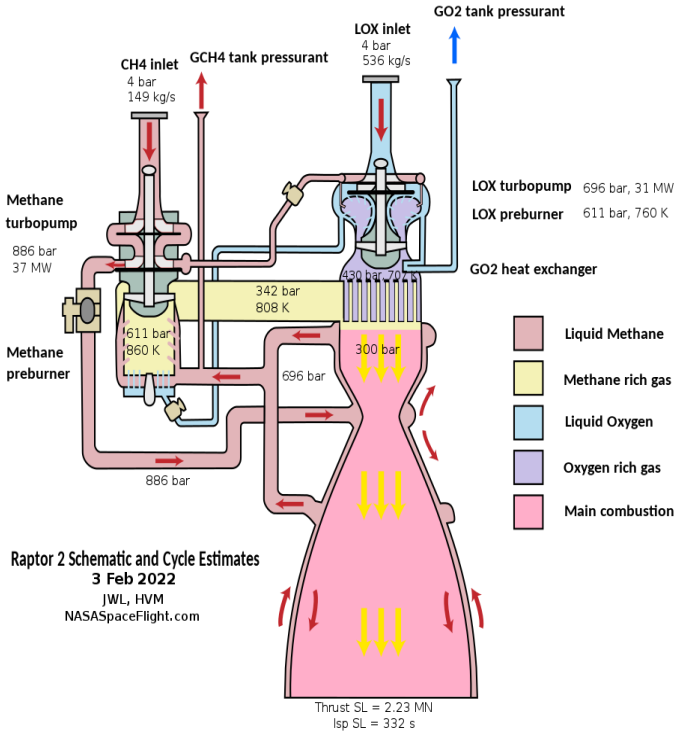

Figure 6: Raptor Engine Cycle Diagram

MATERIALS AND METHODS

For the CFD analysis, a basic CAD geometry was first drawn for the Raptor engine. In this drawing process, the dimensions were made based on the reference values of ER=35 shown in Figure 7. After the CAD geometry was created, preparations were made for the CFD analysis. The first step was to create a surface mesh from the CAD geometry. Volume mesh elements with the same edge length as the surface mesh elements were derived. Adjustments were made in the mesh parameters until mesh metrics like skewness and orthogonal geometry showed good values, and a mesh of sufficient quality to achieve mesh independence was obtained. Then, other interfaces necessary to set up the CFD analysis were opened, and the relevant parameters were defined.

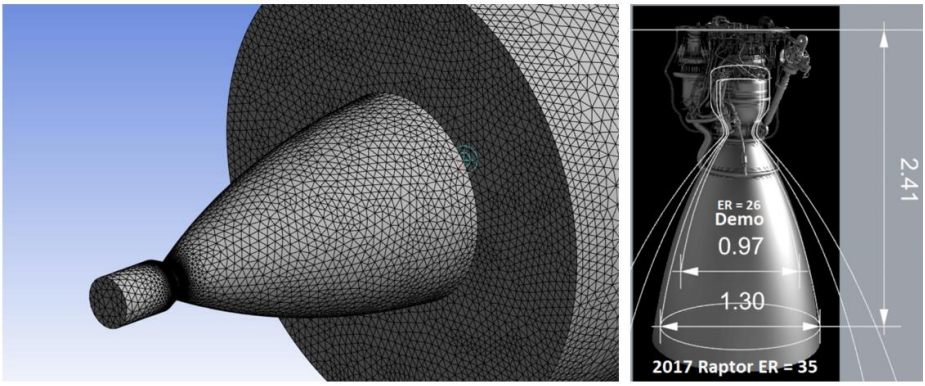

Figure 7: ER=35 Model Mesh

Input pressure and mixture ratio values were taken from NASA's CEA for combustion chamber calculations. In the interface where the material arrangement is made and seen in Figure 8, the fluid selection was made assuming an ideal gas for density properties. In addition, specific heat, molecular weight, and thermal conductivity values were entered as seen below. Due to the nature of the rocket engine, the viscosity of the fuel mixture will also not remain constant. The Viscous Sutherland Method is a method used to calculate the viscosity value of fluids in relation to temperature. Viscosity is an important property that defines the internal friction resistance of a fluid and plays a significant role in the analysis of fluid mechanics and heat transfer. Therefore, accurately estimating the viscosity of the fluid as a function of temperature is important for many applications. The advantage of the Sutherland method is that it can accurately calculate viscosity at low and high temperatures. However, at low temperatures, it would be more appropriate to use more sensitive models, especially for fluids in the liquid state. Therefore, the "Sutherland" method has been chosen to calculate the change in viscosity.

$$\mu = \mu_0 \frac{T_0+C}{T+C} \left(\frac{T}{T_0}\right)^{3/2} \quad (1)$$

In equation 1 above, μ(T) is the viscosity of the fluid at temperature T, μ_0 is the viscosity of the fluid at the reference temperature T_0, and C is a value known as the Sutherland constant (Sutherland, 1893). This method is

usually used to calculate the viscosity of gases, and for gases, the Sutherland constant is usually 110.4 K.

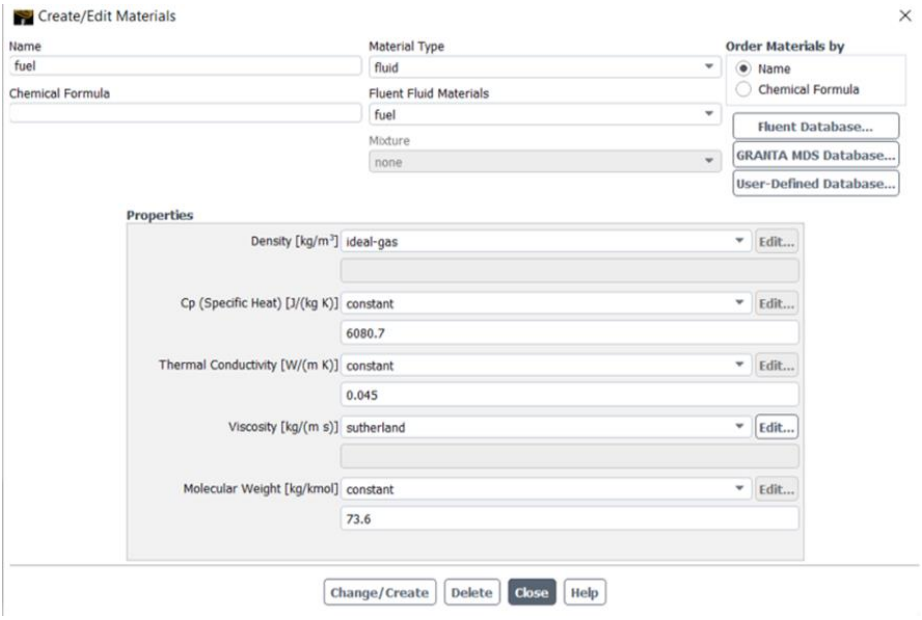

Figure 8: Properties of Material

As seen in Figure 9, since the speed of the fuel mixture is not known for the input condition, the pressure inlet parameter was defined based on the pressure at the input cross-section. After the input pressure data of 300 bar taken from NASA's CAE was defined, the supersonic initial gauge pressure value was found as a result of a calculation assuming isentropic compressed flow.

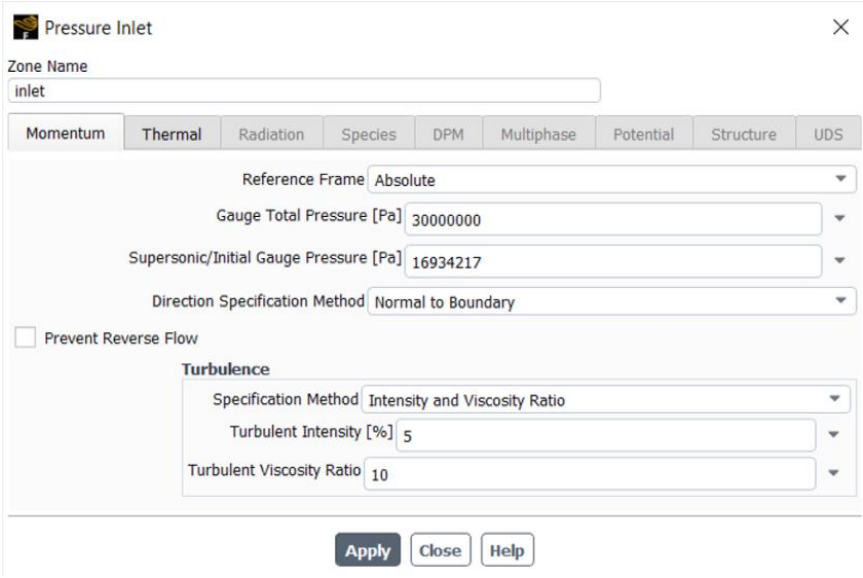

Figure 9: Definition of Inlet Boundary Condition

The scalar magnitude of the temperature input condition, which is located in the second tab of the interface related to the pressure inlet parameter shown in Figure 10, was defined as 3762.41 K in Kelvin.

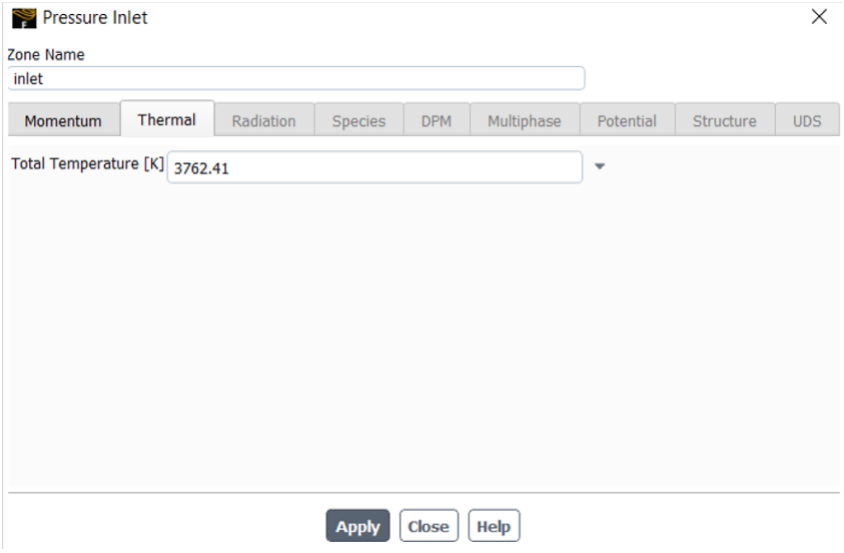

Figure 10: Defition of Inlet Temperature Condition

In the interface related to the pressure outlet parameter shown in Figure 11, there are two different tabs for momentum and thermal conditions. The value to be entered for the gauge pressure parameter in the first tab needs to be set at 101325 Pa by referring to the atmospheric pressure at sea level, as the thrust values are given as thrust sea level. In addition, the scalar magnitude of the temperature condition found in the second tab has been defined as 293 K, equivalent to 20 degrees Celsius, in correspondence with the National Institute of Standards and Technology (NIST).

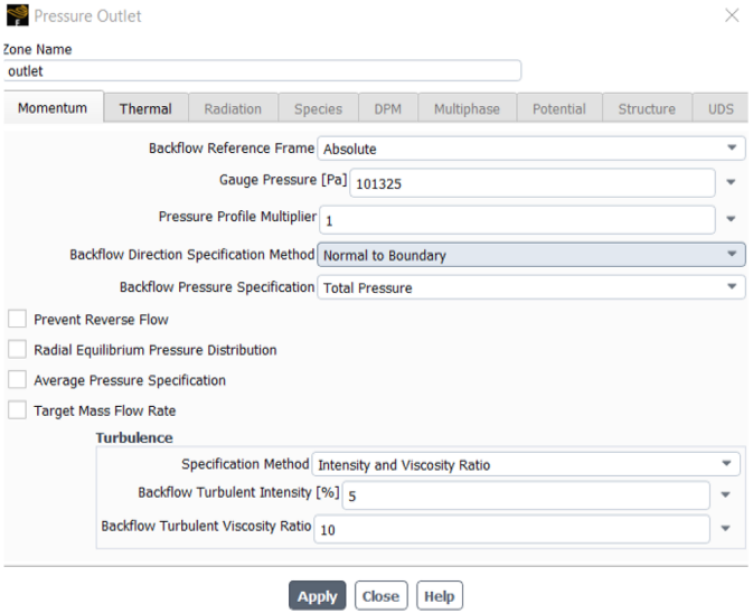

Figure 11: Definition of Outlet Boundary Condition

In the interface shown in Figure 12, a turbulence model must be selected from the list pertaining to turbulence models. The k-omega model is widely used in CFD (Computational Fluid Dynamics) analyses to calculate turbulence effects and predict the characteristics of turbulent flow.

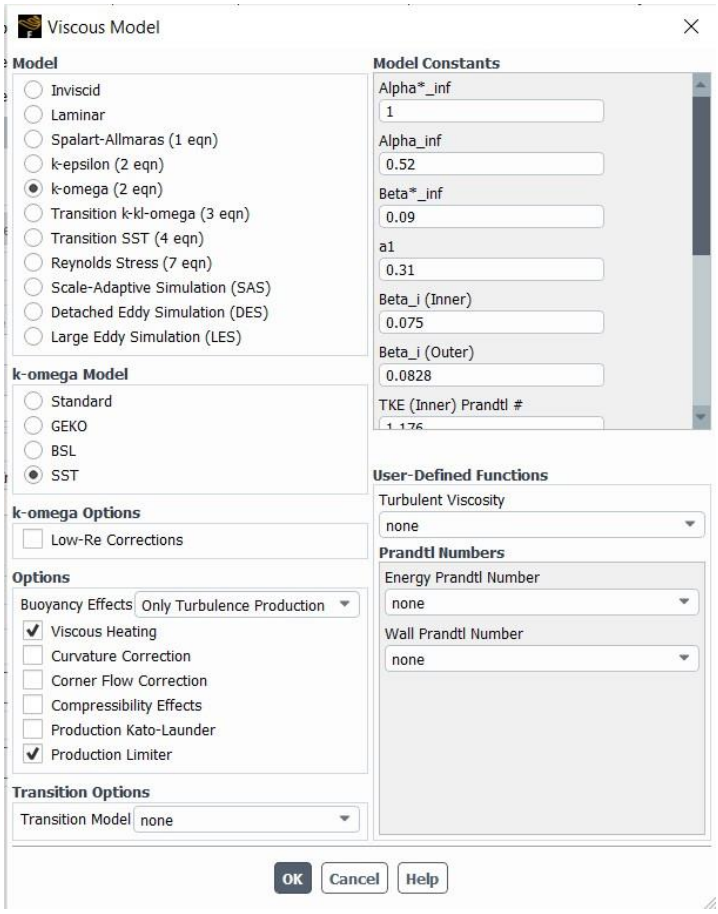

Figure 12: Setting of Viscous Model

The k-omega model uses two carrier variables named k and omega. These variables are called turbulence kinetic energy (k) and scaling frequency (omega). While turbulence kinetic energy represents the intensity of turbulent motion, the scaling frequency determines the size and interactions of turbulent structures. The k-omega model simulates turbulent flow by solving additional equations called k and omega equations, along with the Navier-Stokes equations. These additional equations are used to calculate the spreading rate of turbulence, turbulence energy production, turbulence viscosity, and other features associated with turbulence.

Such turbulence models are used to predict complex turbulent flows with less computational cost and are often preferred in industrial applications in CFD analyses. There are different variations of k-omega turbulence models used in mathematical modeling of turbulent flows.

The standard k-omega model is the basic version of the k-omega turbulence models. It is a suitable choice especially for smooth fluid flows such as high-pressure flows and circular pipes. However, it may not give sufficient results for turbulent flows involving rotational movements such as severe rotational motion and turns.

The GEKO (Generalized k-omega) model is an improved version of the k-omega model. This model is designed to more accurately predict turbulent flows where there are rotational movements and severe rotational motions. Therefore, it is a more suitable choice for rotating flows.

The BSL (Baseline) k-omega model is a variation aiming to perform better under low Reynolds numbers of turbulent flows. The Reynolds number is a parameter where the turbulence effects of the fluid become significant. The BSL model is a suitable choice to get accurate results under low Reynolds numbers.

The SST (Shear Stress Transport) k-omega model aims to achieve accurate results both near the wall surfaces and in the free flow area of turbulent flows. This model combines the advantages of k-epsilon and k-omega models and performs well across a wide flow spectrum. The SST model is a popular choice that can generally be used in various flow conditions.

Considering the suitability and effects of the differences between these variations for the rocket thrust analysis scenario and supported by the literature, the k-omega model was preferred in the choice of the turbulence model to complete the CFD analysis of the liquid-fueled rocket engine with low computational cost, and the SST variation was used in this study.

RESULTS

After all parameters were defined, the CFD analysis was run and converged in 450 iterations. In Figure 13, cross-sections of temperature results are seen. The temperature profile on the left is a section of the mixture of methane and oxygen fuel, while the temperature profile on the right shows a cross-section of the temperature profile for FLP fuel.

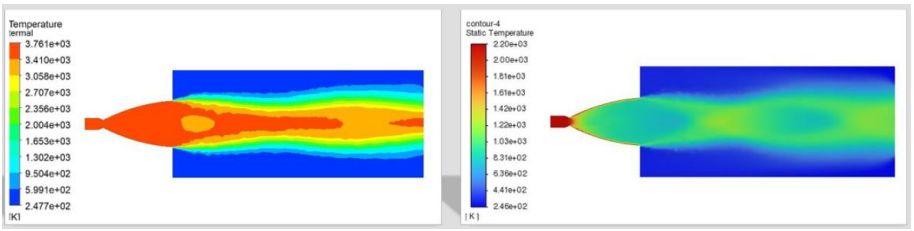

Figure 13: Temperature Profiles

In Figure 14, velocity profiles are seen. The velocity profile on the left is a section of the mixture of methane and oxygen fuel, while the velocity profile on the right shows a cross-section of the velocity profile for FLP fuel, and the velocity profile at the nozzle exit for FLP fuel turned out to be higher.

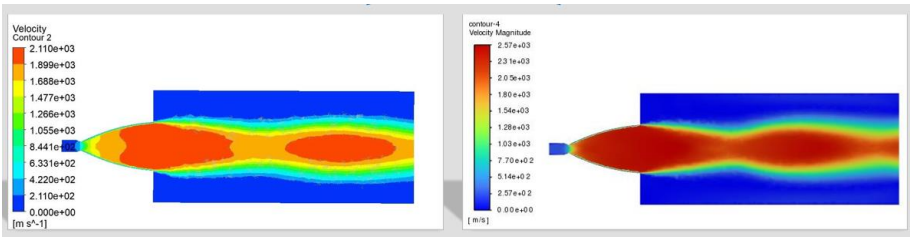

Figure 14: Speed Profiles

As a result of certain equations using the pressure, velocity, and density values obtained from the analysis, the values of mass flow rate and thrust force were found. The relevant values are given in Figure 15. It was observed that the average of the thrust force values is 1.74 MN.

X [m]	Pressure [Pa]	Velocity [m s^-	Density [kg m^-	Mass Flow	THRUST
0.00E+00	2.86E+07	2.11E+03	2.88E-01	7.89E+02	1.80E+06
1.67E-02	2.86E+07	2.11E+03	2.89E-01	790.9043355	1805552.939
3.33E-02	2.86E+07	2.11E+03	2.90E-01	793.9776119	1812156.275
5.00E-02	2.86E+07	2.11E+03	2.91E-01	797.0840412	1818920.06
6.67E-02	2.86E+07	2.11E+03	2.92E-01	800.2236434	1825846.973
8.33E-02	2.86E+07	2.11E+03	2.93E-01	803.3745521	1832759.526
1.00E-01	2.86E+07	2.11E+03	2.94E-01	806.1011453	1838917.854
1.17E-01	2.86E+07	2.11E+03	2.95E-01	808.9529904	1845561.741
1.33E-01	2.86E+07	2.11E+03	2.96E-01	811.8315589	1852289.941
1.50E-01	2.86E+07	2.11E+03	2.98E-01	816.3609831	1860505.237
1.67E-01	2.86E+07	2.11E+03	3.01E-01	824.3147108	1874613.137
1.83E-01	2.86E+07	2.11E+03	3.04E-01	832.2717854	1888904.148
2.00E-01	2.86E+07	2.10E+03	3.07E-01	840.2257889	1903154.427
2.17E-01	2.86E+07	2.10E+03	3.10E-01	846.9620617	1913344.811
2.33E-01	2.86E+07	2.10E+03	3.13E-01	854.5938365	1923116.048
2.50E-01	2.86E+07	2.10E+03	3.17E-01	865.0918484	1934016.389
2.67E-01	2.86E+07	2.10E+03	3.22E-01	876.7448853	1941311.687
2.83E-01	2.86E+07	2.09E+03	3.26E-01	888.3745315	1948447.853
3.00E-01	2.85E+07	2.09E+03	3.31E-01	900.1869823	1931498.458
3.17E-01	2.85E+07	2.09E+03	3.36E-01	913.0304594	1922446.909
3.33E-01	2.84E+07	2.08E+03	3.44E-01	931.0352225	1874979.325
3.50E-01	2.84E+07	2.08E+03	3.51E-01	948.8383089	1826880.373
3.67E-01	2.83E+07	2.08E+03	3.58E-01	966.5112222	1711323.21
3.83E-01	2.81E+07	2.07E+03	3.65E-01	984.0659397	1566750.966
4.00E-01	2.79E+07	2.07E+03	3.72E-01	1001.724825	1233541.432
4.17E-01	2.76E+07	2.07E+03	3.79E-01	1019.867662	909054.4999
4.33E-01	2.72E+07	2.07E+03	3.87E-01	1039.577565	431082.3321

Figure 15: Thrust Force Results (CH4+LOx)

In Figure 16, as a result of certain equations using the pressure, velocity, and density values obtained for FLP, the values of mass flow rate and thrust force were found. The average value of the thrust force was found to be 0.74 MN.

X [m]	Pressure [Pa]	Velocity [m s^-1]	Density [kg m^-3]	Mass Flow	THRUST
0.00E+00	2.84E+07	2.50E+03	1.98E-01	6.41E+02	8.83E+05
1.67E-02	2.84E+07	2.50E+03	1.98E-01	642.914259	886223.1635
3.33E-02	2.84E+07	2.50E+03	1.99E-01	644.10184	888694.2067
5.00E-02	2.84E+07	2.50E+03	1.99E-01	645.315951	890891.6456
6.67E-02	2.84E+07	2.50E+03	1.99E-01	646.556133	894337.6863
8.33E-02	2.84E+07	2.50E+03	2.00E-01	647.822816	897931.4163
1.00E-01	2.84E+07	2.50E+03	2.00E-01	649.124356	901268.6938
1.17E-01	2.84E+07	2.50E+03	2.00E-01	650.45811	905613.6377
1.33E-01	2.84E+07	2.50E+03	2.01E-01	651.966258	911355.2181
1.50E-01	2.84E+07	2.50E+03	2.02E-01	655.723181	921927.6718
1.67E-01	2.84E+07	2.50E+03	2.03E-01	658.995155	931228.052
1.83E-01	2.85E+07	2.50E+03	2.04E-01	662.358179	940400.6202
2.00E-01	2.85E+07	2.50E+03	2.05E-01	665.867022	948958.1119
2.17E-01	2.84E+07	2.50E+03	2.06E-01	669.389577	956431.9901
2.33E-01	2.84E+07	2.50E+03	2.07E-01	672.92533	962144.3831
2.50E-01	2.84E+07	2.50E+03	2.09E-01	677.716532	963853.1628
2.67E-01	2.84E+07	2.49E+03	2.10E-01	682.501486	964529.0496
2.83E-01	2.84E+07	2.49E+03	2.12E-01	687.281499	954513.2641
3.00E-01	2.84E+07	2.49E+03	2.14E-01	692.055188	932714.2025
3.17E-01	2.84E+07	2.49E+03	2.15E-01	696.823566	895456.3567
3.33E-01	2.83E+07	2.49E+03	2.18E-01	703.957665	841479.3441
3.50E-01	2.82E+07	2.49E+03	2.20E-01	709.825618	731836.909
3.67E-01	2.81E+07	2.48E+03	2.21E-01	714.025672	593853.5867
3.83E-01	2.79E+07	2.48E+03	2.24E-01	723.490274	384088.8535
4.00E-01	2.77E+07	2.48E+03	2.27E-01	732.936341	119670.0808

Figure 16: Thrust Force Results (FLP)

CONCLUSION

In NASA Spaceflight, the average thrust force is stated as approximately 2.23 MN for the case where the exhaust gas is redirected to the combustion chamber. In this study, when the intermediate stage in which the exhaust gas is redirected to the combustion chamber is excluded, it was observed that the average of the thrust force values dropped to 1.74 MN. Therefore, it was determined that the staged combustion cycle increases the thrust force by 25%.

One of the main reasons for working with FLP fuel is as follows: During the use of carbon-containing fuels like CH4 (methane), a large amount of carbon is released into the environment and it is clear that it damages nature, but FLP fuel does not contain carbon and have easier logistics can be a solution to this problem. However, as numerical results also show, the thrust force obtained from FLP fuel is at least half less. It was observed that the thrust force dropped from 1.74 MN to 0.74 MN. Therefore, it cannot give the capacity to free high-mass rockets from the effect of gravity and access space. It is thought that the use of FLP fuels is more suitable in smaller scale, low altitude rockets.

REFERENCES

Bilstein, R. E. (1999). Stages to Saturn: A Technological History of the Apollo/Saturn Launch Vehicle. DIANE Publishing Company.

Center, E. M. K. S. (2004). *NASA - Robert Goddard: A Man and His Rocket*.

Gisler, M., & Sornette, D. (2009). Exuberant innovations: The Apollo program. *Society*, *46*(1), 55–68. https://doi.org/10.1007/S12115-008-9163-8/FIGURES/1

Reddy, V. S. (2018). The SpaceX Effect. *Https://Home.Liebertpub.Com/Space*, *6*(2), 125–134. https://doi.org/10.1089/SPACE.2017.0032

Rocket - Liquid Fuel, Propulsion, Engines | Britannica. (2023). Retrieved August 4, 2023, from https://www.britannica.com/technology/rocket-jet-propulsion-device-and-vehicle/Liquid-propellant-rocket-engines

Seedhouse, E. (2022). The Engines. *SpaceX*, 40–57. https://doi.org/10.1007/978-3-030-99181-4_3

Sutherland, W. (1893). LII. The viscosity of gases and molecular force. *The London, Edinburgh, and Dublin Philosophical Magazine and Journal of Science*, 36(223), 507-531.

V-2 rocket - Wikipedia. (2023). Retrieved August 4, 2023, from https://en.wikipedia.org/wiki/V-2_rocket

Young, A. (2008). The Saturn V F-1 Engine. *The Saturn V F-1 Engine*. https://doi.org/10.1007/978-0-387-09630-8

CHAPTER 7

HYDROGEOCHEMICAL CHARACTERIZATION AND HEALTH IMPLICATIONS OF FRESHWATER SPRING IN THE FATMALI-ÖNSEN REGION, TURKEY

Prof. Dr. Yusuf URAS[1*]

MSc. Şule TÜRKÖNER[2]

Prof. Dr. Yağmur UYSAL[3]

[1] Kahramanmaras Sutcu Imam University, Geological Engineering Department, Kahramanmaras, Turkey. uras74@gmail.com; ORCID: 0000-0001-5561-3275

[2] Kahramanmaras Sutcu Imam University, Geological Engineering Department, Kahramanmaras, Turkey.

[3] Mersin University, Environmental Engineering Department, 33343, Mersin-Turkey. yuysal@mersin.edu.tr; ORCID: 0000-0002-7217-8217

*Corresponding Author

Kahramanmaras Sutcu Imam University, Geological Engineering Department, Kahramanmaras, Turkey. uras74@gmail.com

INTRODUCTION

Natural spring waters are valuable sources of freshwater that emerge from underground aquifers, often acclaimed for their purity and potential health benefits. These waters play a crucial role in meeting the drinking water needs of communities around the world. The quality of these spring waters is of paramount importance, as it directly affects public health. Natural spring waters possess certain characteristics that make them unique sources of drinking water, yet their safety for public consumption hinges on a rigorous assessment of their water quality parameters. Spring waters are often believed to be pure due to their origin from deep underground sources. They can contain beneficial minerals such as calcium, magnesium, and potassium, contributing to human health. However, excessive levels of certain minerals can lead to health issues, making it essential to monitor and regulate mineral content (Stupar et al., 2022).

Despite their underground origin, spring waters are vulnerable to microbial contamination from sources such as surface runoff and human activities. Bacteria, viruses, and other microorganisms can pose serious health risks if ingested. Regular testing for microbial indicators like coliform bacteria helps ensure that the water remains safe for consumption (Bratovcic & Petrinic 2020). Natural spring waters can contain various chemicals derived from geological formations or human activities. Heavy metals, nitrates, and organic compounds are among the potential contaminants. These substances, if present above safe levels, can have adverse effects on human health, necessitating rigorous monitoring and treatment processes (Batool et al. 2020). The pH level of spring water influences its taste and how it interacts with the body. Extreme pH values can cause gastrointestinal discomfort. Monitoring pH levels is crucial to prevent any potential health issues related to the water's acidity or alkalinity.

The sources of natural spring waters are vulnerable to pollution, climate change, and other environmental factors. Protecting these sources from contamination is essential for maintaining the quality and availability of these valuable resources for future generations. Governments and health agencies establish regulatory standards for water quality parameters to safeguard public health. These standards define acceptable levels of contaminants, minerals, and other parameters in drinking water. Spring waters must meet these standards to be considered safe for consumption (EPA 2017).

Located 40 km south of the city center of Kahramanmaraş in the Mediterranean region, the areas of Fatmalı and Önsen are noteworthy spots within the region's natural beauty. These locales stand out for their captivating natural landscapes, rich vegetation, and tranquil atmosphere. Fatmalı and Önsen offer ideal settings for nature enthusiasts and visitors to engage in activities such as trekking, hiking, picnicking, and exploring wildlife. Additionally, these areas encompass historical and cultural elements of the region, making them appealing destinations for both relaxation and various recreational pursuits. The primary sources of drinking water in the Fatmalı region are groundwater resources. These resources typically involve extracting water from underground aquifers. These aquifers are layers beneath the ground that carry water and can aid in the natural filtration processes. Groundwater sources in the Fatmalı region play a fundamental role in meeting the drinking water needs of the local population and residents of the area. These water sources are regularly monitored and managed to ensure clean and safe consumption of water. Investigating the hydrogeology of the water sources in this region and determining the water quality parameters of these sources hold significant importance for several reasons.

1. Drinking Water Security: Understanding the hydrogeology of the region's water sources is crucial for ensuring a stable and secure supply of drinking water. By comprehending the characteristics of the aquifers, groundwater flow patterns, and recharge mechanisms, authorities can make informed decisions about water extraction, allocation, and management.

2. Resource Sustainability: Studying the hydrogeology helps in assessing the sustainability of water resources. This includes evaluating the rate of groundwater replenishment compared to withdrawal, preventing overexploitation, and avoiding the depletion of these vital resources for future generations.

3. Preventing Contamination: Detailed knowledge of hydrogeological conditions allows for the identification of potential sources of contamination and pathways for pollutants to enter the groundwater. This information is essential for implementing protective measures to safeguard the quality of drinking water sources and prevent pollution-related health risks.

4. Source Vulnerability: Hydrogeological studies can reveal the vulnerability of water sources to external factors such as climate change, land use changes, and pollution. By identifying these vulnerabilities, authorities

can develop strategies to mitigate the potential impact of such changes on the quality and availability of drinking water.

5. Establishing Water Quality Standards: Determining water quality parameters is essential for establishing appropriate standards for safe drinking water. By analyzing the chemical composition of the water, authorities can ensure that it meets health-based guidelines, protecting the public from potential contaminants.

6. Health and Well-being: The quality of drinking water directly impacts public health. Investigating water quality parameters helps identify potential health hazards, such as excessive mineral concentrations or microbial contamination. This information enables timely interventions and treatments to ensure the safety of the water supply.

7. Regulatory Compliance: Water quality parameters are often regulated by governmental and health agencies to ensure the safety of drinking water. By determining and monitoring these parameters, authorities can ensure compliance with established standards and regulations.

8. Data-Driven Decision Making: Hydrogeological research and water quality parameter determination provide a scientific basis for decision-making processes. Whether it's setting extraction rates, implementing treatment methods, or planning for water infrastructure, data-driven decisions lead to effective and sustainable management.

In this study, we aimed to analyze the hydrogeochemical attributes of drinking water resources of Fatmalı-Önsen region, focusing on water quality parameters. Our primary objective was to establish a potential connection between apparent public health concerns, and the utilization of various natural water sources in this area. In order to achieve this, we conducted thorough geological, hydrogeological, and medical geological investigations specific to the Fatmalı-Önsen region.

The research inquiries guiding this study encompassed: (1) Understanding the hydrogeological sustenance of underground water resources in the Fatmalı-Önsen region, (2) Determining the temporal origins of these water sources, and (3) Evaluating the suitability of the utilized water resources for drinking purposes according to established standards. In order to conclude, this study delves into a comprehensive exploration of the hydrogeochemical aspects of drinking water resources in the Fatmalı-Önsen

region. In conclusion, investigating the hydrogeology of the region's water sources and determining water quality parameters are essential steps towards ensuring a safe, reliable, and sustainable drinking water supply. These practices are instrumental in protecting public health, preventing contamination, and making informed decisions for the management of precious water resources. This paper explores the significance of natural spring waters and their water quality parameters in safeguarding public health.

2. MATERIAL AND METHODS

In this section, we delve into the characterization of the geological structure, hydrogeological features, and water resources within the Kahramanmaraş Fatmalı-Önsen region. In order to accomplish this, we first outline the sampling locations and provide a comprehensive overview of the geological composition of the study area. Following this, we focus on the hydrogeological attributes of the region, aiming to understand the groundwater dynamics and characteristics. Subsequently, we present the methods and procedures employed in the characterization and analysis of the water resources. This section serves as the foundation for our comprehensive assessment of the geological and hydrogeological aspects of the Fatmalı-Önsen region.

2.1. Sampling Locations and Geology of the Study Area

Water samples from the Fatmalı-Önsen region were systematically collected over the course of a year during distinct periods, encompassing both dry and rainy seasons. This approach aimed to establish the condition of the predominant drinking water sources within the region. This assessment considered not only the geological characteristics of the area but also sought to determine the potability of these water sources. The sampling efforts were directed towards four specific water sources, namely the Atatürk Fountain (FA-1), Kancıkdere Fountain (KD-2), Kişifli Spring (FG-3), Pınarbaşı (OKB-4) fountain, and Hacıağlar (İncirlipınar) fountain (OH-5) all situated within the confines of the Fatmalı-Önsen region (Figure 1).

Figure 1. View of the Water Resources of Fatmalı-Önsen Region (FA-1, KD-2, FG-3, OK-4, OH-5)

The study area is effectively situated within the 1/25,000 scale Kahramanmaraş M37-d3 map. The formations visible in this study area are not grouped under a single age category within this context. Instead, they are treated as separate entities, classified based on age from the oldest to the youngest among themselves. Consequently, the geological map of the study area encompassing the drinking water sources in the Fatmalı-Önsen region has undergone revisions (Figure 2).

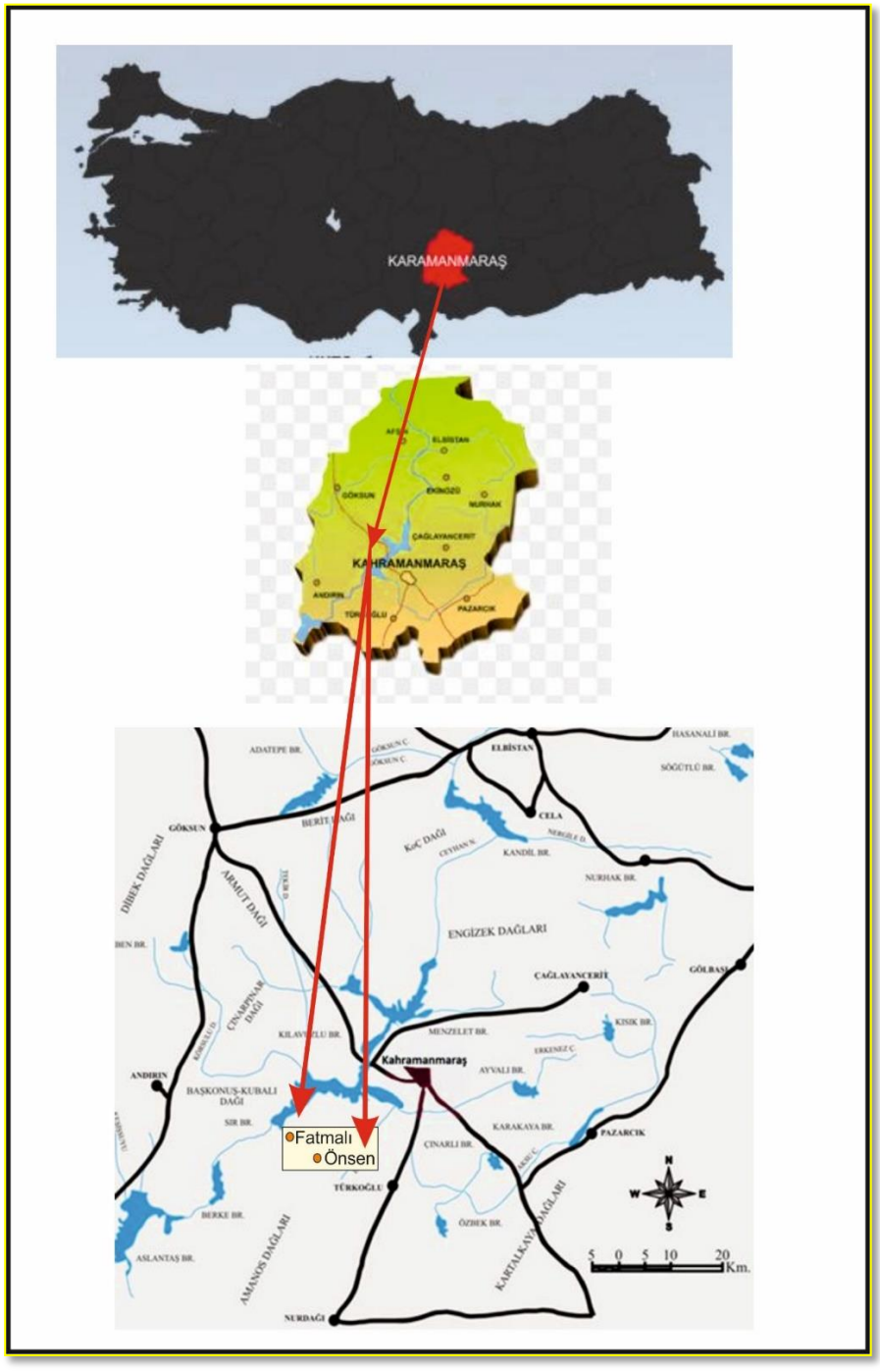

Figure 2. Location Map of the Investigated Region

It was determined that they were formed within the alternation of sandstone, shale, siltstone, quartzite, and dolomite within the Ordovician aged tut formation of the Southeast Anatolian autochthon. The formations outcropping in the study area are not described in a single age order in this section, but are handled separately, independently of each other, with the age order from oldest to youngest. The geological map of our study area, where the drinking water sources of Fatmalı-Önsen location are located, has been revised (Figure 3)

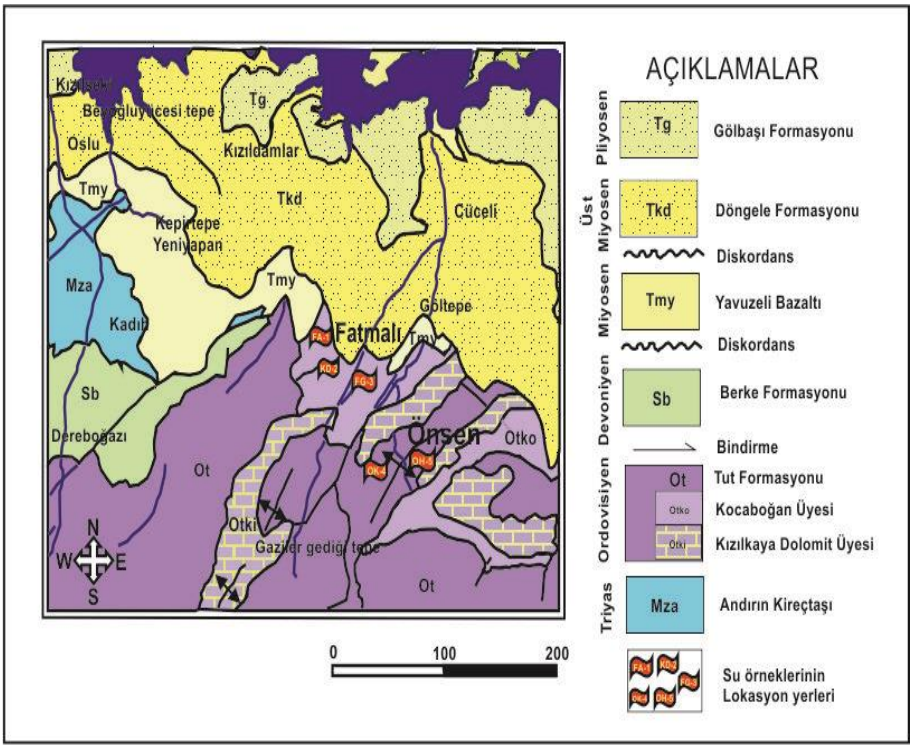

Figure 3. Geological Map of the Region (modified from MTA 2008).

2.1.1. The Gölbaşı Formation (Tg):

Baydar and Yergök (1996) used the name Gölbaşı formation for the first time for the unit, which includes conglomerate, sandstone, marl and tuff lithologies, whose typical outcrops are observed around Gölbaşı Lake in Adıyaman province Gölbaşı district and generally deposited in the lake environment. The unit is generally characteristic with its soft topography and yellowish-gray appearance. Gölbaşı formation generally consists of shale, clayey limestone and siltstones observed in places between these lithologies. The shales should be bluish-gray, thin-bedded, unstable, dispersed and

splintered. Marl and clayey limestones are yellowish-gray colored, thin-medium bedded, carbonate cemented, medium strength, cracked and fractured. Among these lithology, there are gray colored, thin bedded, loosely attached siltstones with polygenic elements. Gölbaşı formation overlies all older units with angular unconformity, and is overlain by talus and alluvium with angular unconformity. Baydar and Yergök (1996) suggested that the Gölbaşı formation, which they gave Pliocene age, had a thickness of 194 m around Gölbaşı and was deposited in lake or marsh areas that developed under the influence of tectonic forces. The Gölbaşı Formation, a prominent geological unit, is found in various regions and holds significant insights into the Earth's geological history. Comprising sedimentary rocks, the formation's deposits provide valuable evidence of past environmental conditions and depositional processes. The Gölbaşı Formation typically consists of layers of sandstone, siltstone, shale, and limestone, reflecting diverse sedimentary environments such as fluvial, lacustrine, and deltaic settings. Its distinct stratigraphic characteristics and fossil content enable geologists to decipher the evolution of landscapes and ecosystems over time, shedding light on the dynamic interplay between climate, tectonics, and sedimentary processes. The Gölbaşı Formation's multifaceted composition and geological significance make it a focal point for studies aimed at unraveling the Earth's geological heritage and understanding the intricate mechanisms shaping its surface.

2.1.2. Döngele sandstone member (Tkd)

The unit, which generally consists of alternating yellowish-gray sandstone, siltstone and mudstone, and is best exposed in the vicinity of Süratı, Tanır, Döngel and Karaağaç, was first introduced by Gül (2000) as the Döngele sandstone member. The unit, which has wide outcrops in Kahramanmaraş and its vicinity, is characteristic with its flat topography and yellowish-gray uniform appearance. The sandstones in the unit; It is gray, yellowish-gray in color, thin-medium bedded, varying in size from fine sand to coarse sand, partly parallel, partly tangential-cross-layered, carbonate cemented and polygenic elements. siltstones; It is yellowish gray in color, thin bedded, medium strength carbonate cemented and polygenic elements. The mudstones and claystones alternating with these units are yellowish-greenish gray, thin-bedded, unstable, splintered and carbonate-cemented. The unit generally presents a highly folded and fractured structure. Baydar and Yergök (1996) stated that the unit conformably overlies the Lower Miocene aged Zeytin formation, overlies the Eocene aged Midyat formation with angular

unconformity, and is also laterally and vertically transitional with other members of the Yenicekale formation. The researchers stated that the thickness of the unit reached up to 1000 m. In previous studies, no fossil finds were found in the unit. However, due to the Middle Miocene age of the Parpiyayla limestone member, which it shows a lateral and vertical transition, the Döngele sandstone member is assumed to be of the same age. Baydar and Yergök (1996) suggested that the Döngele sandstone member was deposited in a deeper part of the Middle Miocene sea than the Parpiyayla limestone member.

The Döngele Sandstone Member is a notable geological unit recognized for its distinctive characteristics and contributions to the understanding of regional geological history. This member is part of the larger geological sequence and is often found in specific regions, offering insights into past depositional environments and geologic events. Comprising primarily sandstone deposits, the Döngele Sandstone Member showcases the sedimentary history of its formation. It is often associated with fluvial environments, indicating deposition in river systems. The sandstone layers within this member might exhibit variations in grain size, sorting, and sedimentary structures, providing clues about the energy and conditions of the ancient river systems. Fossil evidence within the Döngele Sandstone Member, if present, can offer insights into the organisms that existed during the time of deposition, helping paleontologists reconstruct the paleo environment and its inhabitants. Additionally, its distinct stratigraphic characteristics make it valuable for correlation with other geological formations, aiding in understanding the broader geological context of the region. Geologists study the Döngele Sandstone Member to unravel the geological processes that shaped it, including factors like sediment transport, water currents, and depositional changes over time. This member's examination contributes to a comprehensive understanding of the geological evolution of the area it is found in, helping scientists piece together the puzzle of Earth's history.

2.1.3. Yavuzeli Basalt (Tmy)

The Upper Miocene-aged basalts were introduced as the "Yavuzeli Basalt" by Yoldemir (1987a). This unit is present in the ridges northwest of Dehliz, the Kazankıran Mountain south of Pazarcık, the eastern and western parts of the Narlı Plain, and the northern and northwestern areas of Karacasu Village. The basalts exhibit various shades of reddish, dark brown, dark gray, and black colors. They are massive, occasionally with very thick layers, and

porous, with calcite amygdules and calcite fillings in pores that can reach up to 15-20 cm. The lavas sometimes include tuffaceous contributions and display brecciated appearances.

The unit, observed as olivine basalt and amygdule-bearing olivine basalt, consists of lavas that reached the surface through fractures developed due to faults. The basalts unconformably cover all older units. Based on radiometric dating conducted by Yoldemir (1987a), their age is determined to be around 12.1 million years (Middle Miocene). However, according to Ulu et al. (1991), they are estimated to be around 7-8 million years old (Upper Miocene). The burial of Middle Miocene units by basalts in the Kahramanmaraş Basin can be interpreted as data supporting their Upper Miocene age. Yavuzeli Basalt is an important geological formation located in Yavuzeli district in Turkey's Southeastern Anatolia Region. This basalt formation is an issue that affects the geological features of the region and is studied in various scientific researches. Yavuzeli Basalt is known as a layer formed by basalt, which is a hard, dense and dark colored stone on the surface as a result of volcanic activity. This formation occurs when lava that spreads to the surface during lava flows or volcanic eruptions cools and solidifies. Basalt can often be broken up into hexagonal prism-like columns, making it visually recognizable.

The geological and geomorphological features of Yavuzeli Basalt play an important role in understanding the volcanic past and geographical structure of the region. In addition, factors such as the origin, ages, and environmental effects of this formation have been studied by geologists and researchers. In conclusion, Yavuzeli Basalt is an important geological formation located in the Southeastern Anatolia Region and formed as a result of volcanic activity. This formation plays an important role in geological research and understanding the geological history of the region.

2.1.4. Berke Formation (Sb)

The Berke Formation is prominently observed in the southwestern region of Kahramanmaraş, lying between the Hartlap and Berke villages. This geological formation is characterized by its sequence of yellow and light green laminated layers of thin-bedded shale and phyllite alternations. The formation seamlessly overlies the Tut Formation, showing a harmonious transition between the two. The Berke Formation measures around 600 to 800 meters in thickness. In terms of its age and regional correlation, it is believed

to belong to the Silurian period (Baydar and Yergök, 1996). The Berke Formation stands as a remarkable geological unit, found in diverse regions. It is composed of a mixture of sandstone, mudstone, and shale, which provides valuable insights into past environmental conditions and the sedimentary processes that contributed to its formation. The presence of this formation sheds light on the dynamic geological history of the area and offers important clues about the changing landscapes and ecosystems of the past. The Berke Formation is often associated with marine environments, suggesting that it was deposited in ancient seas. The distinct sedimentary layers within the formation can provide clues about the energy levels and conditions of the water during its deposition. Fossil content within the Berke Formation can offer valuable information about the organisms that inhabited these ancient seas, aiding paleontologists in reconstructing past marine ecosystems. Geologically, the Berke Formation provides important stratigraphic and sedimentological information, helping geologists understand the region's history and the changes that have occurred over time. This formation's composition and characteristics play a crucial role in piecing together the larger geological puzzle of the area where it is found. In summary, the Berke Formation is a significant geological unit that contributes to our understanding of past marine environments and the geological history of the region. Its composition, sedimentary layers, and fossil content offer valuable insights into the Earth's ancient seas and the organisms that inhabited them.

2.1.5. Tut formation (Ot)

The Tut Formation, as observed at the base of the units belonging to the Arabian autochthon in the study area, was first identified and named by Ketin (1966). This geological formation is characterized by an intercalation of various rock types including tawny-brown quartzite, shale-sandstone, gray-black colored dolomite-dolomitic limestone, pink-purple colored clayey limestone, thin-bedded black colored claystone, and alternating layers of yellow dolomite-dolomitic limestone-clay limestone. Additionally, there are gray-olive green colored claystone and siltstone intercalations within the formation.

The Kızılkaya Dolomite Member (Otki) is the portion of the Tut Formation that includes interbedded dolomite and dolomitic limestones. Another member within the Tut Formation is the Kocaboğan Member (Otko), characterized by alternating claystone, siltstone, and milestone layers. This detailed stratigraphic description was provided by Ketin (1966). The Tut

Formation, with its diverse rock types and distinctive members, contributes to our understanding of the geological history and characteristics of the study area, particularly within the Arabian autochthon.

2.1.6. The Kocaboğan Member (Otko)

This member is situated at the uppermost part of the Tut Formation and consists of olive-green, dark gray, fine to medium-bedded, clayey limestone, shale, greensand, greenish-purple, gray, and violet-colored, laminated, fine to medium-thick bedded sandstone, and quartzitic sandstone interbeds. The clayey limestone layers within this member are discontinuous and occur sporadically, often exhibiting laminations and leaf markings. On the surfaces of these layers, ripple marks, raindrop impressions, and traces of organisms can be observed. Above this level, sandstone and conglomeratic quartzite are found laterally and vertically.

The quartzites found within the Kocaboğan Member, with intermittent layers of clay and siltstone, are thickly bedded, siliceous, hematitic, and micaceous. They display white, yellow, and occasionally purple hues. The Tut Formation is accepted as having an Early Ordovician age through regional correlation. However, according to Lahner (1972) and Dean and Monod (1985), it is believed to be of Late Ordovician age. In terms of stratigraphic and lithological characteristics, the Tut Formation can be correlated with the Sadan Formation in the Derik region, the Çardakyayla Formation in the Hassa area, and the Değirmentaşı Formation northeast of Tufanbeyli.

2.1.7. Kızılkaya Dolomite Member (Otki)

This member consists of interbedded dolomite, dolomitic limestone, clayey limestone, and shale layers. At its base, there are gray and black-colored, hard, angular, fractured dolomite and dolomitic limestone layers. These layers' fractures are filled with calcite and quartz. They are thick-bedded, massive, occasionally laminated, and highly resistant, displaying remarkable durability. Above this level, there are pink-purple colored, medium-bedded clayey limestone layers. Further upward, the member comprises yellow-colored, medium-bedded dolomite and dolomitic limestone layers occasionally interspersed with clayey limestone.

2.1.8. Andırın Limestone (Mza)

Triassic-Cretaceous aged limestone formations were called "Andırın Limestone." This unit is widely spread across extensive areas north of the Sürgü-Elbistan faults and west of the Andırın Thrust Belt, exhibiting a rugged and morphologically distinct appearance. The limestone constituting the unit displays local color variations, ranging from gray to dark gray, white, and yellow. It is characterized by fine to medium-thick beddings, occasionally massive layers, significant karstic features, solution cavities, dissolution surfaces, and generally strong to very strong durability. The upper levels often contain chert, chert-marl interbeds, or reefal limestone. This unit, occasionally rich in fossil content, is highly tectonized, extensively fractured, and jointed. The fractures are filled with calcite. In certain areas, the unit exhibits recrystallized limestone features and presents sparitic or micritic textures. Within the study area, it is thrust to the south and east, forming slices and nappes. North of the Sürgü Fault, the unit is juxtaposed with Permian and older Yoncayolu, Çayderesi Nergile formations, Berit Metaophiolite, and Eocene-aged Ballıkısık Formation with tectonic contact. Its age ranges from Upper Triassic to Lower Cretaceous, as determined by Perinçek and Kozlu (1984). In the Bolkardağı-Aladağ region, the Andırın Limestone can be correlated with the White Aladağ Tekeli within the Bozkır unit, as presented by Tekeli et al. (1984), demonstrating a tectonic slice according to Özgül (1976) and Gül et al. (1984).

2.2. Hydrogeology of The Area

Kahramanmaraş province is located in the Southeastern Anatolia Region of Turkey. The hydrogeological structure of the province is quite diverse, and groundwater resources play a significant role in this geographical area. The hydrogeology of Kahramanmaraş relies on the presence of different geological formations. Among these formations, there are limestone, sandstone, shale, and dolomite. This diversity influences the formation of groundwater resources by creating different capacities for water transport and storage.

The Fatmalı-Önsen region is situated to the south of Kahramanmaraş city. The hydrogeology of this area is closely related to the surrounding geological structures. The variety of surface rocks affects the movement and storage of groundwater. Particularly permeable rocks like limestone and dolomite allow groundwater to flow, while less permeable rocks like shale can restrict its movement. Groundwater resources play a vital role in meeting the

drinking water needs of the local population across Kahramanmaraş province. However, the sustainable management and protection of water sources are crucial, especially considering factors such as population growth and increased industrial activities. Therefore, a more comprehensive understanding of the hydrogeological structure in the region is necessary, and appropriate management strategies should be developed to ensure the sustainable use of water resources.

Due to its geographical location where three separate geographical regions (Mediterranean, Eastern Anatolia, and Southeastern Anatolia Regions) come closest to each other, Kahramanmaraş province exhibits three different climate types simultaneously. As elevation increases, the northern parts of the province have a completely continental climate, while the southern parts generally have characteristics closer to a "Modified Mediterranean Climate." Consequently, it can be said that the study area experiences hot and dry summers and relatively rainy and mild winters. Based on long-term (1970-2016) average monthly precipitation data (TSMS, 2016), it can be noted that months such as January, February, March, April, May, October, November, and December have average precipitation values exceeding 40 mm in the study area and its vicinity. On the other hand, June, July, August, and September exhibit average precipitation values below 10 mm. Accordingly, it is observed that the region receives consistent rainfall during the winter and spring months, while the summer months are dry. Long-term (1970-2016) data for maximum monthly precipitation values (TSMS, 2016) indicate intense rainfall exceeding 100 mm during December, January, and February, whereas the period between June and September sees precipitation levels drop below 10 mm. Furthermore, according to long-term (1970-2016) data on maximum snow depth (TSMS, 2016), the study area is covered with snow between December and March, with the thickest snow cover recorded in February.

Due to the rainy and mild climate characteristics described above, the Tut Formation in the study area, covering a vast expanse, presents a highly jointed and fractured structure due to intense tectonic influences. This structure renders the Tut Formation permeable on the surface, allowing water to percolate downward, and it gains a suitable aquifer quality for storing subsurface waters. In the Fatmalı-Önsen region where this study was conducted, the terrain features make it conducive for the Tut Formation to be permeable and acquire a suitable aquifer quality for storing subsurface waters.

The sources of groundwater in the Fatmalı-Önsen region are provided by five springs named as Atatürk fountain (FA-1) in Fatmalı, Kancıkdere fountain (KD-2) in Fatmalı, Kişifli Spring (FG-3) in Fatmalı, Pınarbaşı fountain (OK-4) in Önsen, and Hacıağlar (İncirlipınar) fountain (OH-5) in Önsen. The fractured and jointed structure of the Tut Formation, combined with the permeable characteristics of the terrain, allows surface waters to infiltrate and contribute to the groundwater system. This hydrogeological setting is significant as it facilitates the natural storage and movement of water within the subsurface, ultimately influencing the availability of water resources in the Fatmalı-Önsen region.

2.3 Methods

In order to assess the conformity of five distinct water sources utilized for drinking water supply Atatürk fountain (FA-1), Kancıkdere fountain (KD-2), Yazılı Kilise Fountain (YK-3), Kişifli Spring (FG-3), Pınarbaşı fountain (OK-4) and Hacıağlar (İncirlipınar) (OH-5)–with drinking water standards, water samples were acquired from these specific sampling locations (Figure 4). Key parameters including pH, temperature, electrical conductivity (EC), and dissolved oxygen (DO) were promptly measured upon sample collection. For the remaining water quality indicators, samples were carefully transported under cold chain conditions to the laboratory and subsequently stored at 4°C within a refrigerator.

Subsequent to transportation, comprehensive analyses encompassing heavy metals and anion-cation compositions were carried out utilizing advanced techniques such as ion chromatography, inductively coupled plasma mass spectrometry (ICP-MS), and ICP-optical emission spectrometry (ICP-OES) at ACME Analytical Laboratory in Vancouver, BC, Canada. In order to undertake isotope analyses – for instance, Oxygen-18 (^{18}O), deuterium (^{2}H), and tritium (^{3}H) – technical support was garnered from the Technical Research and Quality Control Department (TRQC) of Ankara State Hydraulic Works General Directorate.

Guided by the results garnered, a comprehensive classification of the water samples was performed, with an additional emphasis on exploring potential correlations among various parameters. The fundamental determinant influencing the chemical and physical characteristics of water resources within a region resides in the lithological traits of the geological formations through which these water bodies traverse. Thus, the initial step

involved determining the hydrogeochemical properties of the water resources within the investigation zone and subsequently associating these findings with the lithological units prevalent in the region. Furthermore, in an attempt to uncover any conceivable implications of drinking water resources on human health, an endeavor was made to establish a link between the hydrogeochemical attributes of the water sources and the prevalent hearing loss among the local populace.

3. RESULTS and DISCUSSIONS

In this section, we present and delve into the outcomes of our comprehensive analysis and characterization of the Kahramanmaraş Fatmalı-Önsen region's water resources. Beginning with the hydrogeochemistry, we explore various aspects such as the Wilcox and U.S. Salinity Laboratory diagrams, anion-cation ranking, Piper diagram, Schoeller diagram, isotopic composition, and relationships between isotopes. These findings not only shed light on the quality and origin of the drinking water sources but also provide valuable insights into their suitability for consumption and potential health implications. Through a detailed examination of these results, we aim to gain a deeper understanding of the complex dynamics governing the water resources in this region, facilitating informed decisions for sustainable water management and safeguarding public health.

3.1. Hydrogeochemistry

In order to evaluate the drinking water sources in the Fatmalı-Önsen region, a comprehensive assessment of water quality parameters was conducted. This assessment encompassed the measurement of various key factors, including temperature, pH, electrical conductivity (EC), alkalinity, trace element concentrations, anion-cation composition, and metal concentrations, as detailed in Table 1. In addition to this, General Quality Criteria by Classes of Inland Water Resources were evaluated and shown in Table 2. Due to temperature fluctuations ranging between 16°C and 17°C throughout the year, the water sources in the Fatmalı-Önsen region generally fall under the category of cold water. While all water sources exhibited similar dissolved oxygen (DO%) values ranging from 2.0% to 3.0%, there was significant variation in Na+ concentrations, spanning from 1.82 to 30.41 ppm. Notably, these Na^+ concentrations remain well below the permissible limits set by both the WHO (200 mg/L) and WPCR (Water Pollution Control Regulation) (125 mg/L), indicating an exceptionally low salt content in these water sources. The consistently low electrical conductivity (EC) values of the

water samples (ranging from 59.42 to 776.92 µs/cm) further affirm the presence of minimal ion concentrations and salinity in these springs. An analysis of pH values for Fatmalı's water sources reveals that all of them have a neutral to slightly basic nature, with pH levels ranging from 6.12 to 8.08.

The content of heavy metals in the water sources of the Fatmalı-Önsen region is also remarkably low. According to the Wilcox diagram (Wilcox, 1955), FA-1, KD-2, and C1-S1 waters are classified as "very good", while FG-3 and OH-5 fall under the C2-S1 category, and OK-4 falls within the C3-S1 category, as per the United States Salinity Laboratory diagram (Figure 5). The water quality of the Fatmalı-Önsen region's sources is assessed using the United States Salinity Diagram, where the horizontal axis represents the electrical conductivity (EC; µS/cm) of the water, and the vertical axis represents the Sodium Adsorption Ratio (SAR) (Figure 6). The intersection point of these values determines the classification of irrigation water. The United States Salinity Diagrams for the water samples within the study area have been provided.

The chemical analysis results were utilized to assess the hydrochemical characteristics of the water sources within the study area. Based on the Piper diagram, it's evident that waters FA-1, KD-2, FG-3, OK-4, and OH-5 display elevated levels of $CaCO_3$ and $MgCO_3$, showcasing carbonate hardness that surpasses the 50% threshold, or carbonate hardness exceeding non-carbonate hardness. These water sources are classified within region 5 of the Piper diagram (Piper, 1944) (Figure 7). This indicates that the majority of the hardness in these waters, exceeding 50%, is primarily attributed to permanent hardness components such as $CaSO_4$ and $MgSO_4$. Notably, KD-2 falls under region 9, signifying that KD-2 belongs to the category of mixed waters with ion concentrations below the 50% threshold. The anion-cation analysis results for the Fatmalı-Önsen water sources are presented in Table 2. Regarding cation ranking, FA-1, KD-2, and OK-4 were found to follow the order of $Ca^{2+} > Na^{+}+K^{+} > Mg^{2+}$. In contrast, the anion ranking for these samples was determined as $HCO_3^{-} > SO_4^{-2} > Cl^{-}$. When examining the water resources using the Scholler diagram (Scholler, 1967) (Figure 8), it becomes evident that these sources fall into distinct categories:"

1. Normal Sulfate Waters: This category suggests that the water samples contain sulfate ions within a normal range. Sulfates in water can come from various sources, including minerals and industrial discharges. Normal sulfate levels are typically considered safe for drinking water.

2. Normal Chloride Waters: Similar to sulfate, chloride levels in these water samples are within a normal range. Chlorides can also originate from geological sources or pollution. Again, normal chloride levels are generally acceptable for drinking water.

3. Hypocarbonated Waters: This category indicates that the water samples have lower concentrations of carbonate and bicarbonate ions. Carbonate and bicarbonate ions contribute to the alkalinity of water. While these ions are important for buffering pH in natural waters, hypocarbonated waters might have a lower pH.

Based on the Turkish Water Pollution Control Regulation (WPCR, 2004) and the guidelines set by the World Health Organization (WHO) for Drinking Water Standards, it is determined that the water sources in the Fatmalı-Önsen region are categorized as Class I and Potable Waters, respectively. This classification implies that these water sources comply with the established standards for safe drinking water, as their levels of sulfate, chloride, and carbonate-bicarbonate ions fall within the acceptable ranges.

Table 1. Geochemistry of the drinking water sources in the Fatmalı-Önsen Region

Geochemical Parameters	Water Sources				
	FA-1	KD-2	FG-3	OK-4	OH-5
Temperature (^{0}C)	15.93±7.57	16.78±5.21	16.03±6.10	16.30±3.69	17.20±1.22
pH	7.16±0.31	6.12±0.43	7.95±0.14	7.77±0.32	8.08±0.09
EC (µS/cm)	135.50±46.43	59.42±13.51	326.08±21.53	776.92±165.77	305.75±39.94
DO (%)	2.92±0.90	2.75±0.75	3.00±0.83	3.08±0.90	2.83±0.83
Na^+ (ppm)	1.82±0.18	1.84±0.10	3.25±0.21	30.41±2.73	2.36±0.12
K^+ (ppm)	0.79±0.11	1.13±0.17	1.07±1.14	9.62±0.96	1.15±0.71
Ca^{+2} (ppm)	13.25±6.35	8.45±5.87	50.37±2.11	106.73±8.22	45.45±0.38
Mg^{+2} (ppm)	12.91±6.63	5.73±4.32	18.74±1.22	23.21±0.50	15.35±0.74
Cl^- (ppm)	4.12±0.51	3.59±0.30	5.23±0.90	49.82±5.56	3.75±0.29
HCO_3^- (ppm)	67.33±39.15	40.88±30.17	234.33±15.73	339.92±20.46	203.00±1.13
SO_4^{-2} (ppm)	4.96±0.88	4.03±0.16	8.26±0.40	36.36±5.86	6.88±0.41
Fe^{+2} (ppm)	10.0±0.03	9.55±0.28	8.99±0.42	9.22±1.18	9.75±0.25

NO_3^- (ppm)	2.43±0.24	2.59±0.16	5.89±0.55	84.10±14.60	7.01±0.42
PO_4^{-3} (ppm)	0.44±0.09	0.78±0.06	0.10±0.03	1.15±0.21	*NA
F^{-1} (ppm)	0.07±0.02	0.07±0.03	0.06±0.02	0.35±0.14	0.06±0.02
Ba (ppm)	0.320±0.012	0.380±0.015	0.340±0.011	0.400±0.022	0.470±0.015
Al (ppb)	3.00±0.15	6.00±0.33	6.00±0.55	1.50±0.18	1.5±0.11
Au (ppb)	<0.05	<0.05	<0.05	<0.05	<0.05
As (ppb)	<0.5	<0.5	<0.5	<0.5	<0.5
Ag (ppb)	<0.05	<0.05	<0.05	<0.05	<0.05
Total Cr (ppb)	6.30±1.17	3.7±0.71	10.2±1.85	13.8±2.25	8.6±1.182
Cu (ppb)	1.00±0.82	1.90±1.10	0.60±0.05	1.95±0.93	0.15±0.07
Hg (ppb)	<0.10	<0.10	<0.10	<0.10	<0.10
Mn (ppb)	1.66±0.05	14.3±1.35	1.42±0.73	0.43±0.21	0.05±0.01
Ni (ppb)	<0.20	<0.2	<0.2	<0.2	<0.2
Sn (ppb)	<0.05	<0.05	<0.05	<0.05	<0.05
Pb (ppb)	7.3±3.25	4.3±1.10	45.2±5.85	2.6±0.84	1.3±0.07
Pt (ppb)	<0.01	<0.01	<0.01	<0.01	<0.01
Ru (ppb)	<0.05	<0.05	<0.05	<0.05	<0.05
Zr (ppb)	<0.02	<0.02	<0.02	<0.02	<0.02

EC Electrical conductivity, DO dissolved oxygen

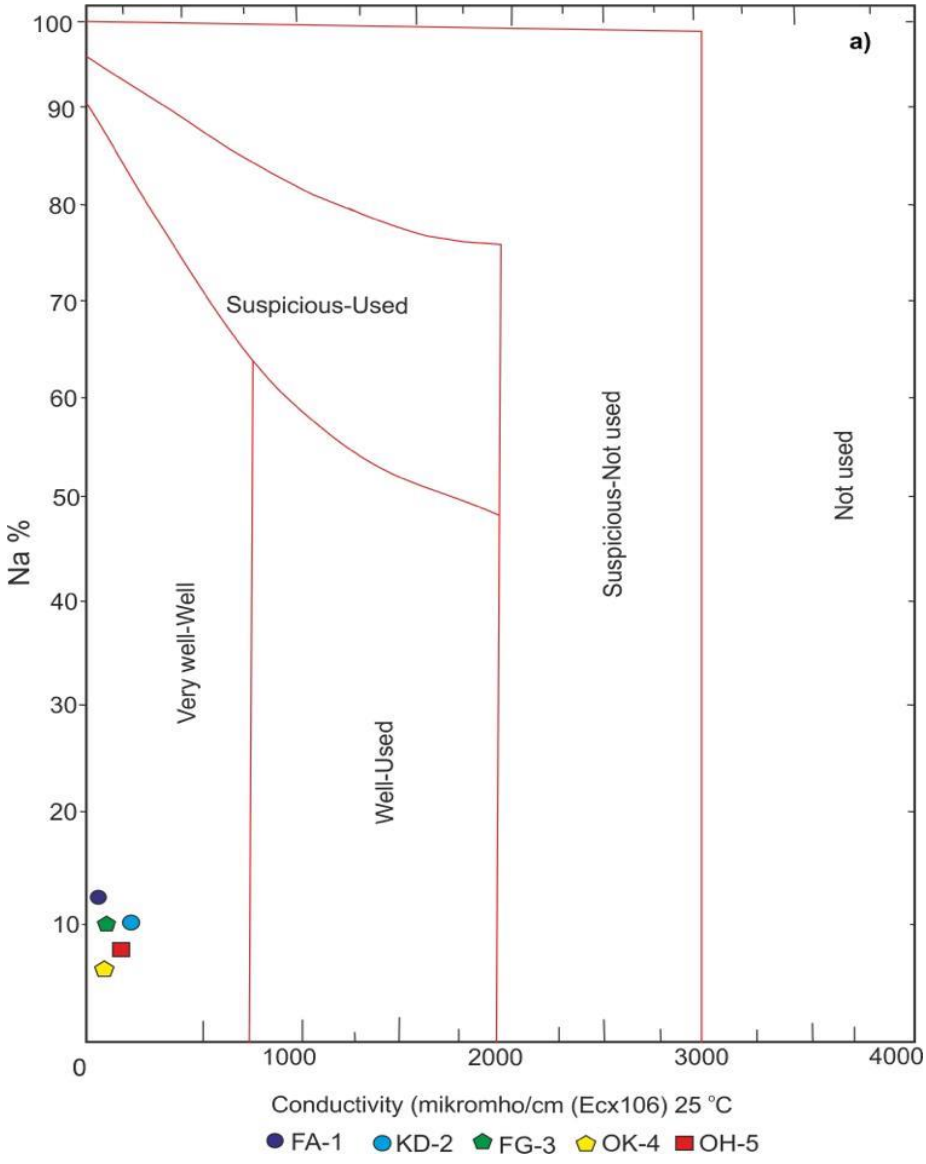

Figure 4. The Wilcox diagram of Fatmalı-Önsen drinking water sources

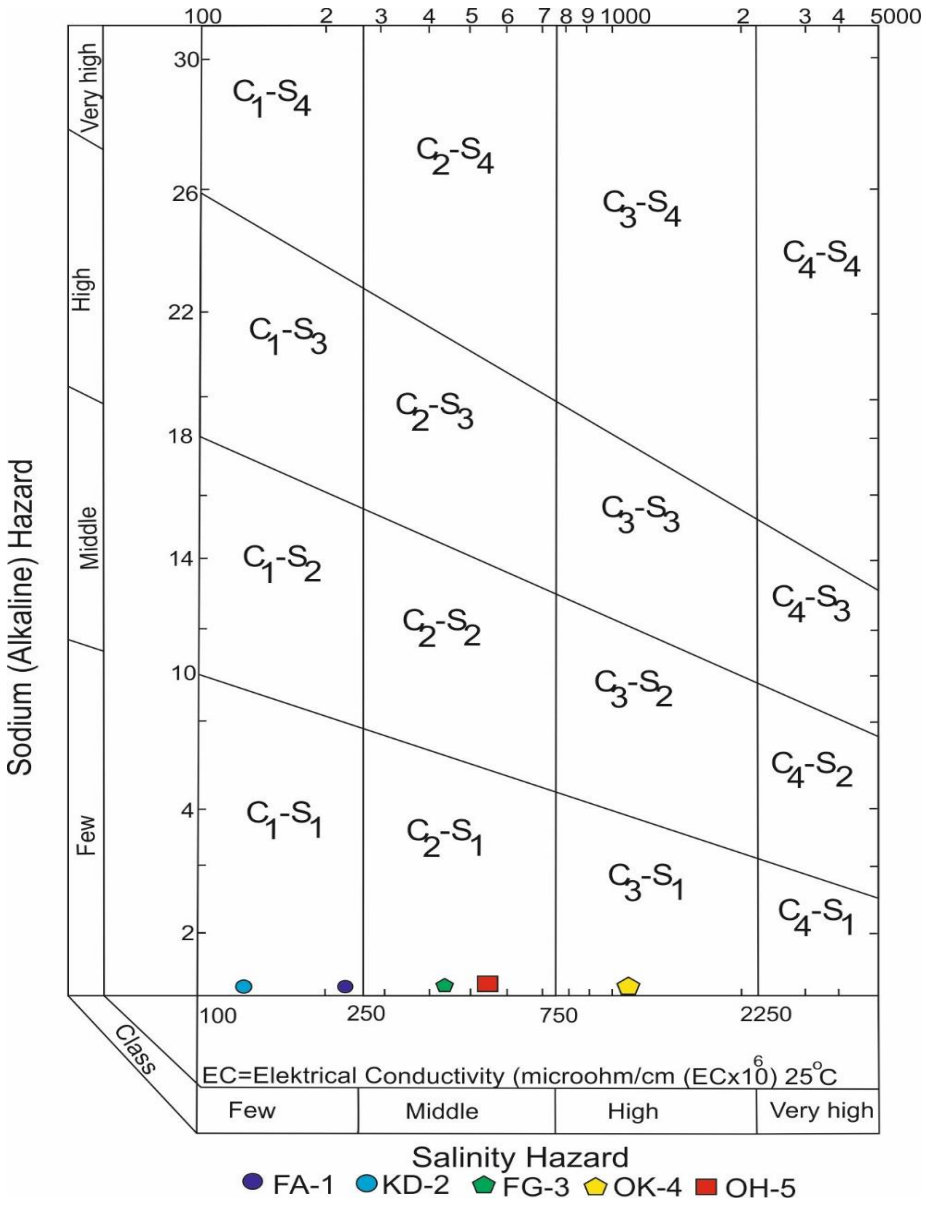

Figure 5. The U.S. Salinity Laboratory diagram of the drinking water sources of Fatmalı-Önsen

Table 2. The anion–cation ranking of drinking water sources of Fatmalı-Önsen

Sample	Cation Ranking	Anion Ranking
FA-1	Ca^{2+}> Na^{+}+K^{+}> Mg^{2+}	HCO_3^-> SO_4^{-2}>Cl^{--}
KD-2	Ca^{2+}> Na^{+}+K^{+}> Mg^{2+}	HCO_3^-> SO_4^{-2}>Cl^{-}
FG-3	Ca^{2+} > Mg^{2+}> Na^{+}+K^{+}	HCO_3^-> SO_4^{-2}>Cl^{-}
OK-4	Ca^{2+}> Na^{+}+K^{+}> Mg^{2+}	HCO_3^-> Cl^{-}>SO_4^{-2}
OH-5	Ca^{2+} > Mg^{2+} > Na^{+}+K^{+}	HCO_3^-> SO_4^{-2}>Cl^{-}

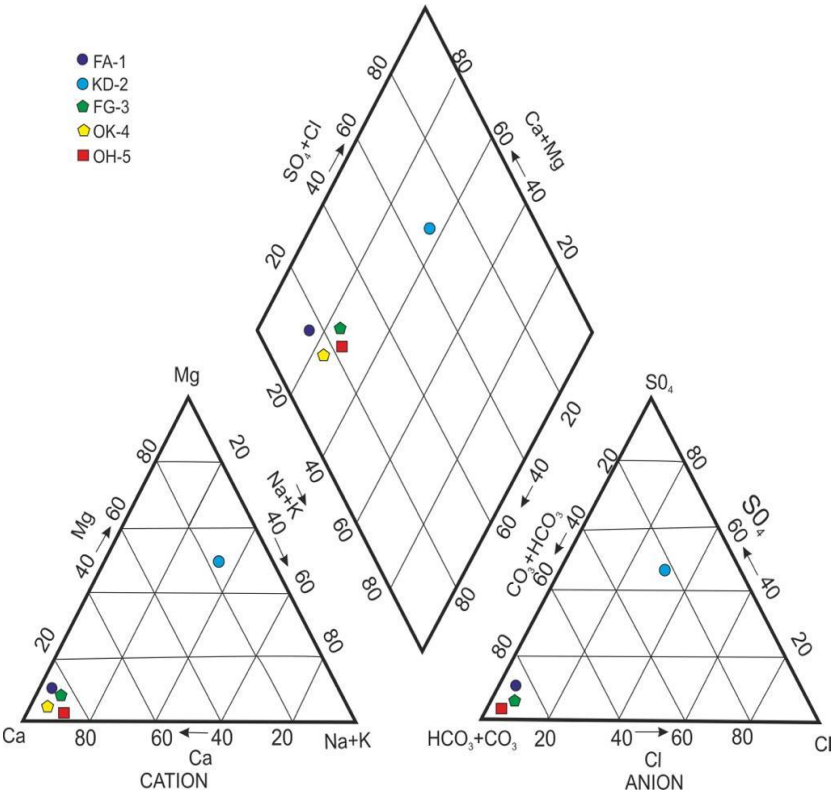

Figure 6. The Piper diagram illustrates the composition of drinking water sources in the Fatmalı-Önsen region

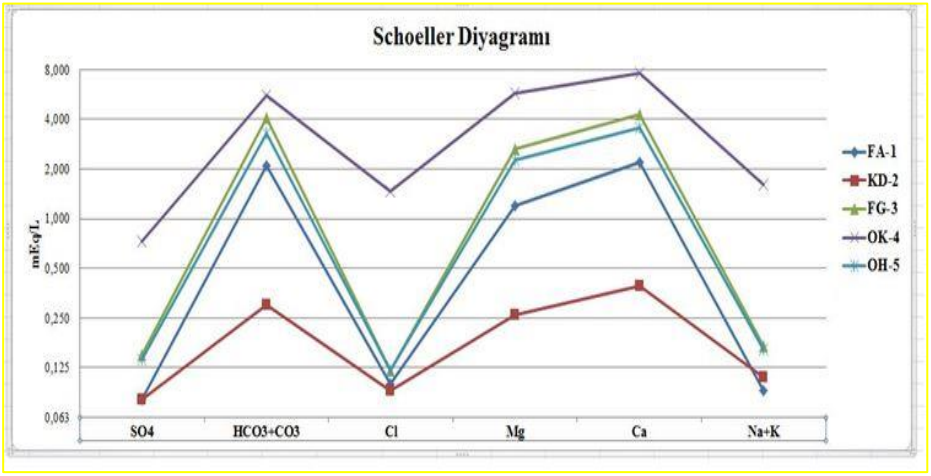

Figure 7. Schoeller diagram of Fatmali-Önsen water sources

The interpretations of the ion concentrations of the Fatmalı-Önsen region's spring waters were made using circular diagrams (**Fig. 10**). In these diagrams, which represent the total ionization in the water via radius, cations are placed in the northern half of the circle, and anions in the southern half. The sum of cations and anions is 100 meq/L, equivalent to 180º. The total mineralization in mg/L is indicated at the center of the circle. Here are the fundamental results and interpretations of these diagrams:

1. Ion Variations: The analyses did not reveal significant changes in anion and cation ions in water samples taken in different months. Therefore, it is possible to say that the water sources are fed from the same aquifer.

2. Same Aquifer Source: The results indicate that the spring waters originate from the same underground water source. This suggests that the water composition remains stable over time, even during different sampling periods.

These circular diagrams help us better understand the chemical composition and source of the Fatmalı-Önsen region's spring waters. The fact that they are fed from the same aquifer is important information for the management and sustainability of these water sources.

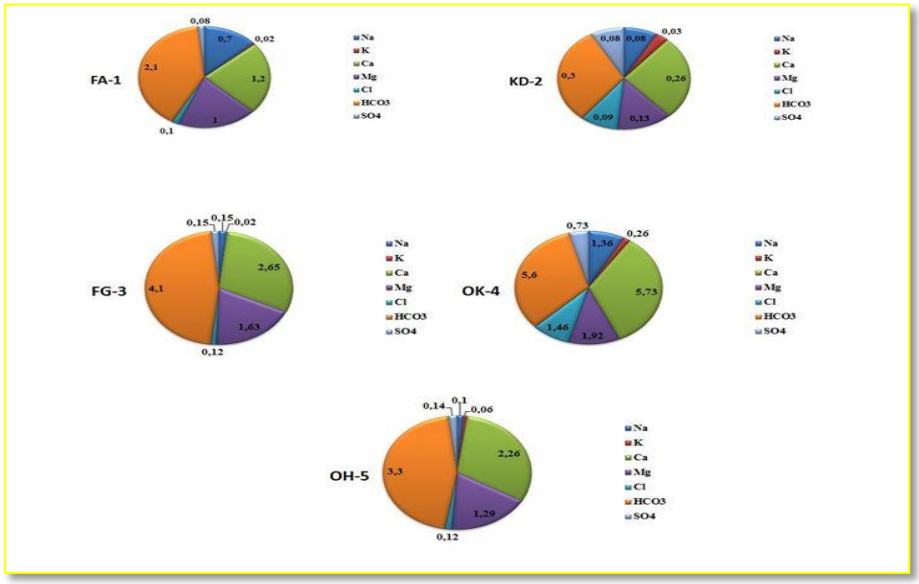

Figure 8. Pie diagram of water resources of Fatmali-Önsen region.

3.2. The results of isotopes

The study involved the use of environmental isotopes, including tritium (^{3}H), oxygen-18 (^{18}O), and deuterium (^{2}H), to gain insights into the properties of the aquifer and the interaction between water and rock in the underground water resources of Fatmalı-Önsen. These isotopes can provide valuable information about the source and history of the water. Here are the key findings and interpretations from the isotope analysis:

1. Recharge Elevation Values: By analyzing the isotopic composition of the water samples, the recharge elevation values were calculated. This information can help understand the source of the water and its movement within the aquifer.

2. Comparison with Global and Mediterranean Waterlines: The results were compared with two important reference lines: The Global Meteoric Waterline (GMWL) and the Mediterranean Waterline (MWL), both of which are used to interpret stable isotope data in hydrology. This comparison can provide insights into the origin and history of the water.

3. Source of Aquifer Recharge: Based on the isotope analysis, it was determined that the aquifers supplying the drinking water sources in Fatmalı-Önsen primarily receive their water from surface precipitation, including rainfall and snowmelt. This finding suggests that the aquifers are primarily

recharged by water from rainfall and snowfall events. In summary, the use of environmental isotopes in this study helped identify the source of recharge for the aquifers in Fatmalı-Önsen. The analysis indicates that these aquifers predominantly receive water from surface precipitation, highlighting the importance of understanding the hydrological processes in the region for sustainable water resource management.

Based on the provided information, it has been determined that the water resources in the Fatmalı-Önsen region fall between the global meteoric water line (GMWL) and the Mediterranean water line (MWL). This suggests several important conclusions regarding the aquifer system:

1. Precipitation as the Main Source: The aquifers in this region are primarily replenished by meteoric precipitation, such as rain and snow. The fact that these water resources fall between GMWL and MWL implies that the aquifers are directly fed by precipitation without significant evaporation losses.

2. Subsurface Accumulation: The interpretation suggests that the underground waters, which feed these water resources, are formed through the accumulation of precipitation beneath the ground. This occurs as the precipitation infiltrates through cracks, fractures, and faults in the subsurface geology.

3. Rising and Faults: The stored groundwater appears to rise along faults and active cracks within the subsurface. This rising process allows the accumulated groundwater to reach the Earth's surface, making it accessible as water resources.

4. Deuterium Excess Calculation: Deuterium excess values were calculated using the provided formula, which can provide further insights into the water's isotopic characteristics and the processes affecting it.

In summary, the isotopic analysis and interpretation indicate that precipitation plays a crucial role in replenishing the aquifers in the Fatmalı-Önsen region. The water accumulates underground and rises along geological features like faults, ultimately forming the accessible water resources in the area. Deuterium excess calculations provide additional data for understanding the water's isotopic composition (Table 4).

Table 4. Results of the $\delta^{18}O$, $\delta^{2}H$, and ^{3}H analyzes

Water sources	Date (dry/rainy period)	Oxygen-18 δ^{18} O (‰)	Deuterium δ^{2}H (‰)	Excess value (d_e) (‰)	Tritium (^{3}H)
FA-1	Augt/Jan	-8.31/-9.88	-48.70/-48.81	22.38/30.23	3.62/2.71
KD-2	Augt/Jan	-8.93/-10.04	-49.27/-49.80	48.34/30.52	2.92/2.37
FG-3	Augt/Jan	-8.30/-9.46	-46.24/-46.83	20.16/28.35	3.04/3.10
OK-4	Augt/Jan	-8.44/-9.46	-46.59/-45.14	20.93/29.42	2.53/3.16
OH-5	Augt/Jan	-8.58/-9.32	-47.01/-47.70	21.63/30.30	3.88/2.59

According to the $\delta^{18}O$-^{3}H diagram, it can be concluded that the groundwater sources in the Fatmalı-Önsen region have been fed by low-level sources with short circulation times (Figure 9-a). Tritium (^{3}H) is a radioactive isotope with a very short half-life (12.43 years) that enters the hydraulic system through precipitation, both natural and artificial, driven by cosmic radiation. Tritium-containing waters are considered as modern waters with transit times ranging from 5 to 10 years (Clark and Fritz, 1997). The Cl-^{3}H diagram reveals that the aquifer representing the Fatmalı-Önsen region water sources is primarily fed by relatively short-term young groundwater characterized by high Tritium and low chlorine content (Figure 9-b). However, according to the ^{2}H-^{3}H relationship, OK-4 source appears to have a slightly longer circulation time compared to other water sources (Figure 9-c).

The high ^{3}H concentration and low electrical conductivity values suggest that the groundwater in the region has a short water-rock interaction time, minimal interaction between groundwater composition and geological units, and a groundwater residence time of less than 50 years (Carreira et al., 2013) (Figure 9-d). Based on the isotopic analysis and interpretation, it can be concluded that the general lithological characteristics of the Tut Formation, within which the Fatmalı-Önsen water sources are located, are in good alignment. The Tut Formation typically commences with lithologies comprising dolomite-dolomitic limestone and clayey limestone at the base, transitioning upward into shale-sandstone, quartzite, and quartzitic conglomerate. Furthermore, being subjected to low to moderate regional metamorphism at the upper Ordovician age, this unit has acquired increased resilience against weathering, particularly in the levels of dolomite-dolomitic limestone, clayey limestone, and quartzite, which have become more resistant

due to the effects of metamorphism. Additionally, even if precipitation infiltrates slightly below the quartzites, the metamorphism-induced strengthening of these lithologies has made them more durable against weathering. Therefore, it can be inferred that these lithologies, especially the marbleized dolomite-dolomitic limestone and clayey limestone, which have undergone substantial metamorphism, could not have remained underground long enough to be dissolved by water due to the deformation they have experienced over time.

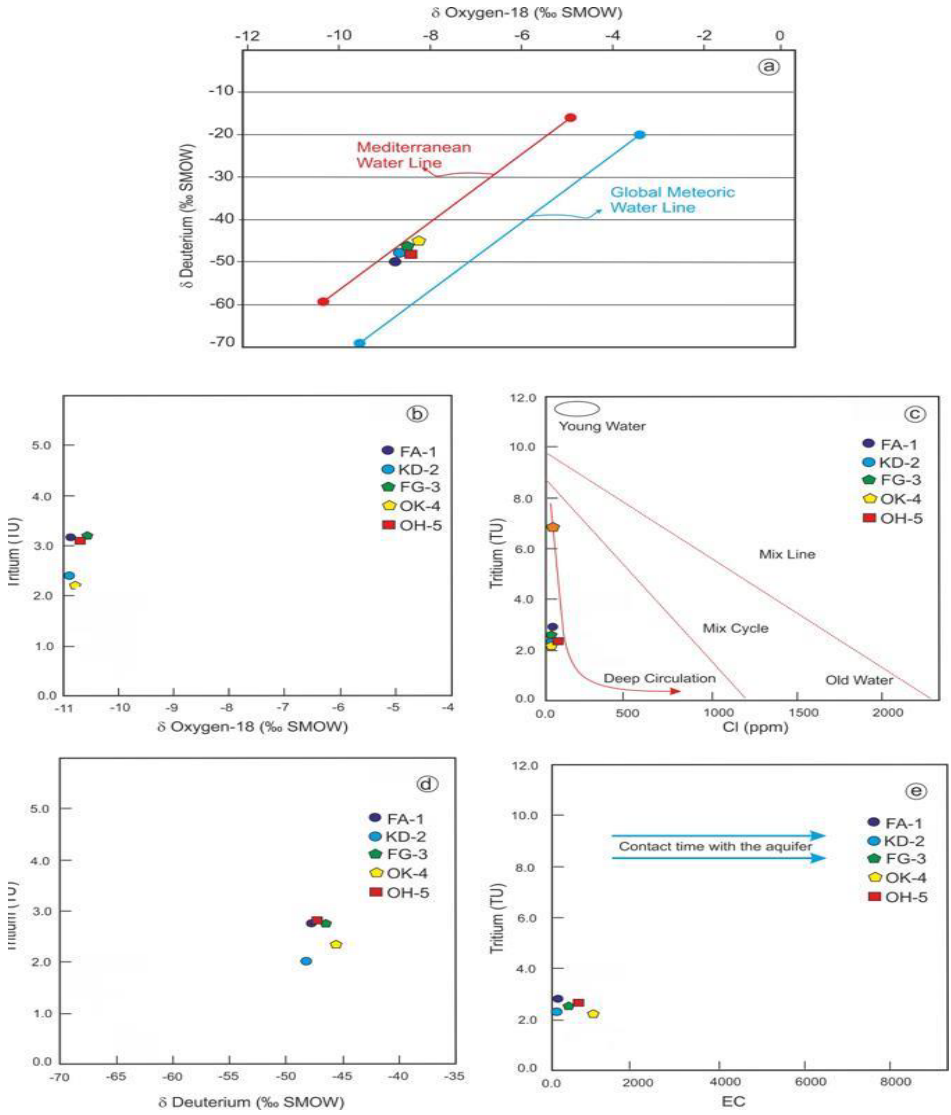

Figure 9. The Relationship Between Isotopes of Drinking Water Sources of Fatmalı-Önsen (a) δ18O-3H; TU relationship, b) Cl-TU relationship, c) (δ2H)–TU relationship, d) (EC; S/cm)–TU) relationship

3.3. Evaluation of water quality in terms of health

Contaminants present in drinking and utility water sources can present substantial risks, particularly to children. Nitrate is one such contaminant. Nitrates are a colorless, odorless, and tasteless compound that can be detected in well water and certain groundwater sources. From a chemical perspective, nitrates can be denoted as NO_3 and NO_3-N (nitrate-nitrogen). In accordance with EPA guidelines, the maximum allowable level is 10 mg/L NO3-N or 45 mg/L NO3. When evaluated from a medical geology perspective, the drinking water sources in Fatmalı-Önsen, particularly the water source identified as OK-4, exceed the standard drinking water limits, especially concerning nitrate levels. Previously, it was believed that nitrate levels exceeding these thresholds were harmful to infants and could lead to blue baby syndrome. However, recent studies have suggested that directly linking nitrate in drinking water to the occurrence of methemoglobinemia in infants may be overly simplistic. Nitrate might be one of several factors that could contribute to the development of this condition. Therefore, regular monitoring of drinking water sources and maintaining nitrate levels within the limits set by health authorities is crucial. Additionally, preserving water sources and preventing contamination play a critical role in safeguarding public health in the region.

CONCLUSION

Natural spring waters are not only sources of hydration but are also often associated with potential health benefits. However, ensuring their safety for public consumption requires a comprehensive understanding of the various water quality parameters. Regular monitoring, adherence to regulatory standards, and protective measures for water sources are all essential to guarantee the health and well-being of communities relying on these natural resources. Proper monitoring and management of water quality parameters are vital to prevent potential health risks associated with microbial contamination, excessive minerals, chemicals, and other pollutants. Considering the high Tritium concentrations and short underground water circulation times observed in the Fatmalı-Önsen spring waters, it can be concluded that these waters are young and fresh. This suggests that the water sources respond quickly to surface rainfall events, and the groundwater storage capacity is limited.

Such sources are often more rapidly renewable. From a human health perspective, these fresh waters offer several advantages. They provide a clean, fresh, and satisfying source of water. However, the sustainability and protection of these sources are crucial. Issues such as overuse, contamination, or drying up of local water sources imply that these sources could be at risk from a health and safety standpoint. Furthermore, the chemical composition of these waters is essential. High mineral content can increase mineral intake through water consumption or lead to adverse health effects. Therefore, regular chemical analyses of the waters and monitoring their compliance with drinking water standards are essential. In conclusion, the impact of the Fatmalı-Önsen spring waters on human health can be positive due to the clean, fresh, and generally low mineral content of the water. However, sustainability and water quality monitoring are crucial. Issues like overuse or contamination of water sources can increase health risks.

REFERENCES

Bratovcic, A., Petrinic, I. (2020). Quality assessment and health safety of natural spring water. Technologica Acta, 13(1): 33–40.

Batool, A., Samad, N., Kazmi, S.S., Ghufran, M.A., Imad, S., Shafqat, S., Shafqat, M., Mahmood, T. (2018). Spring water quality and human health: an assessment of natural springs of margalla hills Islamabad zone-III. International Journal of Hydrology 2(1):41–46. https://doi.org/10.15406/ijh.2018.02.00049

Baydar, O., Yergök, A.F. (1996). Güneydogu Anadolu-Kenar Kıvrım Kusagı-Amanos Dagları Kuzeyi ve Dogu Torosların Jeolojisi. Jeoloji Etütleri Dairesi, Ankara, 90s

Carreira, P.M., Marques, J.M., Nunes, D., Santos, F.A.M., Goncalves, R., Pina, A., Gomes, A.M. (2013). Isotopic and geochemical tracers in the evaluation of ground water residence time and salinization problems at Santiago Island, Cape Verde. Earth and Planetary Science, 7:113–117. https://doi.org/10.1016/j.proeps.2013.03.063

Clark, I., Fritz, P. (1997). Environmental isotopes in hydrogeology. CRC Press/Lewis Publishers, Baton Rouge.

Dean, V.T., Monod, O. (1985). The Lover Paleozoic Stratigraphy and Faunas of The Taurus Mountains Near Beyşehir, Turkey, I., Stratigraphy: Bulletin of Britain Museum of Natural History Geol., 19(8): 411-426.

Gül, M. A. (2000). Kahramanmaraş Yöresinin Jeolojisi. Hacettepe Üniversitesi Fen Bilimleri Enstitüsü Doktora Tezi, 304.

Ketin, İ. (1966). Güneydoğu Anadolu'nun Kambriyen Teşekkülleri ve Bunların Doğu İran Kambriyeni ile Mukayesesi: M.T.A. Dergisi., sayı 66

Lahner, L. (1972). Geologische Untersuchungen an der Oftflanke des Mittleren Amanos: Geotekt. Forshungen, Heft 42.

Özgül, N. (1976). Torosların Bazı Temel Jeolojik Özellikleri T.J.K. Bülteni cilt 19(1):65-78, Ankara

Perinçek, D., Kozlu, H. (1984). Stratigraphy and Structural Relations of The Units in The Afşin-Elbistan-Doğanşehir Region, Eastern Taurus, International Symposium on the Geology of the Taurus Belt, Miner Res. Expl. Inst. Geol. Seoc., 181-198.

Piper, A.M. (1944). A graphic procedure in the geochemical interpretation of water analyses. Eos, Transactions American Geophysical Union, 25:914-928. http://dx.doi.org/10.1029/TR025i006p00914

Schoeller, H. (1967). Geochemistry of groundwater. An international guide

for research and practice. UNESCO, 1967, chap 15, pp 1-18.

Stupar, Z., Levei, E.A., Neag, E., Baricz, A., Szekeres, E., Moldovan, O.T. (2022) Microbial water quality and health risk assessment in karst springs from Apuseni Mountains, Romania. Front. Environ. Sci. 10:931893. https://doi.org/10.3389/fenvs.2022.931893

Tekeli, O., Aksay, A., Ürgün, B. M. ve Işık A. (1984). Geology of the Aladağ Mountains;Geology of The Taurus Belt (edd.: Tekeli, O. ve Göncüoğlu, M.C.), 143-158.

TSMS, Turkish State Meteorological Service (2016). Available at: www.dmi.gov.tr.

U.S. Environmental Protection Agency (EPA) (2018). Water Quality Standards Handbook: Chapter 3: Water Quality Criteria. EPA-823-B-17-001. EPA Office of Water, Office of Science and Technology, Washington, DC. https://www.epa.gov/sites/production/files/2014-10/documents/handbook-chapter3.pdf

Ulu, Ü., Genç, Ş., Giray, S., Metin, Y. Çörekçioğlu, E. (1991). Belveren-Araban-Yavuzeli-Nizip-Birecik Alanının Jeolojisi, Senozoyik Yaşlı ve Volkanik Kayaçların Petrolojisi ve Bölgesel Yayılımı, M.T.A. Rap. No. 9226, Ankara.

WHO, World Health Organization (2017). Guidelines for Drinking-Water Quality: Fourth Edition Incorporating the First Addendum, Geneva. https://www.ncbi.nlm.nih.gov/books/NBK442373

Wilcox, L.V. (1955). Classification and use of irrigation water. US Department of Agriculture, Circular 969, Washington DC.

WPCR, (2004). Water Pollution and Control Regulations. Official Gazette 31.12.2004, No:25687.

Yoldemir, 0. (1987a). Suvarlı-Haydarlı-Narlı Gaziantep Arasında Kalan Alanın Jeolojisi, Yapısal Durumu ve Petrol Olarakları: TPAO Rap. no. 2257, 60s. Ankara.

ISBN: 978-625-367-333-8